CHARACTERIZATION AND ENHANCEMENT OF SAMPLE INTRODUCTION AND ION TRANSMISSION IN COMBINED GAS CHROMATOGRAPHY/TANDEM MASS SPECTROMETRY

By

MARK EDWARD HAIL

A DISSERTATION PRESENTED TO THE GRADUATE SCHOOL
OF THE UNIVERSITY OF FLORIDA IN PARTIAL FULLFILLMENT
OF THE REQUIREMENTS FOR THE DEGREE OF
DOCTOR OF PHILOSOPHY

UNIVERSITY OF FLORIDA

1989

To my loving wife, best pal, and big toe, Amy.

ACKNOWLEDGMENTS

I would like to express sincere gratitude to my graduate research director, Dr. Richard A. Yost, for his guidance and friendship over the past four years. Rick deserves some sort of medal, or perhaps more appropriately, a new prescription for his glasses, for all of the reading and reviewing of manuscripts and thesis chapters that he has done during the past few months. I would like to thank the members of my graduate committee, Drs. James D. Winefordner, Anna Brajter-Toth, Samuel O. Colgate, and Henri A. Van Rinsvelt. I would also like to thank Dr. John G. Dorsey (a fellow Lexingtonian) for his helpful discussions.

I would like to acknowledge the U. S. Air Force Engineering and Services Center at Tyndall Air Force Base and the U. S. Army Chemical Research Development and Engineering Center at Aberdeen Proving Grounds for providing the financial support for this work.

No graduate student would be very productive without the help of the departmental staff. For this reason, I thank Chester Eastman, Vern Cook, and Dailey Burch of the machine shop, and Mark Ross, Steve Miles, and Dean Schoenfeld of the electronics shop. I extend special thanks to Russ Pierce of the electronics shop, who was particularly helpful in answering questions and troubleshooting problems in the electronics lab and in my research.

I would like to thank my friends who made this period of my life so enjoyable, including all of the Yosties, and post-Yostie Jodie Johnson. Special thanks to my two office mates and soon-to-be coworkers, Ken

Matuszak and Dave "Cool One" Berberich. I would also like to thank those that dwelled with me in that most humble abode known as the thunderdome, where one man enters and two people leave. In order of appearance (and in some cases disappearance), thanks to Todd "Spud" Gillespie, Stephen "Judas" Brooks, Mark "Citizen" Barnes, and Jerry "Citrus Connection" Grunewald.

I would like to thank my family, Mom, Dad, Carl Jr., Beccy, and Steve, who have been so supportive.

Finally, I would like to thank my wife, Amy, the person who was always there to pat me on the back, who did my laundry and fed my face when I didn't have time, and who was always there for entertainment just by being herself.

TABLE OF CONTENTS

page

ACKNOWLEDGMENTS iii

ABSTRACT vii

CHAPTERS

1 INTRODUCTION 1

Short GC Columns in GC/MS and GC/MS/MS 1
Short GC Columns at Sub-ambient Pressures 2
Mixture Analysis by GC, GC/MS and GC/MS/MS 4
Organization of Dissertation 10

2 THEORETICAL AND PRACTICAL ASPECTS OF SHORT OPEN TUBULAR COLUMNS AT SUB-AMBIENT PRESSURES IN GAS CHROMATOGRAPHY/MASS SPECTROMETRY 12

Introduction and Theory 12
Experimental Section 15
Calculations 15
Mass Spectrometry 15
Gas Chromatography 16
Average Velocity Measurement 19
Results and Discussion 20
Effect of the Pressure Drop 20
Sub-ambient Inlet Pressures 26
Experimental vs. Theoretical Performance 37
Choice of the Carrier Gas 41
Conclusions 43

3 CONCEPTS FOR PORTABLE GAS CHROMATOGRAPHIC INSTRUMENTATION IN GC/MS: FLOW RATE PROGRAMMING AND DIRECT COLUMN HEATING 46

Introduction 46
Flow Rate Programming 47
Direct Resistive Heating of Al-Clad Capillary Columns . . . 48
GC Probe 51
Experimental Section 52
Experimental Conditions 52
Flow Control System 53
Direct Resistive Heating 57

GC Probe Design 61
Results and Discussion 64
Flow Rate Programming 64
Direct Resistive Heating 77
GC Probe Performance 85
Conclusions 89

4 GAS CHROMATOGRAPHIC SAMPLE INTRODUCTION INTO THE COLLISION CELL OF A TRIPLE QUADRUPOLE MASS SPECTROMETER FOR MASS-SELECTION OF REACTANT IONS FOR CHARGE EXCHANGE AND CHEMICAL IONIZATION 90

Introduction and Theory 90
Experimental Section 93
Mass Spectrometry 93
Gas Chromatography 95
GC/MS Interface 96
Results and Discussion 98
Ionization Energy Measurements 98
Simultaneous Structural and Molecular Weight Information . 101
Selectivity of Ionization 106
Detection Capabilities of GC/MSR/MS 112
Chromatographic Integrity 116
Conclusions 116

5 CHARACTERIZATION AND OPTIMIZATION OF ION TRANSMISSION IN TRIPLE QUADRUPOLE MASS SPECTROMETRY 118

Introduction 118
Experimental Section 119
Instrumentation 119
Procedures 125
Results and Discussion 126
Mass-dependent Optimization 126
Quadrupole Mass Filters 135
Ion Transmission Characteristics of the Center Quadrupole . 140
Ion Transmission at High Collision Energies 153
Conclusions 157

6 CONCLUSIONS AND FUTURE WORK 159

Conclusions 159
Suggestions for Future Work 161
Reduced Column Pressures with Conventional GC Detectors . . 161
Directly-heated Open Tubular Columns 162
Resonance Excitation and Ion Storage in Q2 164

LITERATURE CITED 167

BIOGRAPHICAL SKETCH 173

Abstract of Dissertation Presented to the Graduate School
of the University of Florida in Partial Fulfillment of the
Requirements for the Degree of Doctor of Philosophy

CHARACTERIZATION AND ENHANCEMENT OF SAMPLE INTRODUCTION AND ION TRANSMISSION IN COMBINED GAS CHROMATOGRAPHY/TANDEM MASS SPECTROMETRY

By

Mark Edward Hail

May 1989

Chairman: Richard A. Yost
Major Department: Chemistry

Various theoretical and practical aspects of the use of short open tubular columns in combined gas chromatography/mass spectrometry (GC/MS) and tandem mass spectrometry (GC/MS/MS) have been investigated, including the advantages of low-pressure operation with short and/or wide-bore open tubular columns. It is shown both theoretically and experimentally that short columns with vacuum outlet require sub-atmospheric inlet pressures if optimum gas velocities are to be obtained. The use of sub-ambient inlet pressures is also shown to improve the sensitivity when short columns are used with electron ionization in GC/MS.

Several considerations are addressed for the design of portable GC instrumentation. In particular, exponential flow rate programming as well as resistively-heated aluminum-clad open tubular columns have been evaluated for low-power, high-throughput analysis in GC/MS. Aluminum-clad

open tubular columns are heated directly by applying a voltage across the capillary, and the column temperature is sensed by measuring the column resistance. These investigations have led to the development of a compact gas chromatograph probe for use in GC/MS.

A gas chromatograph has been interfaced to the collision cell of a triple quadrupole tandem mass spectrometer for performing mass-selected ion-molecule reactions. Reactant ions are selected with the first quadrupole and are allowed to react in the second quadrupole collision cell with the effluent from a short open tubular GC column. The ion-molecule reaction product ions are mass-analyzed by the third quadrupole. The advantages of using mass-selected reactions for controlling the selectivity of charge exchange and chemical ionization are demonstrated. In addition, this configuration is shown to provide both structural information and molecular weight information in the same chromatogram by alternating between different reactant ions.

The ion transmission characteristics of a triple quadrupole mass spectrometer (TQMS) have been studied. The unique high level of computer control of the TQMS has allowed for rapid characterization and understanding of the ion optical parameters. Strategies for obtaining optimum ion transmission and minimization of mass dependencies in the ion optics for single MS experiments as well as for MS/MS experiments are discussed.

CHAPTER 1
INTRODUCTION

In this dissertation a variety of concepts are presented for the enhancement of sample introduction and ion transmission in analytical mass spectrometry (MS) and tandem mass spectrometry (MS/MS). Due to the inherent speed and selectivity of MS and MS/MS, considerable attention was devoted to the study of rapid gas chromatographic (GC) separation techniques. A new tandem mass spectrometric method, in which the selectivity of ion-molecule reactions is exploited for gas chromatographic mixture analysis, is also described. Finally, the results of a detailed characterization of the ion optical parameters of a triple quadrupole tandem mass spectrometer are presented.

Short GC Columns in GC/MS and GC/MS/MS

In this research group, it has been found that short GC columns can be used for the extremely rapid analysis of complex mixtures by taking advantage of the inherent selectivity of MS, and particularly MS/MS [1-3]. In the initial results that were obtained with very short (e.g., 50 cm) packed columns, it was found that the sensitivity and selectivity obtainable with short-column GC in conjunction with MS/MS in many cases exceeded that of high-resolution GC/MS (HRGC/MS) [1]. In addition, it was shown that 100 injections per hour could be performed with the short-column method, while only 2 injections per hour could be made with the HRGC/MS method employing an 18 m capillary column [1]. Later, short open

tubular capillary columns were evaluated (including an investigation of the associated chromatographic theory) due to their inherent advantages over packed columns [2,3]. These studies began to demonstrate the advantages of vacuum outlet operation with short open tubular columns. It was found that there were added benefits other than speed of analysis that were important. For instance, because of the high gas velocities and low operating pressures associated with short open tubular columns under vacuum outlet conditions, it was found that solutes tended to elute at temperatures well below their boiling points. Thus, it was discovered that short-column open tubular GC in conjunction with MS or MS/MS was ideal for the analysis of involatile, thermally labile, or polar solutes [2,3]. More recently, McClennen et al. have taken advantage of this and have demonstrated that large involatile and/or polar molecules can be analyzed by examining the Curie-point pyrolysis products of these molecules with short-column GC/MS [4,5].

Short GC Columns at Sub-ambient Pressures

Many of the chromatographic separation techniques currently in widespread use require relatively high operating pressures, namely, high-pressure liquid chromatography (HPLC), supercritical fluid chromatography (SFC), and even high-resolution capillary open tubular gas chromatography (HRGC). In contrast, research in the area of low-pressure separation techniques has been limited. More than 25 years ago, Giddings demonstrated that the minimum analysis times in gas chromatography could be achieved when the column outlet was connected to a vacuum [6]. However, to date, a majority of the research done in high-speed GC has dealt with the use of small diameter columns and the development of high-

speed injectors required for use with these columns [7-13]. Recently, interest in vacuum outlet operation has been renewed, as Leclercq and coworkers have published a number of articles that have addressed the theory and advantages of vacuum outlet operation for reducing analysis times in open tubular GC [14-17].

Vacuum outlet operation in gas chromatography results in lower column pressures, which increases the diffusivity of the solute in the gas phase and leads to increased optimum carrier gas velocities and shorter analysis times [14]. The advantages of vacuum outlet operation are inherently obtained when gas chromatography is combined with mass spectrometry (GC/MS), provided the column is inserted directly into the vacuum of the mass spectrometer. Consideration of the theory indicates that low outlet pressure operation has a more pronounced effect if wide-bore columns [16] and/or short columns [3] are used. As shorter column lengths are used to minimize analysis times, lower inlet pressures are required if optimum chromatographic performance is to be obtained. The use of very short lengths or wide-bore columns is limited when conventional inlet pressures are used because of the gas load imposed on the mass spectrometer. Alternatively, the inlet can be operated at sub-ambient pressures to obtain optimum performance and/or to reduce the flow rate of carrier gas entering the mass spectrometer vacuum system [18]. Unfortunately, the value of sub-atmospheric column inlet pressures has not been widely appreciated, due in part to the difficulty of operating traditional GC injection ports at vacuum.

Mixture Analysis by GC, GC/MS, and GC/MS/MS

Application of short columns with conventional GC detectors has been limited to the analysis of relatively simple mixtures due to the non-selective nature of the detectors and the reduced resolving power of short columns. However, as stated previously, the inherent selectivity of MS and MS/MS can be utilized to atone for the chromatographic resolution lost when shorter columns are used. Perhaps a better comprehension of the additional selectivity of the mass spectrometric detection methods over conventional detection methods in gas chromatography can be obtained by considering the possible cases which result in interferences. These coincidences are summarized in Table 1.1, which shows a comparison of GC employing flame ionization detection (FID) as well as GC with various mass spectrometric detection methods. A schematic comparison of the three mass spectrometric techniques, all of which can be performed on the triple quadrupole tandem mass spectrometer used in this work, is shown in Figure 1.1.

Mixture overlap will readily occur when non-selective detection methods (e.g., FID) are used in complex mixture analysis, unless a column of sufficient length is used to chromatographically separate all possible interferences from the analyte of interest. In many cases, no column, regardless of length, would be sufficient to accomplish this goal; thus, other extraction and sample cleanup procedures must be used in addition to the already time-consuming chromatographic analysis. In addition, since chromatographic resolving power increases only with the square root of the column length, while analysis times increase proportionally with column length, increasing the column length to gain the necessary

Table 1.1. Cases leading to mixture overlap (interferences) in gas chromatographic mixture analysis with flame ionization detection and various methods of mass spectrometric detection. The '?'s in the table indicate the conditions under which targeted mixture components will be obscured by interferences.

Analytical Method			
GC/FID	GC/MS	GC/MS/MS	GC/MSR/MS[a]
Coincidences Resulting in Interferences			
(1) coelute ↓ ?	(1) coelute ↓ (2) produce ions of same m/z ↓ ?	(1) coelute ↓ (2) produce ions of same m/z ↓ (3) fragment to daughter ions of same m/z ↓ ?	(1) coelute ↓ (2) react to form product ions of same m/z ↓ ?

[a] GC/MSR/MS = GC/mass-selected reaction/MS, see Figure 1.1.

Figure 1.1. Schematic comparison of three different combined gas chromatography/mass spectrometric methods which may be performed on a triple quadrupole mass spectrometer: (a) GC/MS, (b) GC/MS/MS, and (c) GC/mass-selected reaction/MS (GC/MSR/MS). The new technique described in this thesis, GC/MSR/MS, involves introduction of the GC column into the second quadrupole collision cell (Q2), rather than into the ion source. Also note the differences in the two MS/MS approaches. In traditional MS/MS, a sample (parent) ion is mass-selected with Q1 and is allowed to fragment via CAD in Q2, whereas in MSR/MS, Q1 is used to mass-select a reactant ion for reaction with sample molecules in Q2.

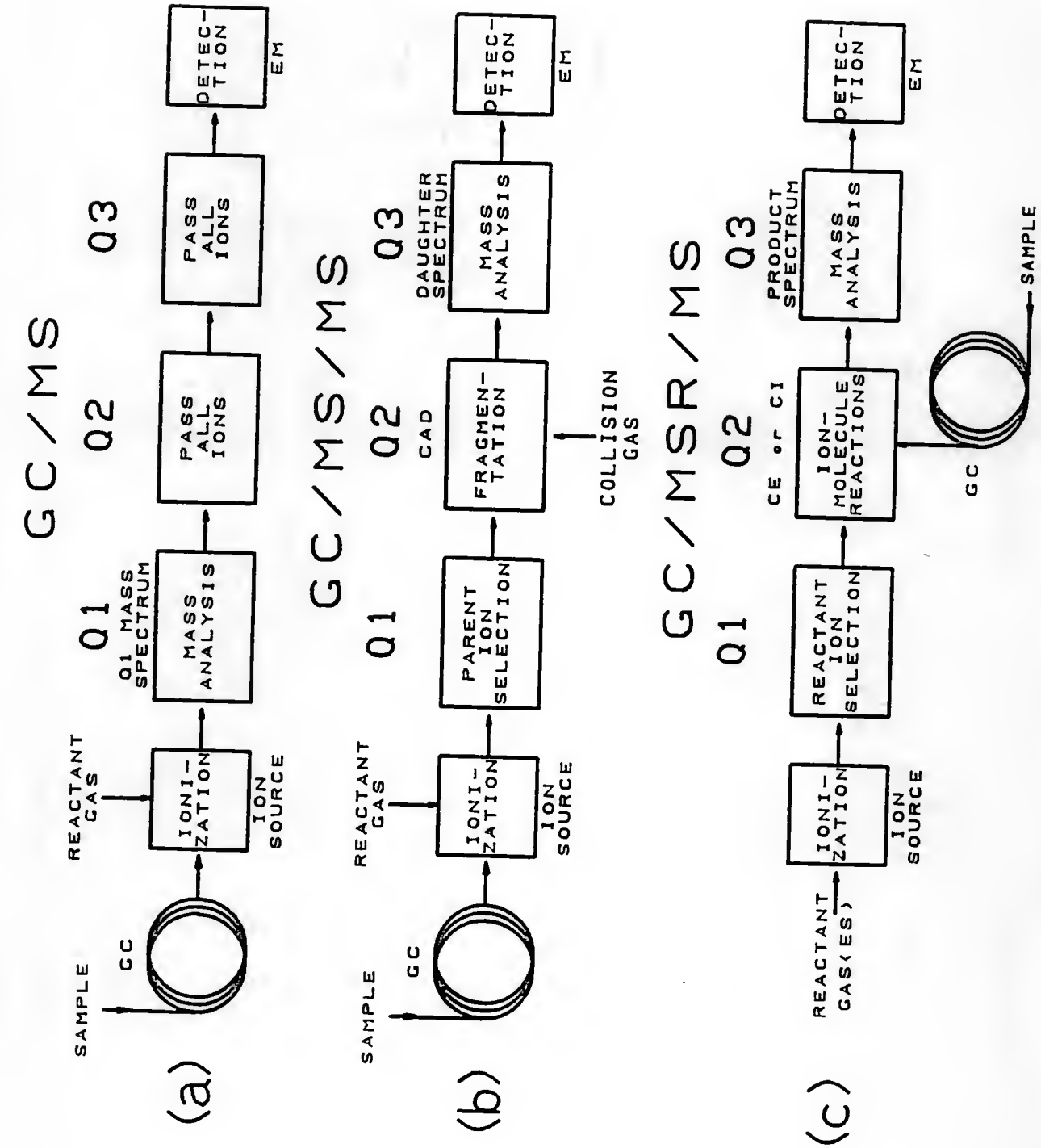
GC/MS
Q1
Q2
Q3
Q1 MASS SPECTRUM
PASS ALL IONS
PASS ALL IONS
DETEC-TION
EM
MASS ANALYSIS
IONI-ZATION
ION SOURCE
REACTANT GAS
SAMPLE
GC
(a)
GC/MS/MS
Q1
Q2
Q3
CAD
DAUGHTER SPECTRUM
PARENT ION SELECTION
FRAGMEN-TATION
MASS ANALYSIS
DETEC-TION
EM
COLLISION GAS
IONI-ZATION
ION SOURCE
REACTANT GAS
SAMPLE
GC
(b)
GC/MSR/MS
Q1
Q2
Q3
CE or CI
PRODUCT SPECTRUM
REACTANT ION SELECTION
ION-MOLECULE REACTIONS
MASS ANALYSIS
DETEC-TION
EM
IONI-ZATION
ION SOURCE
REACTANT GAS(ES)
GC
SAMPLE
(c)

resolution tends to be very costly in terms of the time required for an analysis.

As shown in Table 1.1, the possibilities for interferences in mixture analysis are greatly reduced when mass spectrometric detection is used. In GC/MS (Figure 1.1 (a)), other component(s) of the mixture must coelute with the analyte of interest and must yield ions of the same m/z as the analyte of interest in order for interferences to occur. Even more selectivity is obtainable with GC/MS/MS (Figure 1.1 (b)). In order for mixture overlap to occur in GC/MS/MS, undesirable interferents must not only coelute and be ionized to produce the same nominal mass ions, but the interfering parent ions must also fragment via collisionally-activated dissociation (CAD) to produce all of the same daughter ions as the analyte.

Described in this dissertation is a new GC/tandem mass spectrometric technique, GC/mass-selected reaction/MS (GC/MSR/MS), which involves mass-selection of reactant ions and reaction of these ions with the effluent from a gas chromatographic column. It can be seen from Figure 1.1 (c) that this method involves introduction of the GC column into the second quadrupole collision cell (Q2) rather than into the ion source. This method takes advantage of the intrinsic selectivity of ion-molecule reactions. Hence, for overlap to occur in mixture analysis with GC/MSR/MS, interferences must react in Q2 to produce all of the same m/z product ions as the analyte of interest.

It can be seen from the above comparisons that the added resolution elements available with the mass spectrometric techniques in many cases obviate the need of high-resolution chromatographic separation in mixture analysis. Therefore, the use of short open tubular columns and the

concomitant short analysis times are readily justified. In addition, the capability to perform any of the three GC/MS techniques (GC/MS, GC/MS/MS, or GC/MSR/MS) certainly demonstrates the versatility of the triple quadrupole mass spectrometer (TQMS).

Although instrumentation for MS/MS tends to be rather expensive (e.g., $350,000 for a TQMS) when compared to other analytical techniques (e.g., $15,000 for a GC), it has been pointed out that MS/MS is a cost-effective technique because of the short analysis times that are possible [19]. This is most likely the reason for the increasing popularity as well as the widespread availability of commercial instrumentation for MS/MS. The MS/MS technique has certainly benefited from recent advances in computers and electronics, as these progressions have led to the development of a wealth of new, exciting, computer-controlled instrumentation. One such instrument is the Finnigan MAT TSQ70, which was used throughout this work. This instrument, with its unique level of computer control, has allowed a detailed study of the ion optical parameters and their effects on ion transmission in triple quadrupole mass spectrometry. In fact, many of the undesirable ion optical effects (e.g., mass dependencies) can be avoided due to the capability of this instrument to vary any the ion optical parameters as a function of mass within each mass spectral scan. These types of studies have provided a more thorough understanding of the ion optical parameters that effect the performance of this instrument, which will ultimately improve the analytical capabilities during its use.

Organization of Dissertation

This dissertation is divided into six individual chapters. This chapter has served to present an overall perspective as well as the purpose of the work. Global conclusions and suggestions for future research are found in Chapter 6. Chapters 2-5 make up the body of the dissertation. Due to the widely varying material presented in this dissertation, there is no particular chapter devoted entirely to the description of experimental conditions. Rather, each chapter (of Chapters 2-5) consists of a separate introduction, experimental section, discussion of results, and conclusions.

In Chapter 2, the advantages of utilizing low column pressures with short open tubular columns in GC/MS are examined by consideration of the theoretical chromatographic relationships. In particular, the advantages of operating the column inlet, as well as the column outlet, at sub-atmospheric pressures are stressed. Experimental data are presented that demonstrate the practicality of the combination of short GC columns with mass spectrometry.

In Chapter 3, considerations for portable and/or high-throughput sample introduction schemes for GC/MS are presented, including investigations of exponential flow rate programming and direct resistive heating of aluminum-clad open tubular columns. A portable direct insertion gas chromatograph probe is described that incorporates these concepts.

The fourth chapter describes the GC/MSR/MS technique, including a brief discussion of the utility of selective ion-molecule reactions for mixture analysis. This work represents the first experiments ever performed in which samples are introduced from a GC column into the center quadrupole collision cell of a TQMS. Experimental data are presented that

demonstrate the potential selectivity, detection and screening capabilities of this method. A method is also described which allows for the extremely rapid measurement of ionization energies on the computer-controlled TQMS.

In Chapter 5, the effects of various ion optical parameters of the TQMS for MS and MS/MS are investigated. In particular, it is shown that the mass-dependencies in the ion optics of the computer-controlled TQMS can be minimized, since all of the ion optical parameters may be varied as a function of mass during a mass spectral scan. The insights gained in these experiments have yielded a better understanding of the complex inter-relation of the parameters that affect the performance and reproducibility of the results obtained with this instrument.

CHAPTER 2
THEORETICAL AND PRACTICAL ASPECTS OF SHORT OPEN TUBULAR COLUMNS AT SUB-AMBIENT PRESSURES IN GAS CHROMATOGRAPHY/MASS SPECTROMETRY

Introduction and Theory

In this chapter, various theoretical and practical aspects of the use of short open tubular columns in GC/MS are discussed, including the advantages of low-pressure operation with short and/or wide-bore open tubular columns. It is shown that short columns with vacuum outlet require sub-atmospheric inlet pressures if optimum gas velocities are to be obtained. Since sub-atmospheric inlet pressures are not obtainable with most gas chromatographic inlet systems, a computer-controlled flow control system has been investigated that allows the injection port to be operated at sub-ambient pressures with either split or splitless injections. Plate heights have been experimentally determined at sub-ambient pressures and have been compared with theoretical predictions. The effects of extra column band broadening are evident in the experimental data and demonstrate the need for high-speed injection systems if maximum performance is to be obtained with short columns. The use of sub-ambient inlet pressures is also shown to improve the sensitivity when short columns are used with electron ionization in GC/MS. Finally, it is shown that hydrogen carrier gas can be used to obtain the fastest analyses without altering the relative abundances of ions obtained with methane chemical ionization mass spectrometry.

The theoretical dependence of the plate height, H, on the average gas velocity, υ, in open tubular gas chromatography is given by the Golay equation [20]

$$H = B/\upsilon + (C_g+C_l)\upsilon \tag{2.1}$$

where B is a term relating to the longitudinal diffusion of the solute zone, and C_g and C_l are terms relating to mass transfer in the gas phase and liquid stationary phase, respectively. For open tubular columns employing a thin-film stationary phase, mass transfer in the liquid phase is negligible and C_g dominates [14]. The Golay equation for thin-film columns corrected for gas compressibility [21] can be rewritten in terms of the column parameters yielding [14]

$$H = \frac{2D_{g,o}f}{\upsilon_o} + \frac{(1+6k+11k^2)r^2\upsilon_o f}{24(1+k)^2D_{g,o}} \tag{2.2}$$

where $D_{g,o}$ is the diffusion coefficient of the solute in the gas phase at the outlet pressure, f is the Giddings correction factor, υ_o is the gas velocity at the column outlet, k is the partition ratio, and r is the column radius. The Giddings correction factor accounts for the decompression of the carrier gas when a pressure gradient exists and is given by

$$f = \frac{9(P^4-1)(P^2-1)}{8(P^3-1)^2} \tag{2.3}$$

where P is the inlet to outlet pressure ratio, P_i/P_o. The gas decompression factor approaches a value of 9/8 when large pressure gradients are employed, as in GC/MS. Most commonly, H is expressed in terms of the average velocity, υ. If this is done, υ_o and $D_{g,o}$ of eq 2.2 are replaced by the average velocity, υ, and an average diffusion coefficient, $\bar{D}_g$. An average diffusion coefficient can be estimated from [14]

$$\bar{D}_g = \frac{P_1 D_{g,1}}{\bar{P}} \tag{2.4}$$

where $D_{g,1}$ is the diffusion coefficient at 1 atmosphere pressure, P_1, and $\bar{P}$ is the average column pressure. The length-average column pressure, $\bar{P}$, is dependent on the pressure gradient and is given by [14]

$$\bar{P} = \frac{2P_o(P^3-1)}{3(P^2-1)} \tag{2.5}$$

which reduces to $2P_i/3$ for vacuum outlet conditions.

As shown by eq 2.4, lowering the average column pressure increases the diffusion coefficient. An increase in the diffusion coefficient has been shown to result in an increase in the optimum gas velocity and decreased analysis times [3,14-18]. In addition, a larger $\bar{D}_g$ results in a slower rate of increase of H (from the C_g term) as the gas velocity is increased beyond the optimum. This means that even higher gas velocities can be used without severe losses of efficiency.

There are a number of ways of decreasing the average column pressure. Lower average column pressures are readily obtained if the column outlet is at vacuum as in GC/MS. At lower outlet pressures, the greatest gains in terms of speed of analysis (as compared to normal atmospheric outlet operation) can be obtained if short and/or wide-bore columns are used [3,16]. Lower average column pressures can also be obtained if low-viscosity carrier gases are used [22]; hence, the use of hydrogen as a carrier gas will always result in the shortest analysis times.

Experimental Section

Calculations

All theoretical calculations were done on an IBM PC/XT or a PC/AT, with programs written in TurboBASIC (Borland International). The results of the calculations (e.g., H vs. υ data) were stored on disk in ASCII format, which allowed the data to be retrieved and plotted with a commercially available plotting program (Grapher, Golden Software, Inc.).

Mass Spectrometry

A Finnigan MAT TSQ70 triple quadrupole mass spectrometer was used in these studies. Electron energies of 70 and 100 eV were used for electron ionization (EI) and chemical ionization (CI), respectively. The appropriate interchangeable ion volumes were used to obtain EI and CI spectra. In order to obtain true ion source pressures, indicated ion source pressures were calibrated with a capacitance manometer. This was done by connecting a capacitance manometer (MKS Instruments model 127AA) to the CI ion source via the side flange (normally used for GC/MS transfer line) of the TSQ70. The capacitance manometer was used to calibrate the

ion source thermocouple gauge at various pressures of methane reagent gas. Ion source pressures were determined as a function of flow rate of helium and hydrogen carrier gases by connecting a mass flow controller (MKS 1159A) to the CI ion source and recording the true pressures read from the capacitance manometer. All ion source pressures reported are the absolute pressures obtained from the calibrations. Ion source pressures for chemical ionization were typically 0.2-0.5 torr. The ionizer temperature was 150°C. The preamplifier gain was set to 10^8 V/A; the electron multiplier was operated at 1000 V.

Gas Chromatography

A Varian model 3400 GC equipped with a split/splitless injector with a 2 mm i.d. glass liner was used. Bonded phase fused silica open tubular columns were used with an inner diameter of 0.25 mm and a 0.25 μm film thickness (DB-5, J&W Scientific). Column lengths were typically 3 m. All columns were inserted directly into the ion source. Column efficiencies were measured with n-pentadecane ($C_{15}H_{32}$) with the column and interface at 100°C (k = 32) and an injection temperature of 200°C. For all other applications temperature programming was used with the interface at 150°C. Column temperatures were programmed at a rate of 25°C/min from 50°C to 150°C, after an initial hold period of 12 seconds.

A schematic of the gas chromatographic system, modified to allow for either normal pressure-regulated operation or flow-controlled operation, is shown in Figure 2.1. With valve 1 (V1) rotated to position A, the GC can be operated in the normal configuration with inlet pressures above 1 atmosphere. With V1 rotated to position B, flow regulation is used, allowing inlet pressures above or below one atmosphere to be used. In

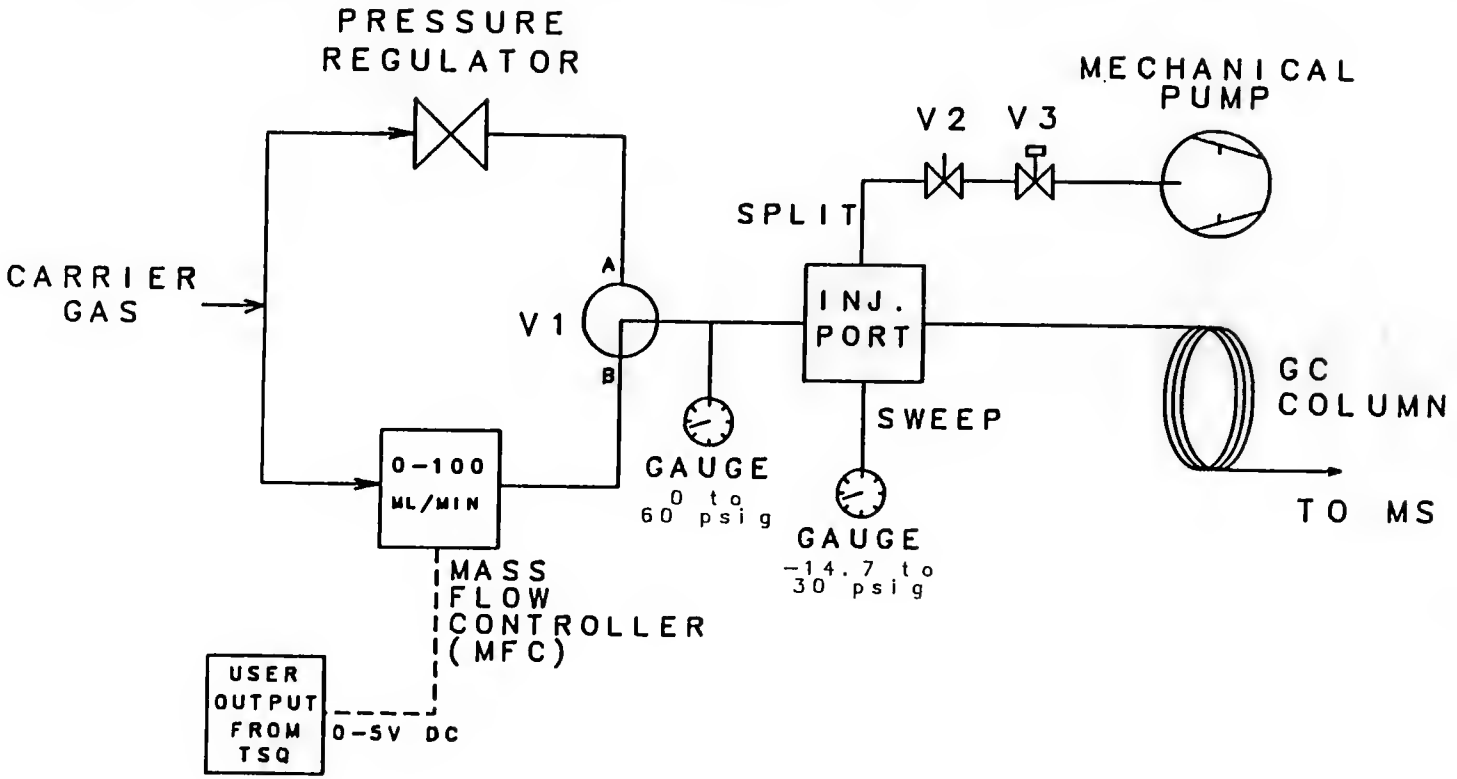

Figure 2.1. Schematic diagram of gas chromatographic flow control system that allows inlet pressures above or below one atmosphere to be used in the injection port.

addition, computer control of the flow controller allows the flow rate of the carrier gas to be programmed with time if desired (see Chapter 3).

The mass flow controller (MFC) used was a MKS model 1159A with a type 246 power supply/digital readout. The output flow rate of the MFC, which has a range of 0-100 mL/min for N_2, is set by a 0-5 V control voltage from the TSQ70. The TSQ70 has two spare digital-to-analog converters (DACs), or user outputs, one of which was used to control the flow rate of the MFC.

In order to achieve the sub-ambient inlet pressures, a 30 L/min mechanical pump (Alcatel model 8A) was connected to the split line of the injection port. A Bourdon tube pressure gauge (Omega Engineering model 30V/30) capable of indicating pressures above or below one atmosphere was connected to the septum sweep of the GC injection port. Valve V2 is a solenoid valve that can be opened or closed under computer control. The inlet pressure in the vacuum inlet mode is determined by the flow rate of carrier gas from the MFC and the adjustment of the needle valve (V3). The occurrence of air leaks in the system was monitored by observing the intensity of the N_2^+ (m/z 28) and O_2^+ (m/z 32) ions. It was necessary to replace the plastic fittings and viton ferrules of the Varian 3400 carrier gas lines with stainless steel fittings to minimize leakage of air into the system. Leakage of air through the septum was minimized by replacing the septum after frequent use (e.g., after 30 injections). Once these steps were taken, no additional increase in the intensity of the air peaks was observed when vacuum inlet operation was used instead of normal atmospheric operation.

During a split injection, samples are injected directly into the low-pressure injection port with valve V2 open; thus, most of the sample is

swept away by the mechanical pump. One of the problems of vacuum inlet GC that has limited its use in the past is that only split injections could be performed. This is certainly a limitation, especially when analyzing samples with analytes present at trace levels. Splitless injection is commonly used for trace analysis [23]. With the flow control system shown in Figure 2.1, the advantages of vacuum inlet GC, as well as splitless operation, can be utilized. A splitless injection is made with V2 initially closed, with the injection port slightly above atmospheric pressure. After allowing ample time for the sample to enter the column, the inlet pressure is then rapidly reduced by opening V2. Based on the internal volume of the injection port (0.24 mL), at a typical flow rate of 5 mL/min, the injection port is completely flushed with carrier gas in approximately 3 s. Thus, leaving V2 closed for any period longer than 3 s should be sufficient time to insure that all the sample has entered the column. Nevertheless, in all experiments utilizing splitless injections reported here, V2 was left closed for 12 s or more.

Average Velocity Measurement

It was found that the average velocity of the carrier gas could not be accurately measured by conventional means with the short columns that were used. Traditionally, the average velocity is determined from the dead time, which is the time required for the elution of unretained air or methane. A 3 m x 0.25 mm i.d. column at 50°C and 1 atmosphere inlet pressure of helium carrier gas has a gas velocity of 240 cm/s and a dead time of 1.25 s. Dead times that are this short are nearly impossible to measure with a reasonable degree of accuracy. An alternative method is to measure the gas flow rate and calculate the gas velocity. This is not

entirely straightforward in GC/MS. One can obtain a measure of the column flow rate by measuring the gas flow rate exiting the forepump of the vacuum system, since all of the carrier gas exiting the column must exit through this pump. However, the pulsations produced by the pump limit the accuracy and precision of this measurement, especially at low flow rates. A more accurate indication of the average gas velocity when short columns are used can be obtained by measurement of the inlet pressure. If the inlet pressure, P_i, is known, the average velocity under vacuum outlet conditions can be calculated from the Poiseuille equation [14]

$$\upsilon = 3P_i r^2/32\eta L \qquad (2.6)$$

where r is column radius, η is the viscosity of the carrier gas at the column temperature, and L is the column length. With the pressure gauge that was used, inlet pressures ranging from -14.7 psig to 30 psig could be measured with a rated accuracy of ± 3% [24].

Results and Discussion

Effects of the Pressure Drop

As was stated previously, lower average column pressures result in increased gas-phase diffusion coefficients and increased optimum gas velocities. Lower column pressures are obtained in GC/MS, since the outlet of the column is at vacuum. Figure 2.2 shows Golay plots (calculated from eq 2.2) demonstrating the effect on the plate height of using vacuum outlet or atmospheric outlet with 0.25 mm i.d. open tubular columns with lengths of 3 m and 30 m. As shown in the figure, the most significant increase in the optimum velocity is obtained with the short

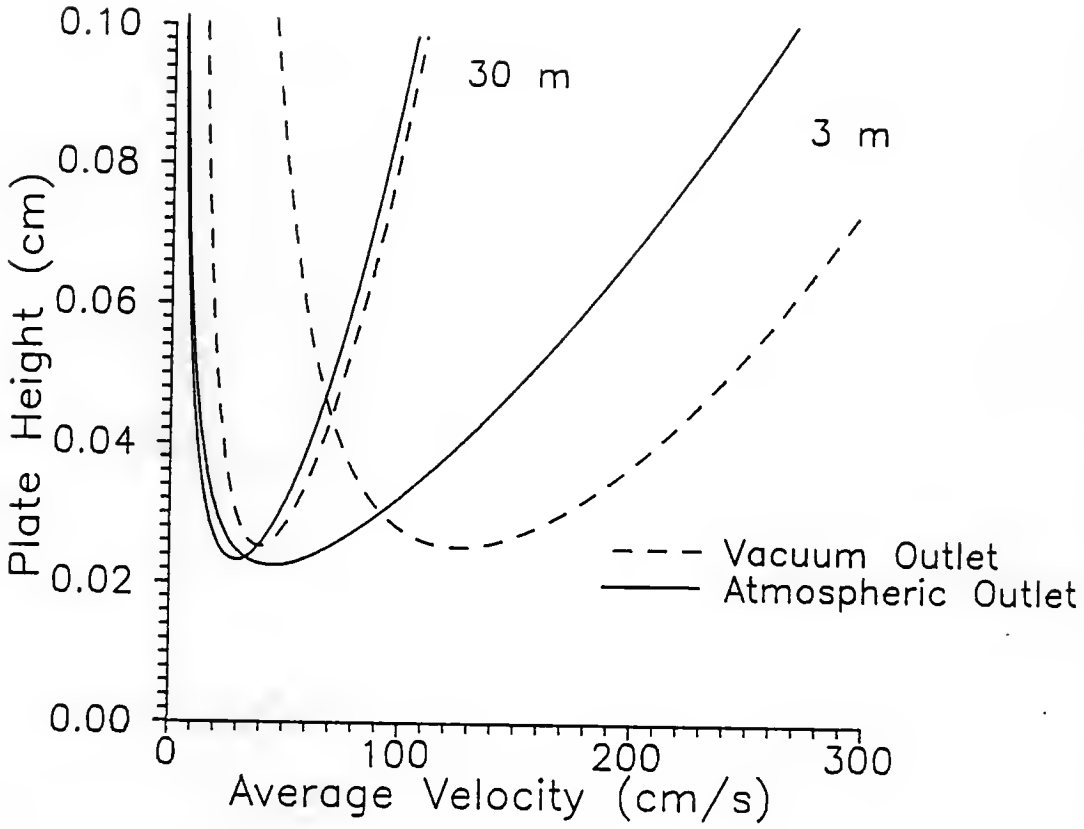

Figure 2.2. Theoretical dependence of plate height on the average carrier gas velocity for 3 m and 30 m 0.25 mm i.d open tubular columns under vacuum outlet and atmospheric outlet conditions. (Conditions: thin-film stationary phase; He carrier gas; k = 10; 100°C; $D_{g,1}$ = 0.27 cm^2/s; η = 2.28 x 10^{-4} poise)

column operated with vacuum outlet. The speed of analysis is ultimately dependent on the gas velocity and the column length. Under vacuum outlet conditions, analysis times are reduced by a factor of 30, if a 3 m column is used instead of a 30 m column, and both are operated at their optimum gas velocities. The reduced analysis times are due to a reduction of the column length by a factor of 10, as well as the increase in the optimum gas velocity by a factor of 3 for the shorter column. In addition, since chromatographic resolution is proportional to the square root of the number of theoretical plates, the resolution lost by using a column that is 10 times shorter is only a factor of the square root of 10 (i.e., 3.16). As shown in Figure 2.2, the theoretical minimum plate heights obtained with vacuum outlet operation are slightly greater than those which are obtained with atmospheric outlet pressure. This can be attributed to the gas decompression term, f, in eq 2.2, which results in an increase of the minimum plate height by a factor of 9/8 (in the worst case) when vacuum outlet is employed instead of atmospheric outlet operation [14].

A better understanding of the effects of the outlet pressure on the plate height for a short column can be obtained from an investigation of the pressure drop. The pressure, p(x), at each point, x, along an open tubular column can be calculated from the inlet pressure, P_i, the outlet pressure, P_o, and the column length, L [25]:

$$p(x) = [(P_o^2-P_i^2)x/L + P_i^2]^{1/2} \qquad (2.7)$$

This equation was used to calculate the pressure at each point along a 3 m x 0.25 mm i.d. open tubular column with various outlet pressures. As

shown in Figure 2.3 (a), the pressures calculated for outlet pressures of 100 torr and 1 torr are virtually the same over most of the length of the column. Figure 2.3 (b) shows the theoretical dependence of the plate height on the average gas velocity for the same outlet pressures used in Figure 2.3 (a). Note that the effects of the outlet pressure on the plate heights calculated are nearly the same with outlet pressures of 100 torr and 1 torr. It is apparent from these data that any GC detector that could be operated at the reduced pressures would offer significant advantages in terms of speed of analysis. In addition, if operation at 1 torr were not possible, operation with outlet pressures of 100 torr should yield nearly the same chromatographic results (at least with the length and diameter column used in this example). Another advantage of the low outlet pressure operation is that chromatograms obtained on a stand-alone GC (e.g., with flame ionization or electron capture detection) could be reproduced on a GC/MS system. If this could be done, routine chromatographic optimization and methods development could be performed on the low outlet pressure GC for analyses to be performed later on the GC/MS system. This would obviate the use of valuable instrument time on a GC/MS system for chromatographic methods development. Investigations in these areas are currently underway in our laboratory.

The effect of the outlet pressure on the optimum velocity is even more pronounced for short wide-bore columns. Figure 2.4 shows the effect of using vacuum outlet or atmospheric outlet on 3 m columns with inner diameters of 0.53 mm and 0.25 mm. As shown in the figure, the use of wide-bore columns when compared to narrow-bore columns of the same length results in a more significant increase of the optimum velocity with vacuum outlet operation. However, it is evident from Figure 2.4 that a lower

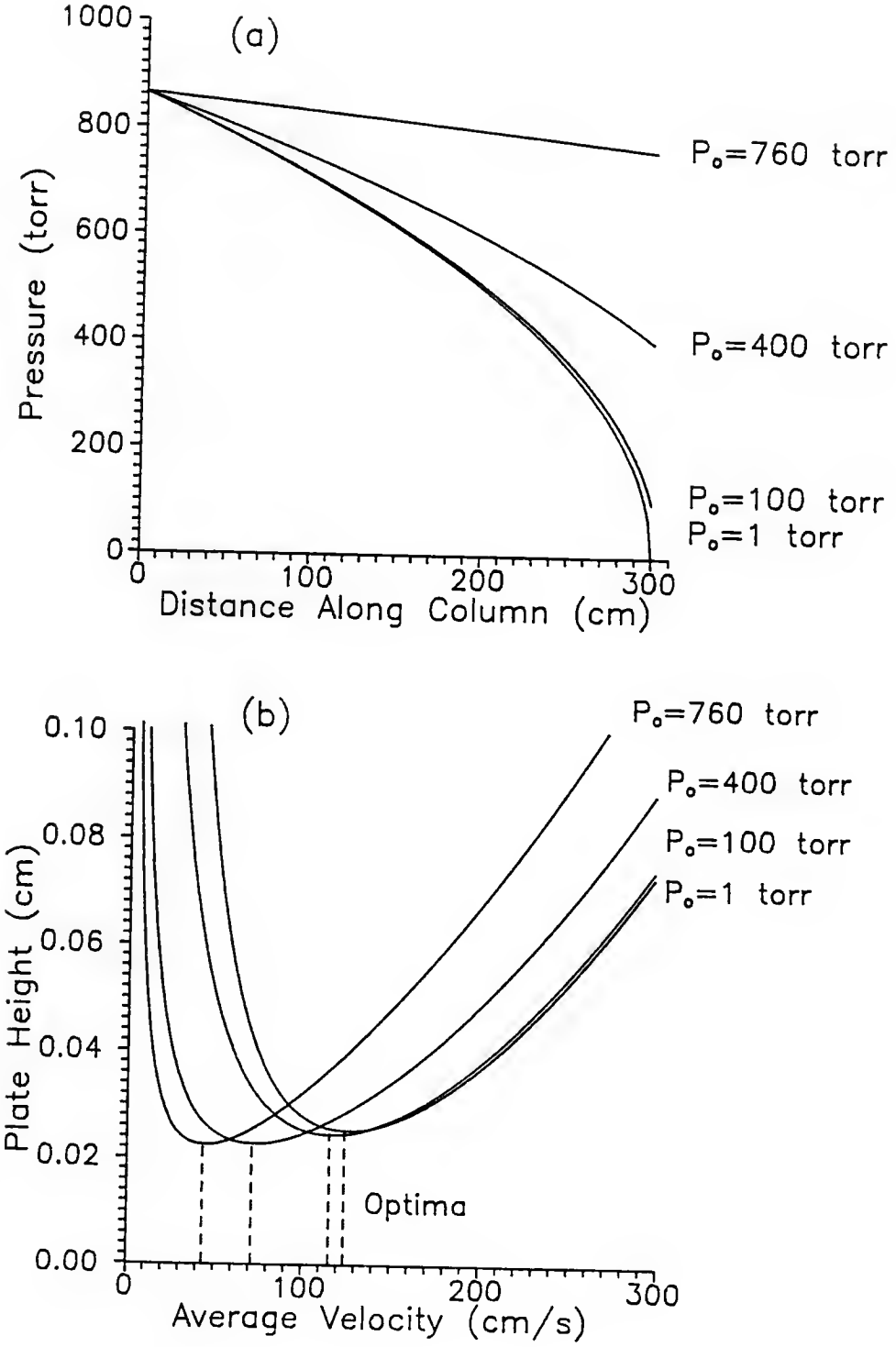

Figure 2.3. (a) Calculated pressures along a 3 m x 0.25 mm i.d. open tubular column with an inlet pressure of 860 torr of helium and various outlet pressures. (b) Theoretical dependence of the plate height on the average gas velocity for the same outlet pressures used in (a). The conditions were the same as those listed with Figure 2.2.

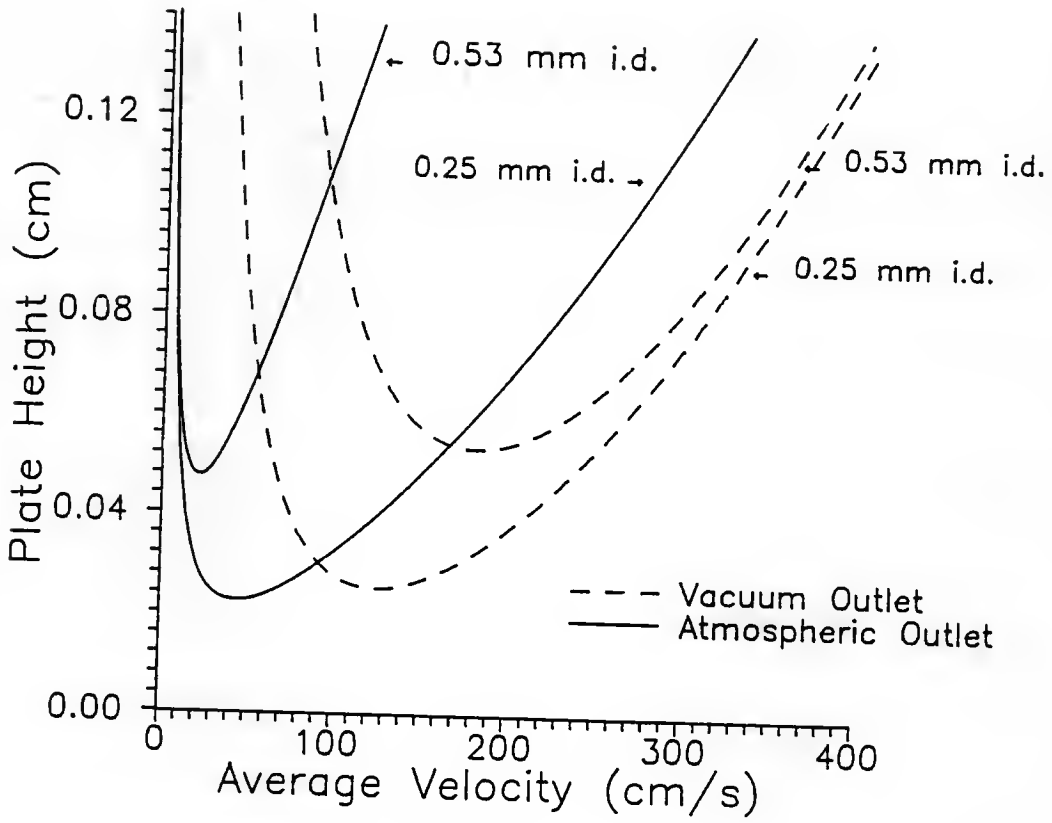

Figure 2.4. Theoretical dependence of the plate height on the average gas velocity for 3 m x 0.25 mm i.d. and 3 m x 0.53 mm i.d. open tubular columns with atmospheric or vacuum outlet operation. The conditions were the same as those listed with Figure 2.2.

minimum plate height can be obtained with the narrow-bore column. Since the maximum number of theoretical plates is equal to column length divided by the minimum plate height, more theoretical plates can be obtained with the narrow-bore column. If a constant number of theoretical plates are required, analysis times will be shorter for the narrow-bore column. For example, approximately 5600 plates can be obtained with the 3 m x 0.53 mm i.d. column at an optimum velocity of 182 cm/s. The same number of theoretical plates and optimum velocity can be obtained with a 1.4 m x 0.25 mm i.d. column. Based on the lengths of the two different diameter columns used to generate 5600 plates, the analysis times should be faster for the narrow-bore column by a factor of 2.1 (i.e., 3 divided by 1.4)

Sub-ambient Inlet Pressures

The optimum gas velocity for thin-film open tubular columns operated under vacuum outlet conditions, $v_{opt,vac}$ can be calculated from [14]

$$v_{opt,vac} = \frac{(P_1 3(1+k)^2 D_{g,1} H_{min})^{1/2}}{(2L\eta(11k^2+6k+1))^{1/2}} \qquad (2.8)$$

where H_{min} is the minimum plate height obtained at v_{opt}. As can be seen from eq 2.8, the optimum velocity is inversely proportional to the square root of the column length; thus, a reduction of the column length results in higher optimum velocities. In addition, the optimum inlet pressure needed to obtain the optimum gas velocity is given by [14]

$$P_{i,opt,vac} = \frac{(72 P_1 L\eta D_{g,1})^{1/2}}{(H_{min})^{1/2} r} \qquad (2.9)$$

Thus, short columns and/or columns with larger inner diameters require lower inlet pressures. In addition, optimum inlet pressures are predicted to be lower for low-viscosity carrier gases. This is demonstrated in Figure 2.5 (a) which shows a plot of optimum velocity vs. column length and Figure 2.5 (b) which shows a plot of optimum inlet pressure vs. column length for 0.25 mm i.d. open tubular columns with both He and H_2 carrier gases. As shown in the figures, short columns with vacuum outlet require sub-atmospheric inlet pressures, if optimum gas velocities and hence, minimum plate heights, are to be obtained. Most GCs designed to be used with open tubular capillary columns utilize pressure regulators that are referenced to one atmosphere, and are incapable of operating with the injection port at reduced pressures. Because of this limitation, the advantages of short-column vacuum outlet GC have never been fully exploited.

Sub-ambient inlet pressures are readily obtained with the flow-regulated system used in this work. The chromatograms shown in Figure 2.6 demonstrate the increased resolution obtained on a 3 m x 0.25 mm i.d. open tubular column when the injection port was operated at a reduced pressure. The chromatogram in Figure 2.6 (a) was obtained with an inlet pressure of 940 torr and a gas velocity of 297 cm/s. For the chromatogram in Figure 2.6 (b), the inlet pressure was kept at 940 torr for the initial 12 s, after which the pressure was reduced to 380 torr and a gas velocity of 120 cm/s. Note that the two components unresolved chromatographically in Figure 2.6 (a) exhibit baseline resolution in Figure 2.6 (b). Moreover, only 35 s of additional time was required for the chromatogram in Figure 2.6 (b).

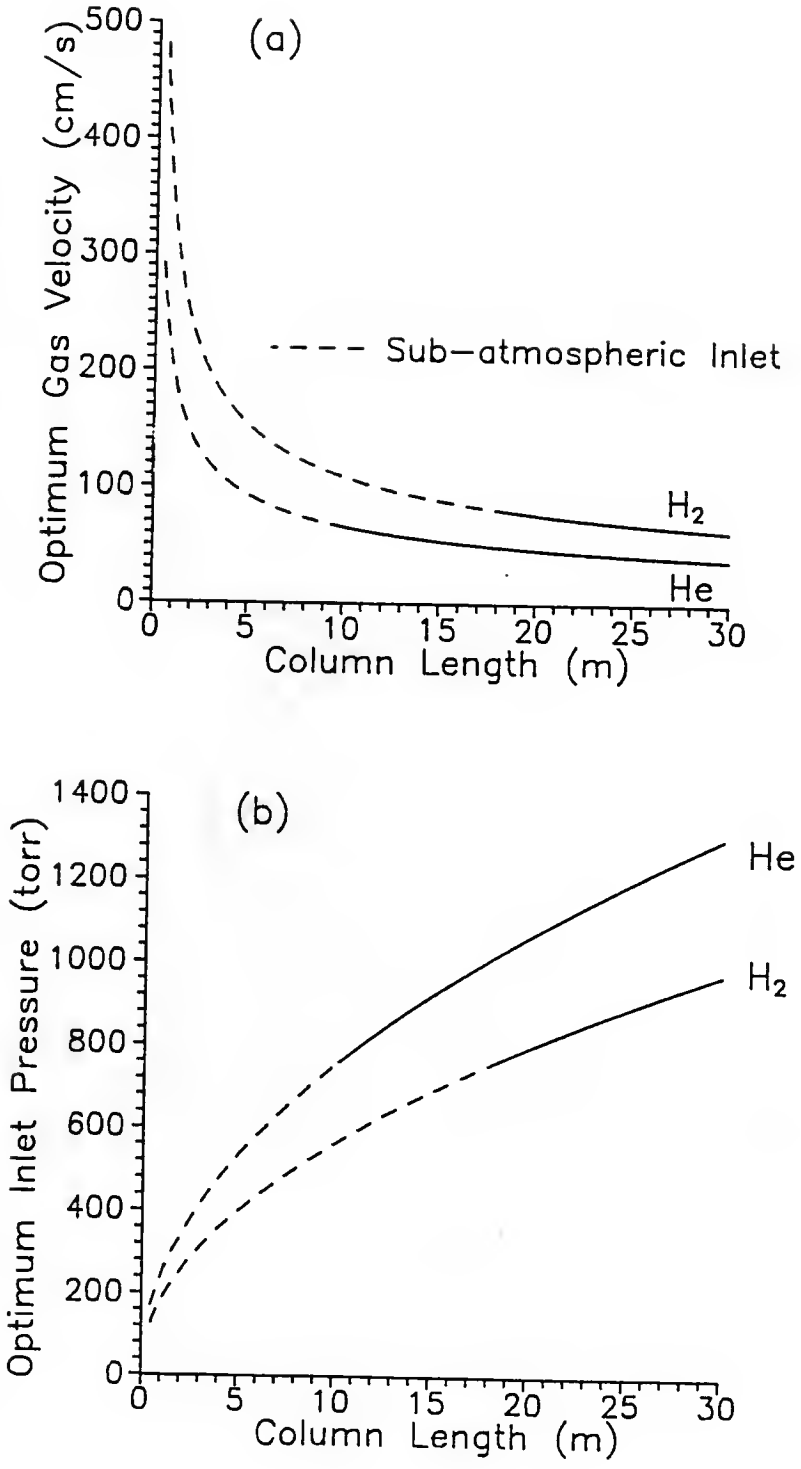

Figure 2.5. Calculated optimum velocity (a) and optimum inlet pressure (b) as a function of column length for 0.25 mm i.d. open tubular columns with helium and hydrogen carrier gases illustrating need for sub-atmospheric inlet pressures with short columns.

Figure 2.6. GC/MS chromatograms obtained with a 3 m x 0.25 mm i.d. open tubular column at two different inlet pressures: (a) P_i = 940 torr, υ = 297 cm/s, (b) P_i = 380 torr, υ = 120 cm/s. Individual traces are for the molecular ions of acenaphthylene (m/z 152) and tetradecane (m/z 198), as well as the reconstructed ion current (RIC) from m/z 35 to 300.

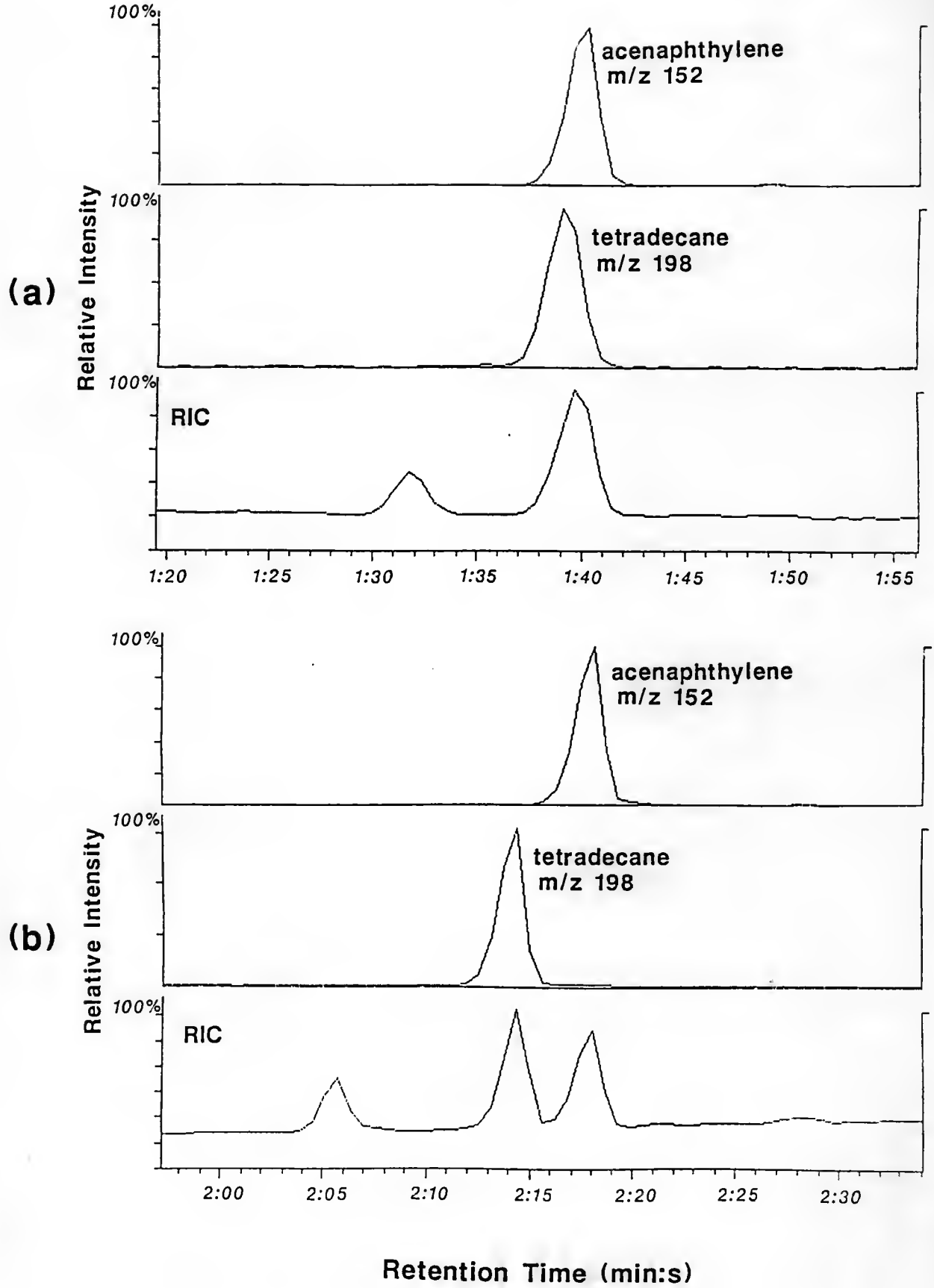
(a)
Relative Intensity
100%
acenaphthylene
m/z 152
100%
tetradecane
m/z 198
100%
RIC
1:20
1:25
1:30
1:35
1:40
1:45
1:50
1:55
(b)
Relative Intensity
100%
acenaphthylene
m/z 152
100%
tetradecane
m/z 198
100%
RIC
2:00
2:05
2:10
2:15
2:20
2:25
2:30
Retention Time (min:s)

It has been suggested that chromatographic analyses be performed at the optimum practical gas velocity (OPGV) rather than the optimum velocity [26,27]. The OPGV has been defined as the velocity that yields the highest number of theoretical plates per unit time [27]. The number of theoretical plates per unit time can be determined by dividing the number of theoretical plates by the retention time (i.e., N/t_R). Thus, if N/t_R is plotted as a function of the average gas velocity, the OPGV will be represented by the maximum on the curve. Figure 2.7 shows examples of these calculated curves demonstrating the determination of OPGVs for 3 m and 30 m 0.25 mm i.d. columns operated with atmospheric and vacuum outlet. For this comparison, the value of the partition ratio (k) was chosen to be 30. Although this is far from the optimum partition ratio of 1.76 suggested by Guiochon [22], a partition ratio of 30 is a typical value with the inherent low operating temperatures employed with short columns. Since chromatographic resolution is proportional to the square root of the number of theoretical plates, the percent resolution lost ($\%R_{lost}$) by operation at any gas velocity other than the optimum is given by

$$\%R_{lost} = 100(1 - (N_{\upsilon}/N_{opt})^{1/2}) \qquad (2.10)$$

where N_{opt} is the number of theoretical plates obtained at the optimum velocity and N_{υ} is the number of theoretical plates obtained at an average velocity, υ.

As shown by the results of this comparison summarized in Table 2.1, vacuum outlet operation results in the shortest analysis times, regardless of whether the columns are operated at their optimum velocities or optimum

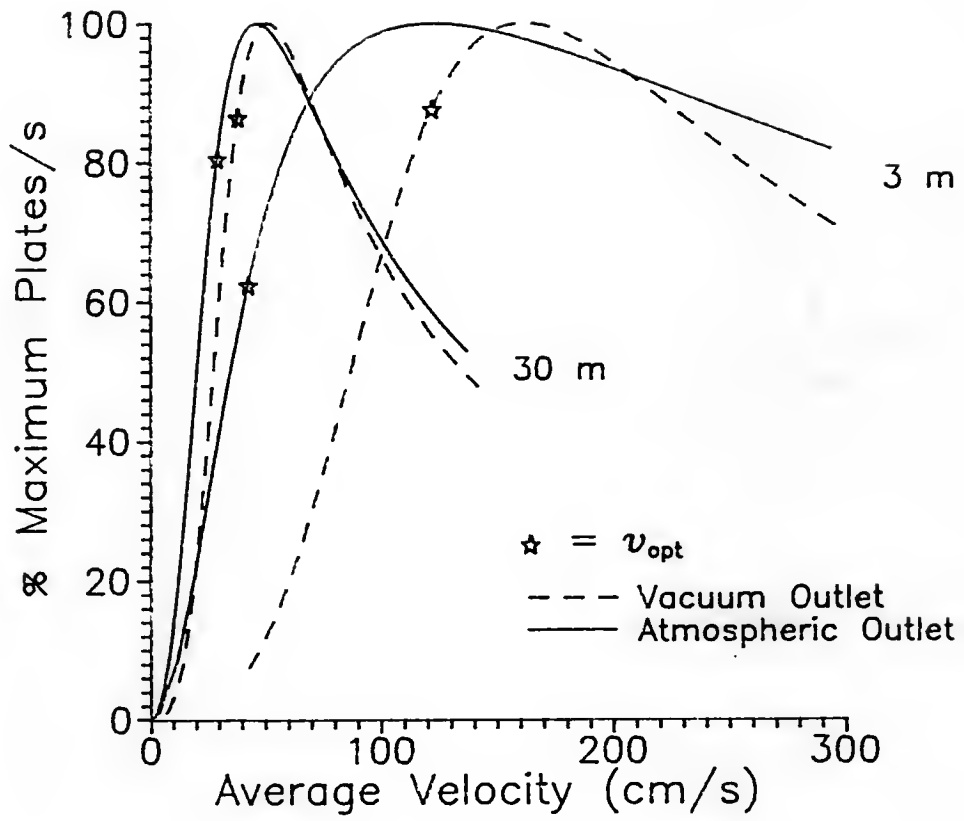

Figure 2.7. Examples of calculated plots to determine optimum practical gas velocities (OPGVs) for 3 m and 30 m 0.25 mm i.d. open tubular columns operated with vacuum or atmospheric outlet. For each plot, the number of theoretical plates generated per second has been normalized to a maximum of 100%. The maxima of the curves indicate the OPGVs, while the stars indicate the optimum velocities. The conditions were the same as those of Figure 2.2, except k = 30.

Table 2.1. Comparison of calculated optimum conditions for 3 m and 30 m 0.25 mm i.d. open tubular columns operated with atmospheric and vacuum outlet.[a]

Column Length (m)	Outlet	υ_{opt}[b] (cm/s)	OPGV[c] (cm/s)	$t_{R,opt}$[d] (min)	$t_{R,OPGV}$[e] (min)	N_{opt}[b]	N_{opt}/t_R (s^{-1})	N_{OPGV}[c]	N_{OPGV}/t_R (s^{-1})	$\%R_{lost}$[f]
3	atm	42	121	3.7	1.3	12814	57.7	7352	94.3	24
3	vac	122	161	1.3	1.0	11408	146.3	10004	166.7	6
30	atm	29	46	53.4	33.7	124003	38.7	97244	48.1	9
30	vac	39	50	39.7	31.0	114031	47.9	99944	53.7	6

[a] same conditions as those of Figure 2.2, except k = 30.

[b] calculated by iteration of eq 2.2

[c] obtained from maxima of curves of Figure 2.7

[d] analysis time obtained with υ_{opt}

[e] analysis time obtained with OPGV

[f] %resolution lost by operation at OPGV, rather than υ_{opt}, calculated from eq 2.10

practical velocities. As stated previously, atmospheric outlet operation results in a lower minimum plate height (typically 10% lower), and thus more theoretical plates at the optimum velocity, than vacuum outlet operation. For example, if operated at their optimum velocities, a 3 m column with atmospheric outlet would yield 5.6% better resolution than a 3 m column with vacuum outlet. However, the analysis times with the 3 m column would be 2.8 times shorter if vacuum outlet was used instead of atmospheric outlet. Moreover, if operated at their optimum practical gas velocities, columns with vacuum outlet would result in faster analyses and more theoretical plates (and hence, better resolution) than columns with atmospheric outlet. For example, analysis times are 0.3 min shorter on the 3 m column with a 15% improvement in the resolution if vacuum outlet at its OPGV is used instead of atmospheric outlet at its OPGV. It can be seen from Table 2.1, that for any column length, vacuum outlet operation yields the shortest analysis times and the highest number of theoretical plates per unit time, regardless of whether optimum velocities or optimum practical velocities are used.

There are other significant advantages of utilizing reduced inlet pressures with short columns in GC/MS. It has previously been reported that short columns result in narrower bands and higher sample concentrations at the detector than long columns [3]; thus, at least from a theoretical perspective, short columns should provide the best possible detection limits. In practice, short columns operated at conventional inlet pressures result in high flow rates of carrier gas into the ion source. In fact, sub-ambient inlet pressures are a necessity if short wide-bore columns are to be used at all in GC/MS, since conventional inlet pressures result in analyzer pressures that are excessive for the normal

operation of the mass spectrometer (see Chapter 3). It is possible that the advantage of low detection limits obtainable with short columns in GC/MS might be lost if excessive flow rates (which can disrupt the ionization process in the ion source) are used. Experience in this laboratory has shown that the sensitivity obtainable with chemical ionization (CI) is not greatly affected by the high flow rates of a different carrier gas (e.g., He or H_2) (see Chapter 3). However, when electron ionization (EI) is used the sensitivity decreases dramatically with increasing flow rates of carrier gas into the ion source, especially when flow rates above ca. 10 mL/min are used. Thus, lower inlet pressures are preferred for use with EI and short columns. The increased sensitivity of the vacuum inlet operational mode is demonstrated in Table 2.2, which shows the integrated peak areas of the molecular ion of n-hexylbenzene obtained with different injection methods and inlet pressures. As shown in the table, splitless followed by low-pressure operation at 560 torr yielded the best sensitivity. The vacuum split injection is inherently less sensitive, since less sample enters the column and is detected. For the splitless injections, the peak areas were significantly lower when the higher inlet pressures (and flow rates) were employed. For example, the peak area obtained by splitless operation with an inlet pressure of 560 torr was approximately two orders of magnitude greater than that obtained at 2155 torr.

The effects of splitless operation on retention times was also studied. Traditionally, both split and splitless operation are performed at constant inlet pressure. Thus, retention times are the same regardless of which mode is used, provided that the same inlet pressures are used. In the splitless method described here, the initial inlet pressure during

Table 2.2. Comparison of peak areas for four different injection of n-hexylbenzene obtained with different injection methods and inlet pressures of He carrier gas.

Injection Method	Inlet Pressure (torr)	Average Velocity (cm/s)[a]	Flow Rate (mL/min)[b]	Peak Area of M^+ (m/z 162)
split[c]	560	176	2.6	2.56×10^6
splitless[d]	560	176	2.6	2.09×10^7
splitless	940	297	5.0	7.95×10^6
splitless	2155	679	30.0	2.11×10^5

[a] average velocities calculated with eq 2.6
[b] indicated flow rates from flow controller
[c] split ratio = 10:1
[d] inlet pressure = 940 torr for initial 12 s, final inlet pressure = 560 torr

injection is much higher than that during the remainder of the elution. Since a change in the inlet pressure results in a change in the gas velocity, it was expected that the retention times for split and splitless operation would not be the same. In order to determine the effects of the large pressure change, the retention times for split injections and splitless injections for a mixture of alkylbenzenes were compared. The results are shown in Table 2.3. The split injection was performed at a constant inlet pressure of 560 torr. The splitless injections were performed with an initial pressure of 940 torr and a final pressure of 560 torr. For splitless operation, the split valve was left closed for 12 s in one case and for 30 s in another. As shown in Table 2.3, the large change in inlet pressure does not greatly affect the retention times, even when a splitless time of 30 s is used. This is most likely due to trapping of the solutes at the head of the column at the initial column temperature of 50°C.

Experimental vs. Theoretical Performance

Figure 2.8 shows a comparison of experimental and calculated (from eq 2.2) plate heights obtained with a 3.1 m x 0.25 mm i.d. open tubular column operated with H_2 carrier gas and the column outlet at vacuum. As can be seen in the figure, the experimental performance at higher velocities is not as good as predicted by theory. The differences in the experimental and theoretically calculated data can be attributed to extra column variances. Extra column contributions are the result of band broadening due to instrumental time constants and, thus are not accounted for in the Golay equation (eq 2.1). The extra column variances result in the addition of a constant band width to the theoretical band width. This

Table 2.3. Comparison of retention times for components of an alkylbenzene mixture utilizing vacuum inlet split and splitless injection.

	Injection Method		
	Split[a]	Splitless, 12s[b]	Splitless, 30 s[b]
Component	Retention times (min:s)		
n-hexylbenzene	1:17	1:14	1:10
n-octylbenzene	2:16	2:14	2:14
n-decylbenzene	3:13	3:12	3:13
n-dodecylbenzene	4:08	4:08	4:09

[a] inlet pressure = 560 torr
[b] inlet pressure = 940 torr for initial 12 s, final inlet pressure = 560 torr

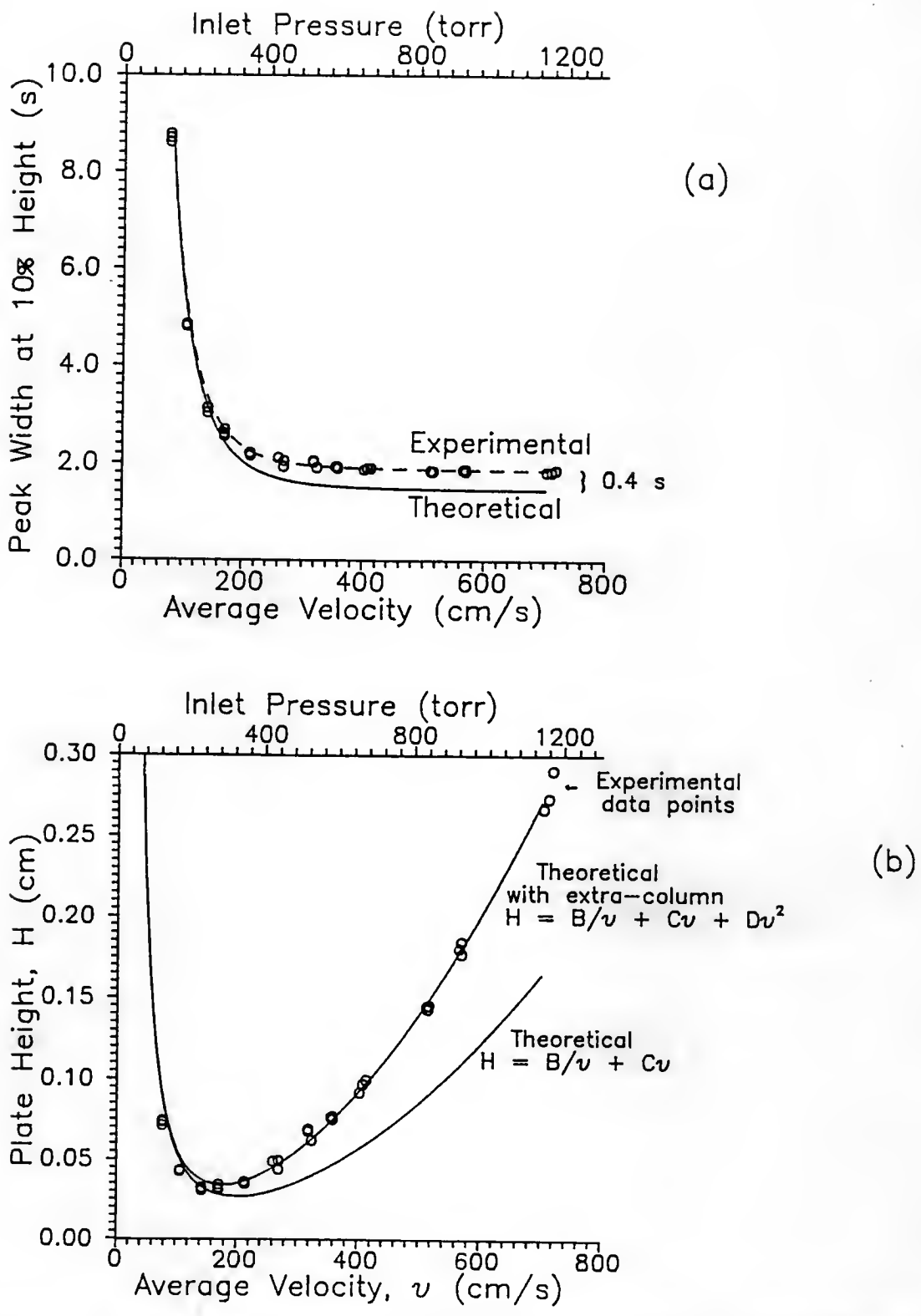

Figure 2.8. Comparison of theoretical and experimental data obtained for a 3.1 m x 0.25 mm i.d. open tubular column at 100°C with hydrogen as a carrier gas: (a) peak widths at 10% height and (b) plate heights. The experimental data agree well with theory if an extra column variance ($\sigma_{ec}^2 = 0.073s^2$) is included in the calculations.

is demonstrated in Figure 2.8 (a), which shows the expected (theoretical) peak widths and the experimentally observed peak widths for n-pentadecane on a 3.1 x 0.25 mm i.d. open tubular column. The extra column band broadening results in an additional 0.4 s to the theoretical band width at 10% peak height. Guiochon et al. have elaborately discussed the role of extra column effects and have stressed their importance in high-speed GC applications where short and/or small diameter columns are used [8]. They demonstrated that an additional term (Dv^2) can be added to the Golay equation which can be used to describe the apparent plate height, H_{app}

$$H_{app} = B/v + Cv + Dv^2 \qquad (2.11)$$

with:

$$D = \sigma_{ec}^2/(1+k)^2L \qquad (2.12)$$

where σ_{ec}^2 is the extra column variance. When eq 2.11 was used with an extra column variance of 0.073 s^2, the resulting curve was an excellent description of the experimental data, as shown in Figure 2.8 (b). As shown in the figure and by eqs 2.11 and 2.12, the extra column contributions become more significant as shorter column lengths or higher velocities are used. It is believed that the instrumental variances observed here arise from sample injection rather than detection. The n-pentadecane used for the plate height determinations was manually injected as a liquid into the hot injection port. There is expected to be a finite time required for vaporization of the sample and entrance of the solute onto the column, which could result in the observed peak broadening. The residence times of samples eluting from the GC column into the ion source is not expected to cause a significant amount of band broadening. In

addition, the data were collected utilizing a scan time of 0.05 s over the m/z of interest, which resulted in at least 40 data points per GC peak. Therefore, no significant time constant was introduced during the data collection. Because of the extra column effects, the use of short columns dictates careful consideration of injection technique and injector design if the maximum performance is to be obtained.

Choice of the Carrier Gas

The importance of the choice of the carrier gas for minimizing analysis times has previously been discussed by Giddings [6]. Hydrogen, which has the largest gas viscosity to diffusivity ratio, is predicted to yield the fastest analyses. This can be seen from the experimentally determined plate heights for H_2 and He on a 3.1 m x 0.25 mm i.d. open tubular column, as shown in Figure 2.9. Hydrogen is preferred, since the optimum velocity is higher and the Golay curve is flatter than that of helium. The dashed line parts of the curves of Figure 2.9 indicate where sub-ambient inlet pressures were used. The use of H_2 results in lower optimum inlet pressures than He as predicted by eq 2.9 and shown in Figure 2.5 (b).

Even though H_2 is predicted to yield the fastest chromatographic analyses, the effects of its use as a carrier gas on resulting mass spectra have not been previously studied. When H_2 is used a carrier gas, H_3^+ ions are produced in the ion source. The presence of these ions does not appear to affect EI spectra and in an EI source do not cause a significant amount of chemical ionization (i.e., no increase in the MH^+/M^+ ratio was observed). This is most likely due to the fact that pressures in the EI ion source are not high enough to cause a significant amount of reaction to occur. However, the reaction of H_3^+ ions with sample molecules

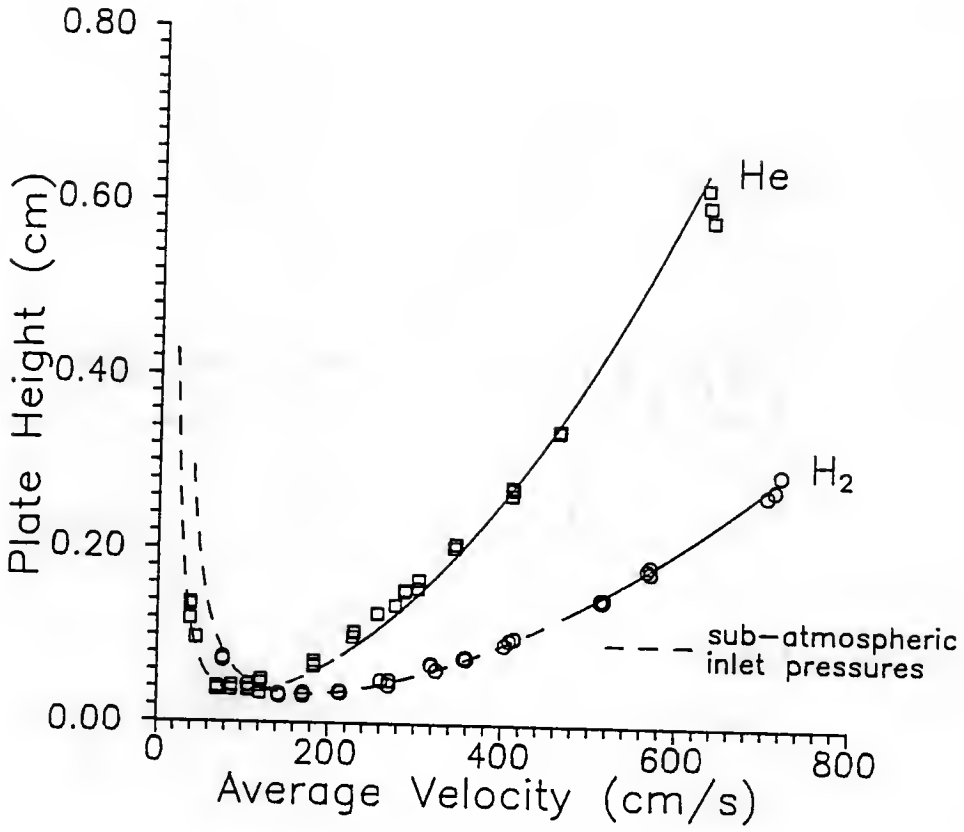

Figure 2.9. Comparison of experimentally determined dependence of the plate height on average velocity for helium and hydrogen carrier gases with a 3.1 m x 0.25 mm i.d. open tubular column at 100°C. The dashed lines indicate where sub-atmospheric inlet pressures are required. The curves were calculated with eq 2.11.

in a chemical ionization (CI) source is possible due to the higher operating pressures. It was also predicted that the H_3^+ ions would alter the mass spectra normally obtained with methane CI. On the contrary, the presence of H_2 carrier gas does not appear to affect methane CI spectra. As shown in Figure 2.10 (a) and (b), the CI spectrum of 2,4 dimethylaniline obtained with 0.5 torr H_2 and 0.2 torr CH_4 (b) is the same as that obtained with 0.2 torr CH_4 and no H_2 (a). In fact, as soon as methane is introduced in the ion source with H_3^+ ions present, the H_3^+ ions disappear. This is apparently due to the fact that the hydrogen reagent ions (H_3^+) are used in the protonation of methane. This is not surprising, since methane has a higher proton affinity than hydrogen [28]. It is expected that similar behavior would be observed with other commonly used proton transfer CI reagent gases (e.g., isobutane, ammonia, etc.) because of the low proton affinity of hydrogen. In the absence of methane, hydrogen can be used as both the carrier gas and the CI reagent gas, as shown in Figure 2.10 (c). The spectra that are obtained with hydrogen CI exhibit more fragmentation than those obtained with methane CI, which is due to the greater exothermicity of the proton transfer reaction between the H_3^+ reagent ions and the sample molecules. With hydrogen CI, no adduct ions are observed as is normally the case with methane CI. The absence of these adducts is often desirable, since their presence may complicate interpretation of the mass spectra.

Conclusions

A better understanding of the influence of the pressure drop on the chromatographic behavior of open tubular columns in GC/MS has allowed for better utilization of the inherent advantages associated with short

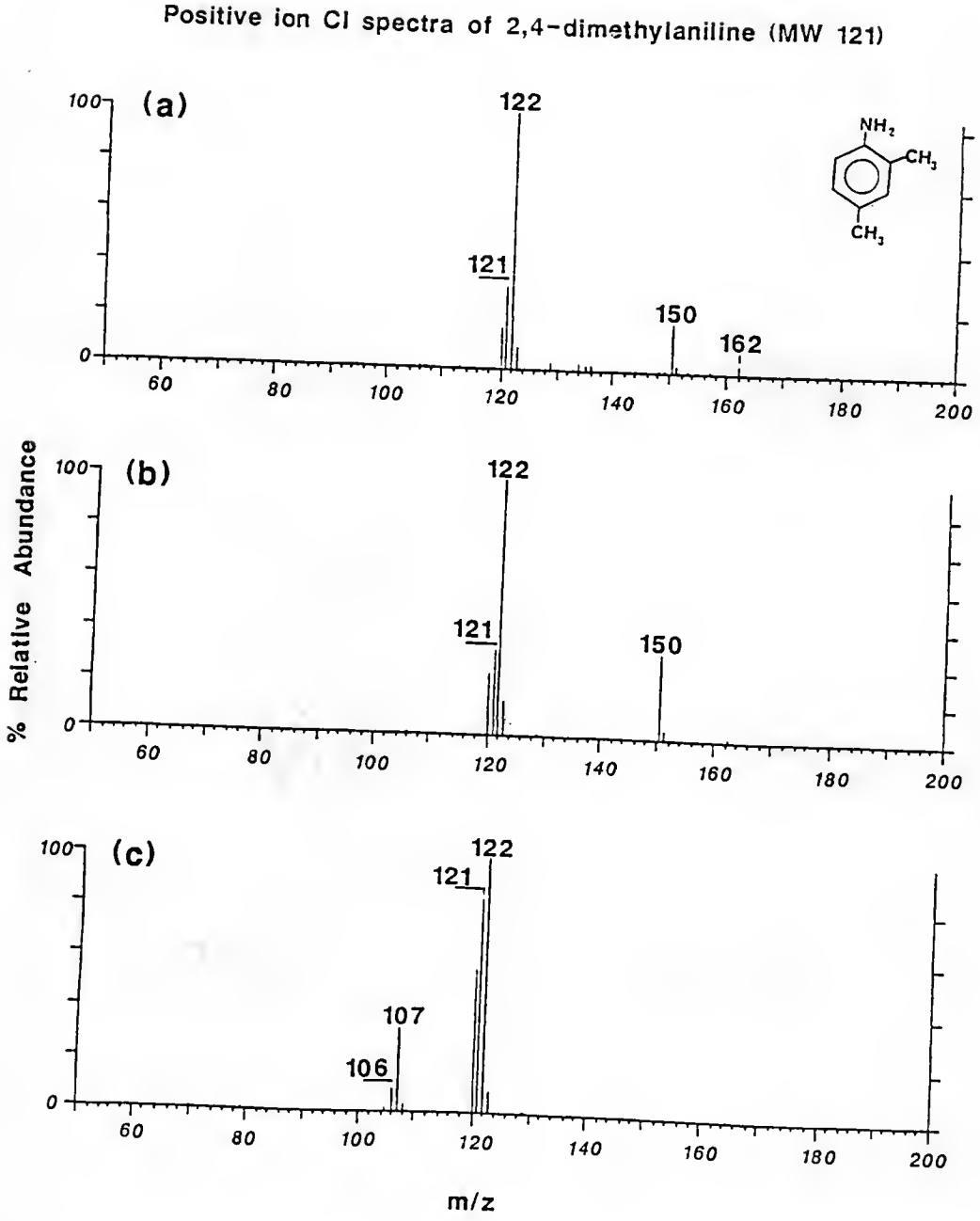

Figure 2.10. Effect of using hydrogen carrier gas on the chemical ionization mass spectra of 2,4 dimethylaniline: (a) 0.2 torr methane and no hydrogen present, (b) 0.2 torr methane with 0.5 torr hydrogen present, (c) 0.5 torr hydrogen and no methane present.

columns. The large pressure drop associated with vacuum outlet GC should not be considered a disadvantage. On the contrary, the low-pressure outlet results in increased optimum gas velocities and decreased analysis times. It has been shown that vacuum outlet operation yields the shortest analysis times, regardless of whether optimum velocities or optimum practical velocities are used. In addition, the chromatographic resolution obtained when optimum practical gas velocities are used is predicted to be higher for vacuum outlet than for atmospheric outlet operation. As shorter column lengths are used with vacuum outlet operation, lower inlet pressures are needed to obtain optimum performance. Sub-ambient inlet pressures can be obtained with a relatively simple flow control system as described here. The capability of splitless operation has greatly extended the utility of vacuum inlet operation. The lower inlet pressures with short columns are also shown to provide the best sensitivity when electron ionization is used, since the flow rates are lower. The use of hydrogen carrier gas results in even lower optimum inlet pressures and higher optimum velocities than helium. Hydrogen can be used as the chemical ionization reagent gas or it can be used in the presence of other commonly used proton transfer chemical ionization reagent gases without affecting the mass spectra.

CHAPTER 3
CONCEPTS FOR PORTABLE GAS CHROMATOGRAPHIC INSTRUMENTATION IN GC/MS: FLOW RATE PROGRAMMING AND DIRECT COLUMN HEATING

Introduction

The object of any chromatographic analysis is the separation and identification of components in mixtures. However, chromatographic mixture analysis is often complicated by the "general elution problem" [29]. This predicament results both in poor resolution in the early part of a chromatogram due to coeluting peaks, and in severe peak broadening near the end of a chromatographic run. In gas chromatography, temperature programming is often used to circumvent this problem. In temperature-programmed GC (TPGC), the column temperature is increased (usually linearly) during the course of the analysis. Since the temperature range covered can be up to 300°C (and higher depending on the stationary phase), TPGC offers a wide dynamic range. In analyses where temperature programming is used, the rate at which samples can be analyzed is not only dependent on the time required by the separation, but also on the time required to equilibrate (cool) the column for the next injection. Since the column temperature is changed by changing the temperature of a large gas chromatograph oven, the rate at which a GC column can be heated or cooled in TPGC is usually slow (typically 50°C/min or less depending on the manufacturer of the GC oven). Moreover, the need to heat a GC oven by conventional convection heating, only to cool it back down, requires

significant amounts of electrical power, making temperature programming unattractive for portable instrumentation.

In this chapter, two approaches to solving these problems are presented. The first approach involved investigation of flow rate programming as a robust alternative to temperature programming. The second approach examined was direct resistive heating of metal-clad capillary GC columns, as opposed to oven (convection) heating. Direct resistive heating is especially exciting, and should be widely applicable in portable GC instrumentation for environmental or process monitoring. The concepts developed in these studies have led to the development of a portable GC probe, which appears to be particularly attractive for future applications involving portable mass spectrometers or as a convenient analytical tool for that could be used in any mass spectrometry laboratory.

Flow Rate Programming

Flow programming of the carrier gas has previously been examined as an alternative to temperature programming [25,29-35]. Use of this technique was limited in the early years of application due to the high inlet pressures required with packed columns. The high permeability of short and/or wide-bore open tubular columns allows for high flow rates to be achieved at relatively low inlet pressures [34]. In addition, it has more recently been shown that exponential flow rate programming under isothermal conditions results in peak distributions that are very similar to those obtained with linear temperature programming [29,33-35]. One advantage of programmed flow GC is that the sample throughput is high, since it is not necessary to wait for the column to cool for the next

injection. Although resetting of the column flow rate is required, this step is essentially instantaneous due to the high permeability of open tubular columns [34]. This technique might prove attractive for a field instrument that could not be rapidly heated and cooled, or in the laboratory where high-throughput analyses are desired. Flow rate programming is well suited for the analysis of thermally labile compounds, since the column can be operated isothermally at relatively low temperatures. It has also been pointed out that bleed of the liquid stationary phase from the column is reduced since lower temperatures are required [34]. This could prove to be an important factor in the reduction of chemical noise at the detector, or could help to extend the life of GC columns. One disadvantage of the method that is evident from GC theory, is that chromatographic efficiency is reduced if the flow rate is increased beyond the optimum. However, as was shown in Chapter 2, optimum flow rates are higher when the column outlet is at vacuum as in GC/MS. In addition, the rate of increase of the plate height is much less for short columns than for long columns, when higher than optimum velocities are used. Nevertheless, as will be shown in this chapter, the maximum allowable flow rate is ultimately dependent on the pumping speed and associated performance of the mass spectrometer.

Direct Resistive Heating of Al-clad Capillary Columns

Another alternative that avoids many of the limitations of oven heating is to heat the column directly instead of by convection. Recently, aluminum-clad fused silica open tubular (Al-clad FSOT) capillary columns have become commercially available (SGE, Quadrex). The potential advantages of directly-heated capillary GC columns have been suggested

[36], but never demonstrated. In Chapter 4 it will be shown that these directly-heated columns can be used as simple transfer lines for introducing samples via GC into the collision cell of a triple quadrupole mass spectrometer. In this chapter, a method is described for heating these columns directly by passing an electrical current through the thin aluminum cladding coated on the outer surface of the column. A method of sensing the temperature of the Al-clad capillary directly, by measuring the column resistance instead of using external thermocouples or other temperature sensors, is also presented.

The principles of resistive heating are relatively simple. When a voltage is dropped across an Al-clad capillary, the column temperature increases depending on the amount of power dissipated. The power dissipated, P, is dependent on the current through the column, i, and the voltage across the column, V.

$$P = iV \tag{3.1}$$

The current is dependent on the voltage drop and the electrical resistance, R.

$$i = V/R \tag{3.2}$$

The electrical resistance is dependent on the length, diameter, and thickness of the Al coating on the outside of the capillary. The amount of heat (or energy) required to increase the temperature of any substance by an increment ΔT is given by [37]

$$Q = mC\Delta T \tag{3.3}$$

where Q is the amount of heat (or energy, J or W-s), m is the mass of the material (g), C is the specific heat of the material (J/g°C), and ΔT is the change in temperature of the material (°C). In addition, since the heat is produced resistively, the amount of energy consumed over a given time period Δt is given by

$$Q = P\Delta t \tag{3.4}$$

From eqs 3.3 and 3.4 it is apparent that objects of large mass require more heat or more power over a given time period to reach a given temperature. Al-clad FSOT GC columns are coated with a very thin aluminum film, and have a very small thermal mass. The low thermal mass of these columns allows them to be rapidly heated and cooled with much less electrical power than is normally required with chromatograph ovens. Since no large oven is needed, direct resistive heating is extremely attractive for use in portable GC instrumentation.

The low thermal mass of the Al-clad columns does present some problems if conventional methods are used to measure the column temperature. Currently, there are no thermocouples or resistance thermometers available that are small enough to accurately measure the temperature of these columns. Even if small sensors are used, placing the sensor against the column causes a local cold spot and leads to inaccurate temperature measurement. An alternative method of measuring the column temperature that avoids this problem is to use the column itself as the temperature sensor. The resistance of any metallic conductor is linearly related to

its temperature over a wide temperature range and is given by [38]

$$R_T = R_o(1 + \alpha T) \qquad (3.5)$$

where R_T is the resistance (Ω) at temperature T (°C), R_o is the resistance at 0°C, and α is the temperature coefficient of resistivity of the metal ($°C^{-1}$). In fact, eq 3.5 is the basis of operation of Pt resistance thermometers, which are widely used in scientific applications. The resistance of a column is readily calculated during resistive heating if the current through the column and the voltage across the column are measured. Once a calibration of temperature versus resistance has been performed, a determination of the column resistance can be used as a direct measure of the column temperature.

GC Probe

The concepts discussed above have been applied in the development of a compact GC probe, which resembles a conventional direct insertion probe, and interfaces with a commercially available mass spectrometer. A GC probe utilizing packed columns operated isothermally has previously been described [39]. The GC probe described here allows the temperature to be rapidly cycled for high-throughput GC/MS analyses requiring very little electrical power. Removal or insertion of the probe from the mass spectrometer is through the normal probe inlet assembly. This facilitates changing of the column or allows for rapid changing to other techniques (e.g., solids probe, FAB, etc.) with minimal effort. Once the probe is removed from the mass spectrometer, the column can be rinsed with solvent without removing the column from the probe. This is attractive in cases

when particularly "dirty" samples are being analyzed, as may be the case for environmental monitoring in the field.

Experimental Section

Experimental Conditions

Mass spectrometry. A Finnigan MAT TSQ70 triple quadrupole mass spectrometer was used for this work. The instrument was tuned with FC43 (perfluorotributylamine) with the GC probe in place. The electron multiplier was maintained at 800-1200 V with the preamplifier gain set at 10^8 V/A. Electron energies of 70 eV and 100 eV were used for electron ionization (EI) and chemical ionization (CI), respectively. Normal Q1 mass spectra were acquired for all MS experiments. Methane reagent gas was used in all CI experiments with ion source pressures of 0.2-0.5 torr. The same removable ion volumes commonly used with the direct insertion probe were used with the GC probe.

Flow rate programming. All experiments with flow rate programming were performed on a Varian model 3400 GC equipped with a split/splitless injector. Open tubular GC columns, approximately 3 m in length with an internal diameter of 0.25 mm and a 0.25 μm film thickness (DB5, J&W Scientific) were used. Injection temperatures were typically 220°C; column temperatures are reported with each analysis.

GC probe. Wide-bore (0.53 mm i.d.) Al-clad FSOT columns with a non-polar 1.0 μm film BP-1 stationary phase (SGE) were used with the GC probe. Narrow-bore columns (0.33 mm i.d., 0.5 μm film, BP-5 stationary phase) were evaluated in terms of heating requirements; however, for all chromatograms obtained with the GC probe, wide-bore columns were used, which allowed for a mechanically simple injection port.

Flow Control System

Flow rate programming. For many of the experiments performed (e.g., exponential flow rate programming and sub-ambient inlet pressure GC) it was necessary to be able to control the column flow rate instead of the column inlet pressure. Several methods for programming the column flow rate have appeared in the literature [25,29-33]. For example, a very simple method of flow programming was achieved by manually manipulating a needle valve in the splitter line [33]. However, due to the imprecision and inconvenience of this method more reliable methods were developed. Others have achieved flow control via feedback from a pressure transducer with a motor-controlled regulator valve [29,34,35]. This type of system first requires a calibration step to determine the dependence of flow rate on inlet pressure. After the flow function is determined and programmed into the computer, the pressure transducer detects any difference between the inlet pressure and the setpoint flow. If a difference is detected, a DC motor adjusts the regulator until the correct flow is achieved. The main disadvantage of this method is the slow response time, since several seconds are required for the motor to reposition the valve. The response time of the flow controller becomes even more important for short columns since the analysis times are typically only a few minutes long. For this reason it was decided that commercially available mass flow controllers would be most suitable for these applications. These types of transducers incorporate thermal mass flow sensors to determine mass flow rates of gases. Sensors placed at both ends of a laminar flow tube detect differences in heat transferred along the tube, and directly relate this difference to the flow rate of the input gas. The measured flow rate is compared to the setpoint value and is adjusted by an electromagnetically

controlled automatic valve. The transducer and controller valve are contained in a single package measuring approximately 1/2 in. x 5 in. x 5 in. An external power supply/readout unit provides the appropriate power, real-time readout of the measured flow, and capability for computer interfacing. The advantages of this system are fast response (500 ms for the transducer), excellent precision (0.2% of full scale), and high accuracy (0.5% of full scale). The flow controller is interfaced to the mass spectrometer electronics via one of two digital-to-analog converters (DACs, known as user outputs) that are variable over the range ± 5 V DC via the TSQ70 trackball or Instrument Control Language (ICL) procedure. A control voltage range of 0-5 V is used to adjust the flow controller flow rate over its full range.

One concern about the use of a mass flow controller was its ability to regulate flow when the output was connected to the vacuum of the mass spectrometer, as it might be in short-column or vacuum inlet GC. In order to test the performance of the transducer in this configuration, the flow controller was utilized to control the input of collision gas into the collision cell of the TSQ70. In fact, this configuration worked so well that a flow controller dedicated for control of collision gas pressure has since been installed.

For exponential flow rate programming experiments, the flow control system was essentially the same as that described in Chapter 2. The only difference was that, instead of a MKS 1159A mass flow controller, a MKS 1259B mass flow controller was used, which has a flow control range of 0-20 mL/min for nitrogen and 0-29.6 mL/min for helium. It was later found that the flow rate range of this flow controller limited the experiments that could be performed. For example, during flow programming

experiments, the split and sweep valves had to be left closed during the entire GC run to obtain the widest range of useable flow rates, which limited analyses to splitless operation. A flow controller with a wider flow rate range (0-100 mL/min for nitrogen) was eventually installed to alleviate this problem. The flow function for an exponential flow program is controlled automatically with the DAC user output of the TSQ70 with an Instrument Control Language (ICL) program. The flow rate at time t, F_t, is given by

$$F_t = F_o + e^{kt} \tag{3.6}$$

where F_o is the initial flow rate and k is a constant. In a flow rate programming experiment, the initial and final flow rates, as well as the time for the delay and end of the programming period are selected and entered into the computer program. The constant, k, is calculated in the computer program such that the flow rate at any time during the analysis is determined by eq 3.6.

GC probe. Since short wide-bore columns (typically 3 m in length) were used in the GC probe, the injection port could not be operated at conventional injection port pressures (i.e., atmospheric pressure and above) without a carrier gas flow rate exceeding the normal operating pressure of the mass spectrometer. Instead, the injection port was maintained at lower pressures (typically 100-200 torr) with the flow control system described in Chapter 2. This system utilized a MKS model 1159A flow controller with a range of 0-100 mL/min for nitrogen and 0-145 mL/min for helium. The use of sub-atmospheric inlet pressures did require some consideration of injection technique, since it was possible for the sample to be prematurely aspirated from the syringe by the vacuum in the

injection port. It was found that the best way to avoid this problem was to use a gas-tight syringe and to draw the sample as well as a small volume (e.g., 1 μL) of air into the syringe barrel prior to injection.

The column flow rate of He carrier gas used with the sub-ambient inlet pressures was typically 3.5 mL/min. Flow rates were determined by measuring the flow output of the flow controller with a soap bubble meter prior to connecting the carrier gas line to the injection port. Davies has shown that, under the conditions of vacuum outlet, flow rates can be calculated by [40,41]

$$Q = 64\pi\eta L^3/9t_o^2 \qquad (3.7)$$

where Q is the flow rate (mL/s), t_o is the retention time of the unretained air peak (s), η is the gas viscosity (poise), and L is the column length (m). However, when short columns are used, the air peak times are so short that they are not easily measured. For example, a 3 m column operated at a typical gas velocity of 300 cm/s has an air peak time of 1 s. As discussed in Chapter 2, the average gas velocity can be calculated if the inlet pressure is known. However, due to the very simple design of the injection port of the GC probe, a conventional pressure gauge could not be used to measure the inlet pressure. Therefore, it was more convenient to measure flow rates instead. Once the flow rates were determined, the inlet pressures and gas velocities were readily calculated. Given that the average gas velocity is

$$\upsilon = L/t_o \qquad (3.8)$$

Average velocities can be calculated if eq 3.8 is substituted into eq 3.7 yielding

$$\upsilon = (375Q/16\pi\eta L)^{1/2} \qquad (3.9)$$

where Q is in mL/min, L is in m, η is in poise, and υ is in cm/s. The inlet pressure (P_i, dynes/cm^2) can be calculated from the Poisuelle equation for vacuum outlet conditions [14]

$$P_i = 32\upsilon\eta L/3r^2 \qquad (3.10)$$

where r is the column radius in cm, and L is in cm. A 3 m wide-bore column, operated at a typical flow rate of 3.5 mL/min of He at 25°C, has a calculated gas velocity of 204 cm/s and an inlet pressure of 146 torr.

Direct Resistive Heating

Electronics. A programmable DC power supply was constructed in-house and was used to control the voltage across the Al-clad GC columns. The electronic components for the power supply are contained in a box which is approximately 10 in. x 6 in. x 3.5 in. A schematic of the overall system electronics is shown in Figure 3.1, with details of the DC power supply shown in Figure 3.2. The output of the power supply (up to 30 V) is controlled by an input control voltage of 0-5 V DC. A DAC from the TSQ70 was used to generate a control voltage for the power supply. The control voltage (from the potentiometer or DAC) is fed into a voltage follower with variable gain. The output of the op-amp provides a bias to the base of power transistor that determines the output of the supply.

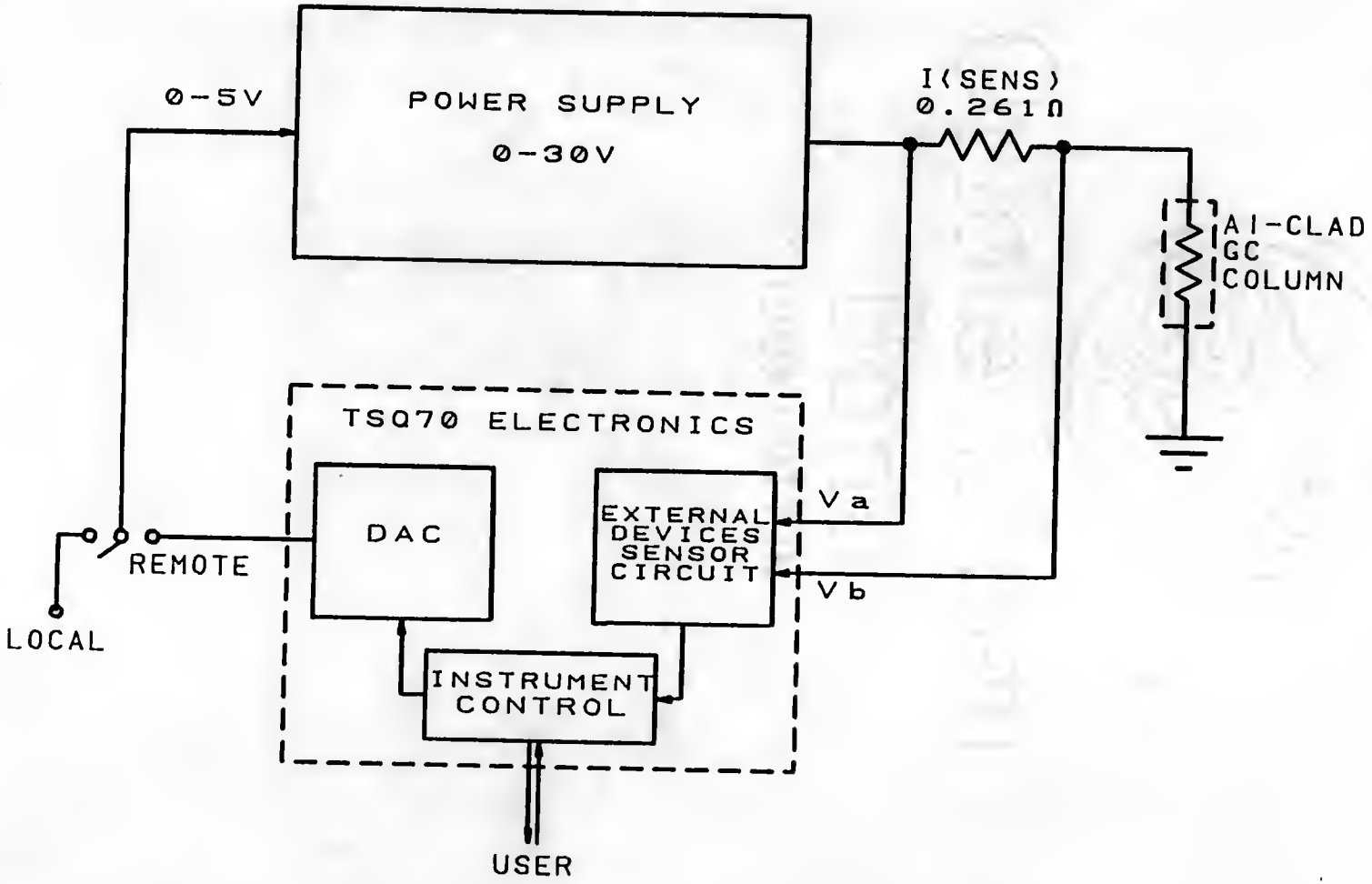

Figure 3.1. Schematic diagram of electronics used for resistive heating and temperature sensing of Al-clad capillary columns.

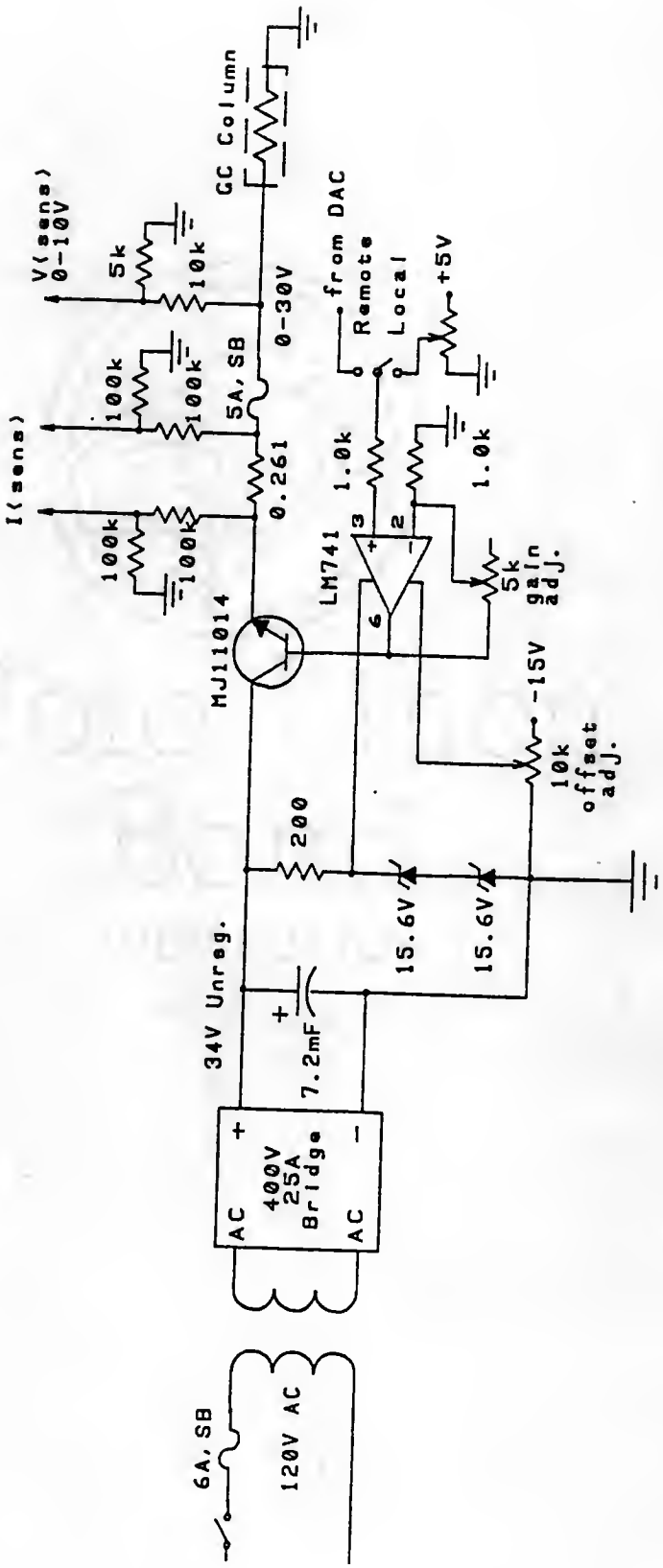

Figure 3.2. Circuit diagram of programmable 30 V DC power supply designed for column heating.

The output of the power transistor is rated at 30 V and 30 A. However, in the present configuration the output of the supply is limited by the transformer, which is rated at approximately 6 A. Typically, the gain of the voltage follower was set such that the power supply yielded the maximum desired temperature at the maximum control voltage. This versatility is important, since a change in the length or diameter of the column changed the amount of power required for the column to reach a particular temperature. No additional circuitry had to be designed to measure the column voltages and currents. The voltage drop across the column, as well as the voltage drop across a 0.261 Ω current sensing resistor were measured with an external devices sensor circuit already present in the TSQ70 electronics. This circuit consists of five differential amplifiers, an analog multiplexer, and an analog-to-digital converter (ADC). The voltages to be determined were fed into two separate differential amplifiers of the sensor circuit. This allows the voltages to be displayed and/or plotted in real time with the computer-controlled TSQ70 and the ICL. Programs were written in ICL that allowed the voltage across the column to be increased linearly with time during the acquisition of data. The linear voltage ramp was used to simulate the linear temperature ramp commonly used in temperature programming. However, it should be pointed out that any desired voltage ramp could be created with this system (e.g., exponential, logarithmic, etc.), by a simple modification of the ICL program.

Temperature sensing. The resistance of the column, obtained by measurement of the voltage and current, was used as an indication of the column temperature. Al-clad GC columns were "calibrated" by placing them in a GC oven (Varian model 3400) and recording the resistances of the

columns as a function of GC oven temperature. A wide-bore Al-clad FSOT column (0.53 mm i.d. x 3.14 m), and two different lengths (4.77 m and 3.05 m) cut from the same narrow-bore (0.33 mm i.d.) Al-clad FSOT column were calibrated using this method. The nominal resistances of these columns were very low (ca. 0.9 Ω/m for the narrow-bore column and 0.5 Ω/m for the wide-bore columns), and thus were too small to be accurately and precisely measured with a typical digital multimeter (DMM). In order to obtain accurate resistance measurements for the calibration, the DC power supply was used to apply a small voltage drop (e.g., 50 mV) across the column. The current through the column and the voltage drop across the column were measured with two DMMs (Fluke model 75). The resistances were then calculated from the voltages and currents measured. The voltages applied during calibration were not high enough to cause a significant amount of column heating.

GC Probe Design

The GC probe is schematically illustrated in Figure 3.3. The 1.27 cm x 28 cm stainless steel probe shaft was adapted from a Finnigan 4500 series ion volume insertion/removal tool. The probe shaft is threaded and screws into one of the two 4 in. square end-blocks (machined from phenolic material). The injection port is positioned in a milled slot on the other end-block and is held firmly in place by a set screw. The column is wrapped around a 2.5 in. diameter Teflon spool. The spool is held between the two end-blocks and contains a slot that allows the column to be inserted through the spool and down the length of the probe shaft. The column is covered with Nextel glass braid insulation (Omega Engineering) and is coiled around the Teflon spool. The insulation serves to

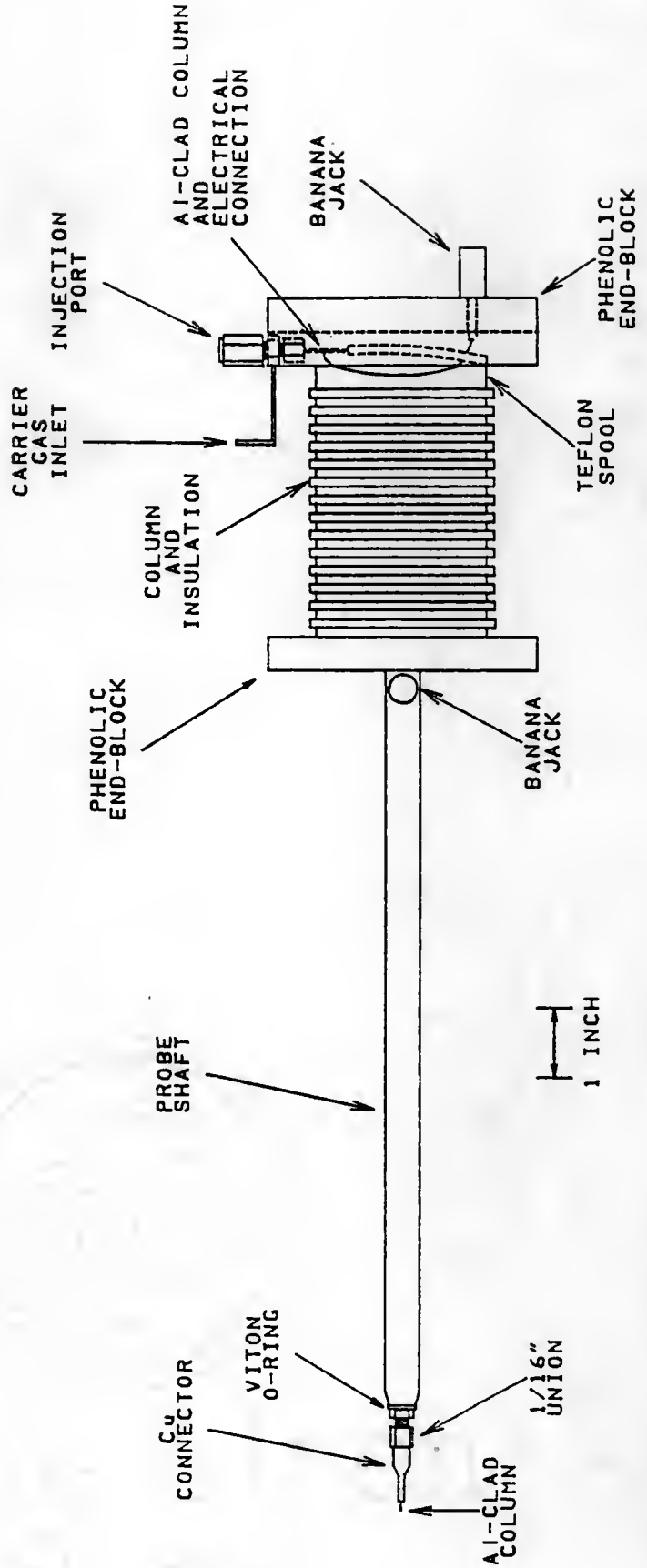

Figure 3.3. Illustration of direct insertion GC probe.

electrically isolate each strand of the coiled column. A 1/16 in. stainless steel union (Swagelok) with a graphitised vespel ferrule and a Viton o-ring are used to form a vacuum-tight seal at the end of the probe shaft. Approximately 2 cm of the column extends from the end of Swagelok union. A copper connector slides over this last few cm of the column and electrically connects the end of the column to the probe shaft. Electrical leads from the DC power supply plug into the banana jacks mounted on the probe assembly. It is very important to minimize the contact resistance of the electrical connections to the column, since poor connections result in power consumption and local heating at the point of contact. In addition, large connectors have a large thermal mass and dissipate heat near the contact. For these reasons, the electrical connection to the head of the column was made with a small removable clip lead. The probe shaft, which is used as a ground return, remains cool during column heating, since the resistance of the probe is much less than that of the columns used. The nominal resistance of the column in the probe was always checked prior to applying power to insure good electrical connections. The GC probe shaft is inserted through the probe inlet assembly and the end of the probe fits firmly against the ion volume contained in the ion source block.

A compact, low thermal mass injection port was fabricated from a 1/8 in. x 1/16 in. stainless steel tube reducing union (Swagelok). For the introduction of carrier gas into the injection port, a hole was drilled into the side of this fitting and a 1/16 in. o.d. stainless steel tube was silver-soldered in place. The wide-bore column is inserted into the smaller end of the union and is sealed with a nut and a graphitised vespel ferrule. The top of the injection port contains an 1/8 in. nut and a

septum. A standard GC syringe (SGE), equipped with a 26-gauge needle, was used to inject samples directly onto the wide-bore columns. The inside of the injection port contains a stainless steel guide, which directs the syringe needle to the column entrance. Upon injection, the syringe needle enters the column and is inserted far enough that the sample is injected past the point where the electrical connection is made. This minimizes sample loss due to unvolatilized components. The injection port remains cold when the column is heated, and thus does not have to be cooled between injections.

Results and Discussion

Flow Rate Programming

Effect of carrier gas flow rates on mass spectrometer performance. Exponential flow rate programming has been used in many instances with conventional GC detectors [25,29-35]; however, the effects of the resultant high (and varying) flow rates on the operation of the mass spectrometer have not been studied. One problem that became apparent from some initial experiments employing electron ionization (EI) was the reduction in the analyte signal (sensitivity) associated with high flow rates of carrier gas into the mass spectrometer ion source. This was briefly addressed in Chapter 2. Initially, it was unclear whether this problem was linked to mass analysis, ion formation, or a combination of both. It is possible that the increased pressure in the mass analyzer (which causes a decrease in the mean free path of the ions) results in scattering losses and a reduction of the number of ions reaching the detector. Analyte signal may also be decreased due to inefficient ion formation with EI. This associated decrease in sensitivity with EI has

also been observed in supercritical fluid chromatography/mass spectrometry (SFC/MS), where the pressure in the ion source is elevated due to the presence of the constantly eluting mobile phase [42].

It was discovered that the problem of reduced analyte sensitivity with high carrier gas flow rates could be overcome by employing chemical ionization (CI) instead of EI. Due to the presence of a reagent gas (e.g., methane) at much higher operating pressures (typically 0.1-1 torr for CI vs. 10^{-4} torr for EI), ion formation with CI appears unaffected by the increase in carrier gas flow rates. Figures 3.4 and 3.5 show a comparison of the performance of EI and methane CI respectively under identical changes in column flow rates. For these experiments, the chromatograms were obtained in the splitless mode with a 3.2 m, 0.25 mm i.d., DB-5 capillary column operated isothermally at 80°C. The sample injected was 30 ng each of C_{14}, C_{15}, and C_{16} n-alkanes. Figure 3.4 shows the chromatograms of the major fragment ion (m/z 85) obtained with EI. For Figure 3.4 (a) the column flow rate was 8 mL/min and that for Figure 3.4 (b) was 20 mL/min. Both traces are plotted on the same time and intensity scale for ease of comparison. The integrated peak areas for the components at the two flow rates are given in Table 3.1. As shown in the table, the m/z 85 peak areas for the three hydrocarbons in a particular chromatogram are reproducible within the expected limits of error. However, the areas of the peaks at the higher flow rate are approximately a factor of four less than the peak areas obtained at the lower flow rate. Although the resulting sensitivity for only one particular ion is considered in this comparison, all of the sample ions were observed to decrease by approximately the same amount. The major sample ions obtained with methane CI of n-alkanes are formed by hydride abstraction to yield

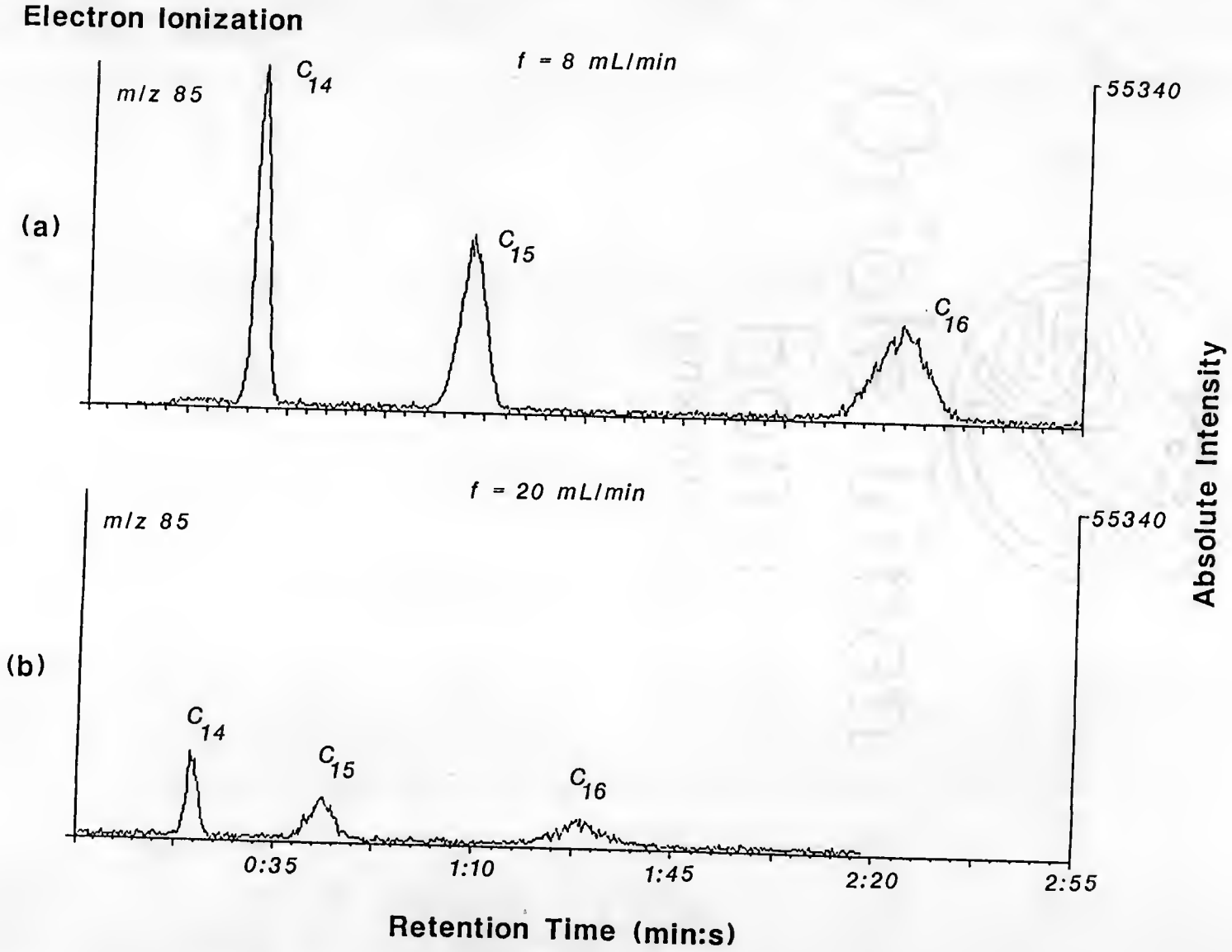

Figure 3.4. Mass chromatograms of m/z 85 from 70 eV EI of n-alkane mixture with (a) 8 mL/min and (b) 20 mL/min He carrier gas flow rates. The sensitivity with EI is drastically reduced when the higher flow rates are used.

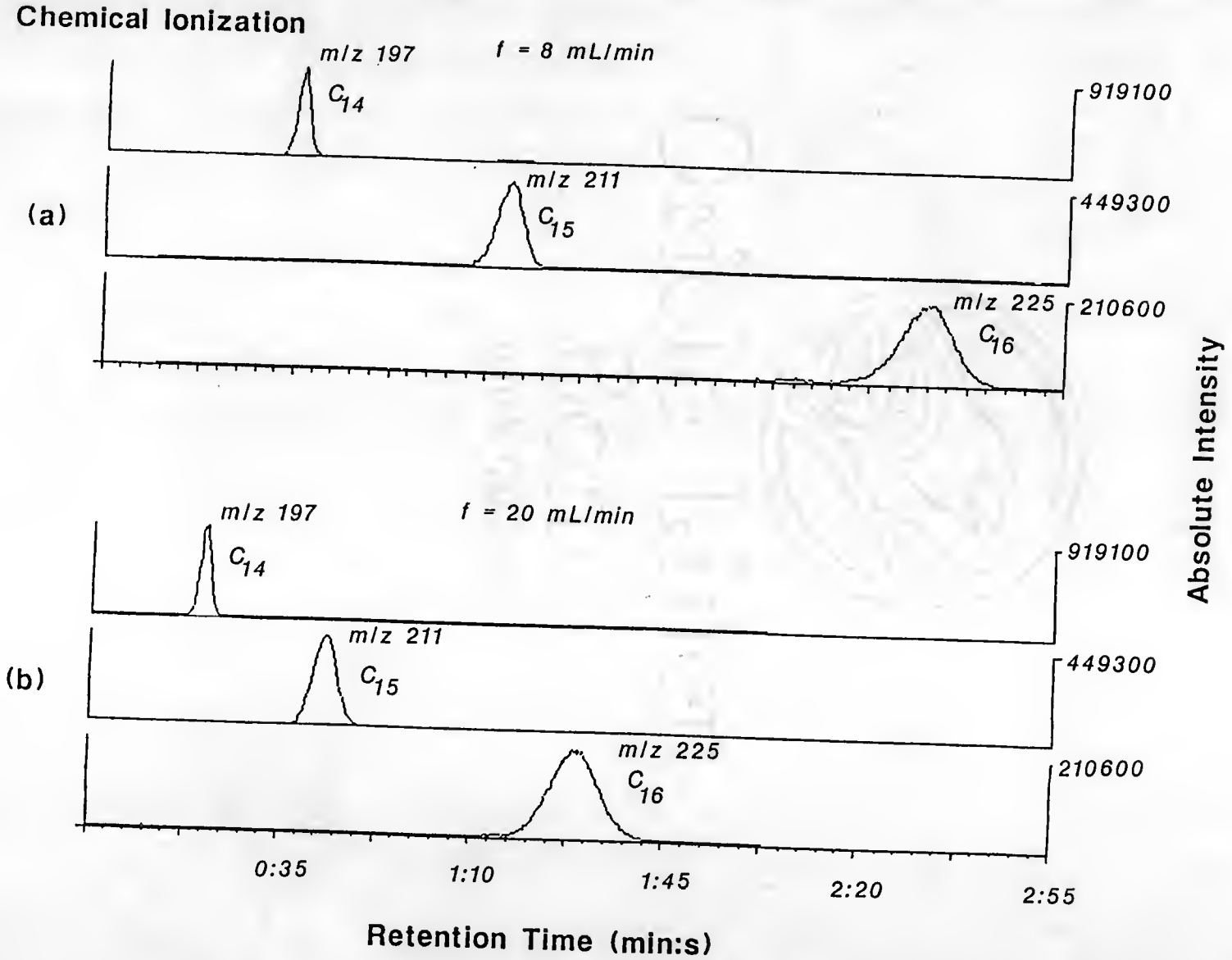

Figure 3.5. Mass chromatograms of major ions obtained with methane CI of n-alkane mixture with (a) 8 mL/min and (b) 20 mL/min He carrier gas flow rates. The sensitivity with CI is apparently unaffected by the increase in flow rate.

Table 3.1. Integrated peak areas for comparison of EI and CI at different He carrier gas flow rates.

Hydrocarbon	m/z	Flow Rate (mL/min)	Ionization Method	Peak Area
C_{14}	85	8	EI	220694
C_{15}	85	8	EI	213729
C_{16}	85	8	EI	227111
C_{14}	85	20	EI	53244
C_{15}	85	20	EI	53148
C_{16}	85	20	EI	52292
C_{14}	197	8	CI	1893613
C_{15}	211	8	CI	1827399
C_{16}	225	8	CI	1617471
C_{14}	197	20	CI	1758975
C_{15}	211	20	CI	1804526
C_{16}	225	20	CI	1679119

$(M-H)^+$ ions. Figure 3.5 shows the mass chromatograms of these ions for the two flow rates. The resultant integrated peak areas for these ions are shown in Table 3.1. As shown in the table, the variation in the peak areas when the flow was increased from 8 to 20 mL/min is insignificant and within the limits of experimental error. These results indicate that the chemical ionization process is less affected by the increased He carrier gas flow rates. This may be due to the fact that sample molecules in the CI ion source exist in a large excess of reagent molecules, thus the variation of He flow rates does not significantly affect sample ionization. The increased sensitivity (larger signal intensities and peak areas) obtained with CI for this alkane mixture can be attributed to the differences in the amount of fragmentation obtained with EI and CI. The EI spectra exhibited a large amount of fragmentation, and thus resulted in an abundance of fragment ions. In contrast, abundant pseudo-molecular ($M-H^+$) ions were obtained with CI with less fragmentation than EI. Thus, the integrated peak areas for one selected ion were larger for CI than for EI.

Once it was determined that EI, but not CI, sensitivity was degraded by high flow rates of He carrier gas, it was postulated that increasing the electron energy might help to improve the sensitivity of EI with the high flow rates of carrier gas. The electron energy, which is the potential difference between the filament and the source block, represents the kinetic energy of the electrons impinging upon the sample molecules. The electron energy is usually set higher in CI than in EI (100 eV instead of 70 eV) to insure that the electrons have sufficient energy to penetrate the source region containing ca. 1 torr of reagent gas. However, experiments have shown that an increase or decrease in electron energy

and/or optimization of any of the other ion optical parameters does not improve the performance of EI when relatively high flow rates are used. These data indicate that CI is the ionization method that should be used if high flow rates (>10 mL/min) of carrier gas are to be used. This is not a severe limitation since CI is often more sensitive than EI and is, thus, usually preferred for trace analysis. In addition, since CI is a "softer" ionization method (less fragmentation than EI), molecular weight information is often more readily obtained. If more fragmentation were desired, it might be possible to employ charge exchange ionization instead of EI or CI, as shown in Chapter 4, and as has been done in SFC/MS [42].

Comparison of temperature programming and flow rate programming. In order to illustrate the similarities and differences of linear temperature programming and exponential flow rate programming, a series of chromatograms was obtained under each set of conditions. In these experiments, a 3 m x 0.25 mm i.d. DB-5 capillary column was used. The sample was a GC test mixture obtained from J&W Scientific that is often used for evaluating the chromatographic performance of non-polar bonded-phase columns. The sample contained 23 ng/μL of each of seven components, which are listed along with their boiling points in the caption of Figure 3.6.

Figures 3.6 and 3.7 show the separation of this mixture with exponential flow rate programming and temperature programming, respectively. Figure 3.6 (a) shows the chromatogram obtained with isorheic (constant flow rate) operation at 5 mL/min of He carrier gas and an isothermal column temperature of 65°C. Figures 3.6 (b) and (c) show the mixture separated isothermally at 65°C using exponential flow rate programming. The rate of the exponential was adjusted such that the final

Figure 3.6. Reconstructed ion chromatograms (methane CI) of GC test mixture obtained on a 3 m column with isothermal operation at 65°C and various flow conditions of He carrier gas: (a) isorheic at 5 mL/min; (b) exponential flow program from 5 mL/min to 30 mL/min in 4 minutes; (c) exponential flow program from 5 mL/min to 30 mL/min in 3 minutes. The components of the mixture and their boiling points are: 1, 2-chlorophenol (175°C); 2, n-undecane (196°C); 3, 2,4-dimethylaniline (214°C); 4, 1-undecanol (243°C); 5, acenaphthylene (270°C); 6, tetradecane (232°C); 7, pentadecane (271°C).

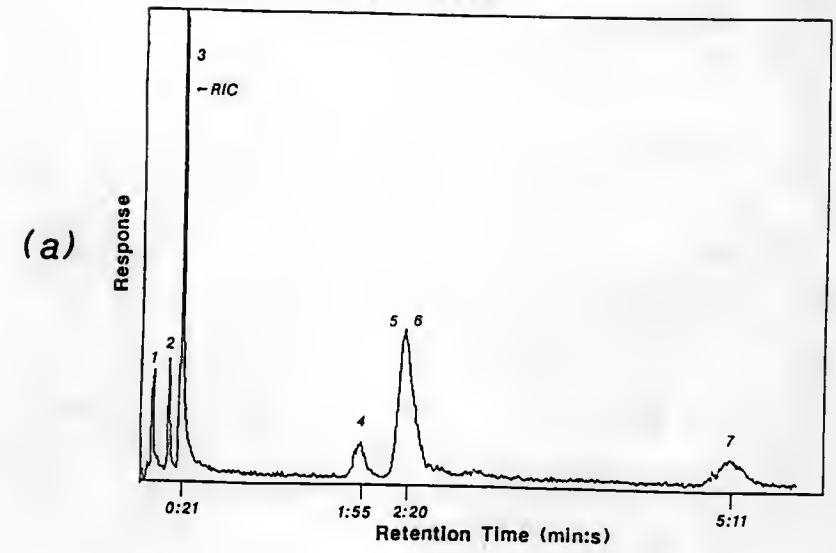
(a)
Response
3
←RIC
1
2
4
5
6
7
0:21
1:55
2:20
5:11
Retention Time (min:s)

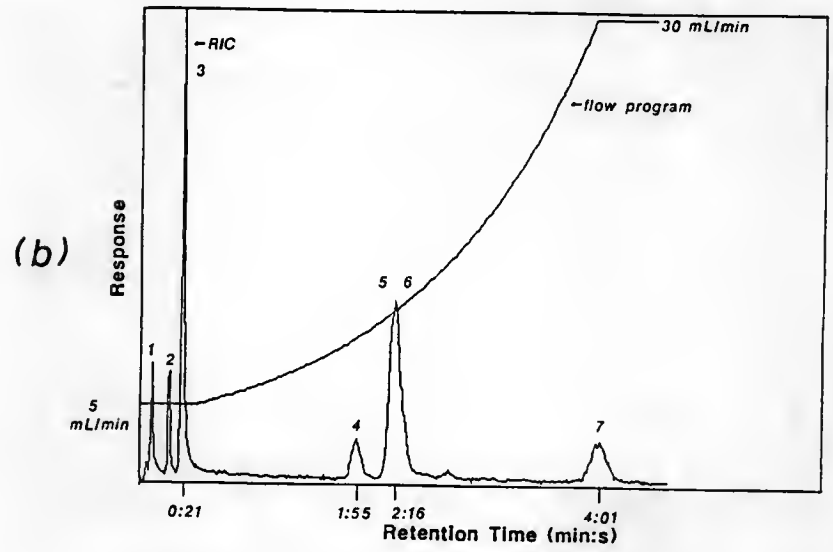
(b)
Response
←RIC
3
30 mL/min
←flow program
5
mL/min
1
2
4
5
6
7
0:21
1:55
2:16
4:01
Retention Time (min:s)

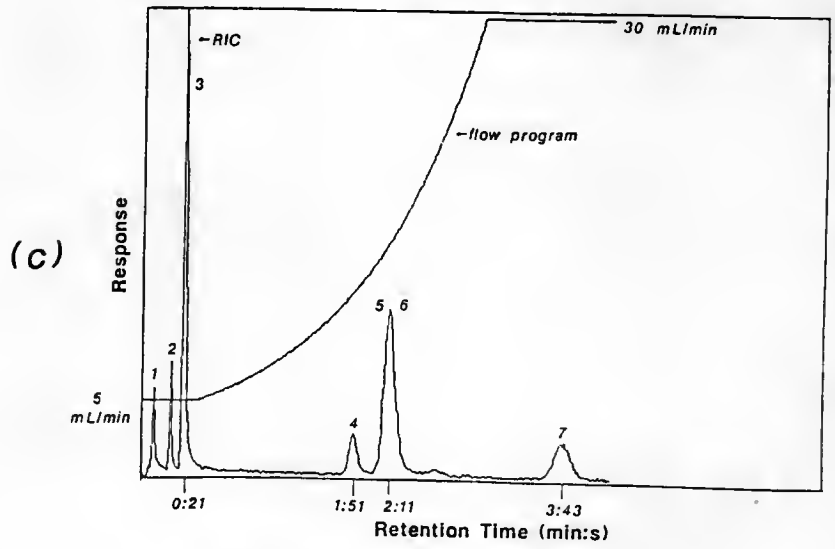
(c)
Response
←RIC
3
30 mL/min
←flow program
5
mL/min
1
2
4
5
6
7
0:21
1:51
2:11
3:43
Retention Time (min:s)

Figure 3.7. Reconstructed ion chromatograms of GC test mixture performed with isorheic operation at 5 mL/min He carrier gas and different temperature program rates: (a) 2°C/min; (b) 5°C/min; (c) 15°C/min. The components of the mixture are identified in Figure 3.6.

(a)

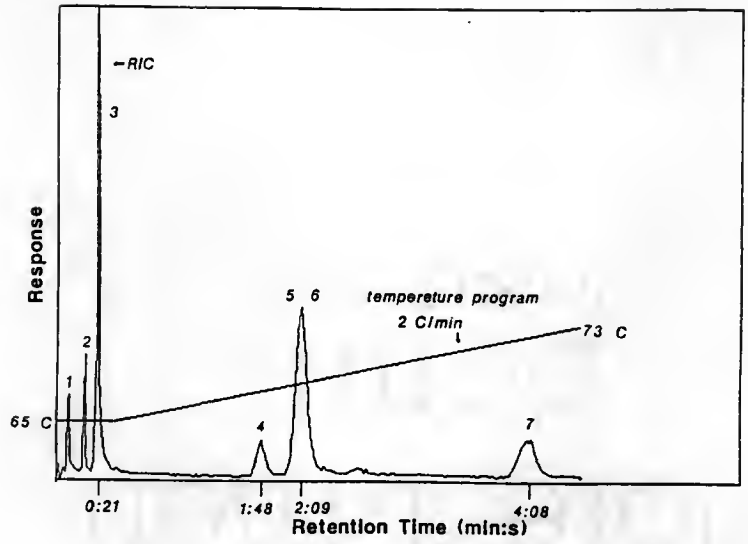
RIC
3
Response
5 6
temperature program
2 C/min
73 C
2
1
65 C
4
7
0:21
1:48
2:09
4:08
Retention Time (min:s)

(b)

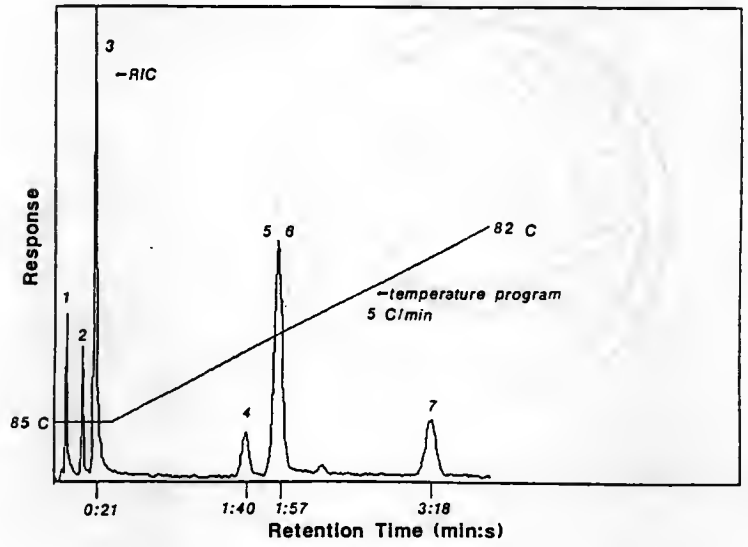
3
RIC
Response
5 6
82 C
temperature program
5 C/min
1
2
85 C
4
7
0:21
1:40
1:57
3:18
Retention Time (min:s)

(c)

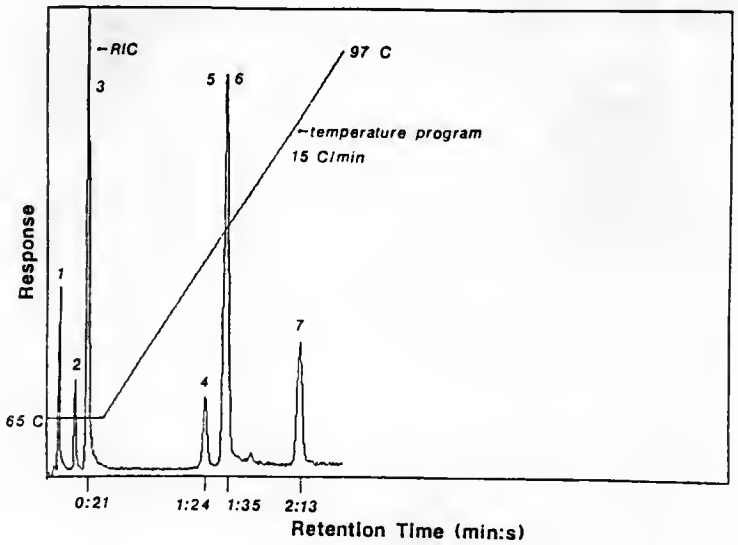
RIC
97 C
3
5 6
temperature program
15 C/min
Response
1
2
7
4
65 C
0:21
1:24
1:35
2:13
Retention Time (min:s)

flow rate of 30 mL/min was reached after 4 minutes and 3 minutes for Figures 3.6 (b) and (c), respectively. Figure 3.7 illustrates isorheic separations of the mixture with temperature programming at rates of 2°C/min, 5°C/min, and 15°C/min. It can be seen from Figures 3.6 and 3.7 that exponential flow rate programming yields similar results to linear temperature programming.

It is evident from this comparison that a change in flow rate does not influence retention as much as a change in temperature. For example, a temperature program rate of 2°C/min and a resulting temperature increase of 8°C over a period of 4 minutes (Figure 3.7 (a)) yielded nearly the same results as an exponential flow program where the flow rate was increased sixfold from 5 mL/min to 30 mL/min in 4 minutes (Figure 3.6 (b)). The differences of temperature and flow rate programming are readily understood if the thermodynamics of the chromatographic process are considered. The retention time, t_R, of a solute is given by [43]

$$t_R = L(1+k)/\upsilon \qquad (3.11)$$

where υ is the average carrier gas velocity, L is the column length, and k is the partition ratio; thus, the retention time is inversely proportional to the average velocity. It is also evident from eq 3.9 that under vacuum outlet conditions the average velocity is proportional to the square root of the column flow rate; therefore, an increase in flow rate by a factor of 6 (e.g., from 5 to 30 mL/min) would decrease the retention time by only the square root of 6 (or 2.4). In contrast, a change in column temperature affects the equilibrium of the solute between the mobile phase and stationary phase, and thus results in a change in the

partition ratio, k. The effect of the column temperature on the partition ratio is given by [43]

$$\ln k = -\Delta G/RT - \ln \beta \qquad (3.12)$$

where ΔG is the change in free energy for the evaporation of the solute from the liquid stationary phase, T is the absolute temperature, R is the gas constant, and β is the volume ratio of the mobile phase to the liquid stationary phase. Consider n-pentadecane, which has a retention time of 311 s on the 3 m x 0.25 mm i.d. column at 65°C. The associated values of k, ΔG, and β for these conditions are 259, -7.9 kcal/mol, and 500, respectively. In order to decrease the retention time of this compound by a factor of 2.4 (the same factor afforded by a factor of 6 increase in flow rate), the partition ratio factor (1+k) of eq 3.11 must also be reduced by this amount (i.e., k must equal 108). From eq 3.12, the temperature must be increased by only 27°C (i.e., to 92°C) to decrease the partition ratio and the retention time by a factor of 2.4.

The calculations discussed above as well as the experimental data demonstrate that a change in temperature has a greater effect on retention than does a change in flow rate; therefore, the range of boiling points spanned in a flow program will not be as large as that obtainable with temperature programming. Nevertheless, the chromatograms obtained with flow programming are certainly an improvement over isothermal operation (Figure 3.6). The range of boiling points covered is still relatively wide, as the components in the test mixture have boiling points ranging from 175°C (2-chlorophenol) to 271°C (pentadecane). Perhaps the real advantage of flow rate programming is the low elution temperatures. The

components of Figure 3.6 eluted as much as 200°C below their boiling points. This benefit might be of particular value in the separation of thermally labile components or if limited power were available for the heating of a portable GC.

Direct Resistive Heating

Calibration of columns for temperature sensing. Data obtained for the calibration of the column resistance vs. temperature are shown in Figure 3.8. The column resistances were normalized by dividing by the length of the column used in the calibration. Length normalization was necessary, since the same length of column was not always used in the GC probe. Once the calibrations were performed, the temperature of a resistively-heated column could be determined from the relationship

$$T = aR/L + b \qquad (3.13)$$

where T is temperature (°C), R is the resistance (Ω), L is the column length (m), and a and b are the slope and y-intercept of the linear calibration curve, respectively. The slopes, y-intercepts, and standard deviations from the linear least squares fits of the calibration data are shown in Table 3.2. As shown in Figure 3.8 and Table 3.2, essentially the same calibrations were obtained for the two different lengths of the narrow-bore column. This is an indication of the uniform thickness of the Al coating. Since these columns were cut from the same original column, no generalizations can be made about the column-to-column uniformity. As shown in Figure 3.8, the resistance of the wide-bore column is less than that of the narrow-bore column. This is due to the fact that there is a

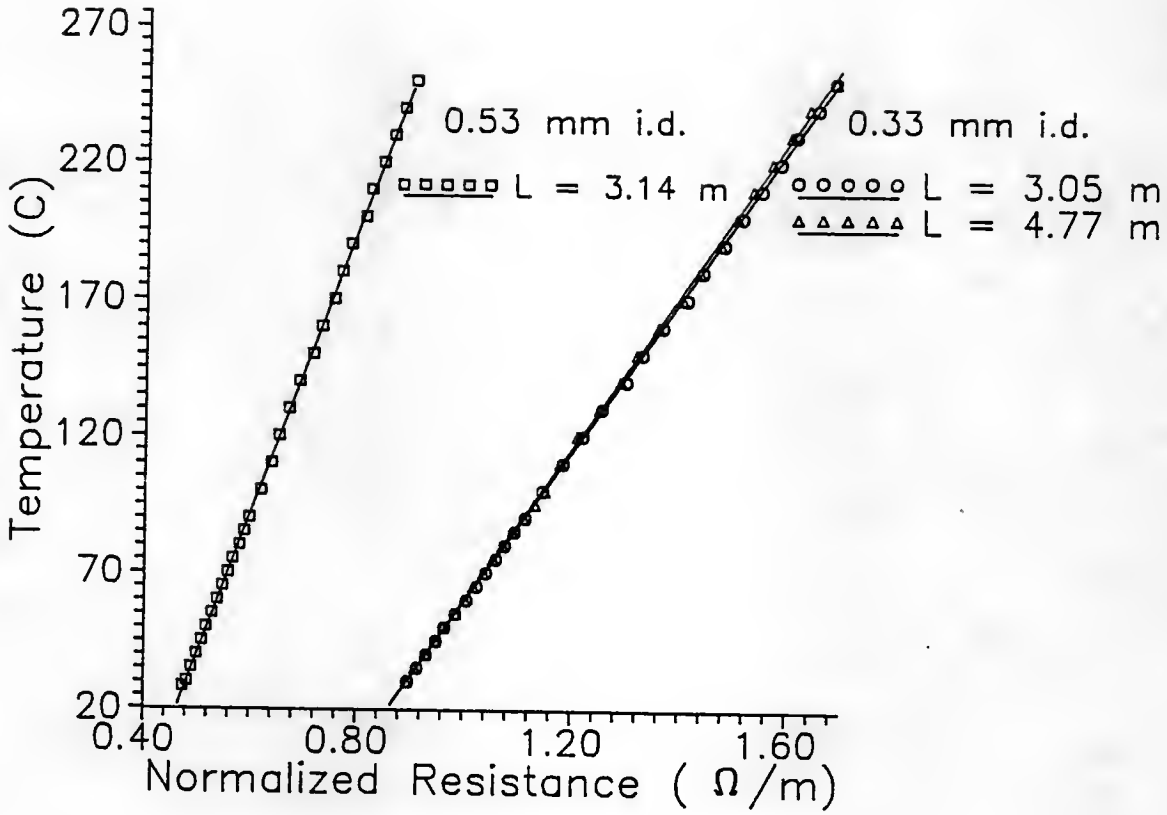

Figure 3.8. Calibrations of column temperature vs. normalized resistance (Ω/m) for two different diameter Al-clad capillary columns. The temperature of a resistively-heated column could be determined from the calibration line with knowledge of the column resistance and the length.

Table 3.2. Results of linear least squares fits of temperature calibrations shown in Figure 3.8.

column	slope ± s.d.[a]	y-intercept ± s.d.[b]	r[c]
0.33 mm i.d. x 3.05 m	276.7 ± 0.7	-217.9 ± 0.4	0.99991
0.33 mm i.d. x 4.77 m	280.4 ± 0.9	-220.8 ± 0.5	0.99987
0.53 mm i.d. x 3.14 m	522.2 ± 1.7	-221.7 ± 0.5	0.99986

[a]slope ± standard deviation, in units of $°C/\Omega m^{-1}$
[b]y-intercept ± standard deviation, in units of °C
[c]correlation coefficient for the linear least squares fit

greater mass of Al per unit length on the wide-bore column, which can be attributed to the greater surface area and/or thicker Al cladding on the wide-bore column. Note that the y-intercepts obtained were practically the same regardless of the column diameter. This can be better understood by a rearrangement of eq 3.5

$$T = R_T/\alpha R_o - 1/\alpha \qquad (3.14)$$

which demonstrates that the y-intercept ($1/\alpha$) is dependent only on the temperature coefficient of resistivity (α), a fundamental property of the metal. Due to the limited availability of these columns, it has not yet been possible to compare calibrations from different columns of the same diameter. If the column-to-column Al coating thicknesses were consistent, then calibrations would not have to be repeated for each new column. Rather, the calibrations would only need to be done for each new diameter column that was used.

One advantage of this method of direct column temperature sensing, since thermocouples or other temperature sensors are not needed, is the simplicity of the electronic circuitry required. This could be an important advantage in the design of portable instrumentation for environmental or process monitoring. Another advantage that is particularly important in this application is that measurement of the column resistance is effectively a length-average temperature measurement. The temperature measured at each point along the column may vary, depending on the insulation and thickness of the Al coating at a particular spot; thus, measurement of the column temperature at one of these spots may not be an accurate representation of the average column

temperature. In addition, we have observed that temperature sensing by conventional means (e.g., with a thermocouple placed in contact with the column) causes the temperature of the column to drop near the point of measurement and leads to inaccurate determinations. This direct measurement of column temperature might be attractive for other applications as well. For example, it is normally assumed that the temperature of a column inside an oven directly follows the oven temperature; this method could be used to directly measure the actual temperature of an Al-clad GC column inside a chromatograph oven.

Temperature response characteristics. As mentioned previously, direct resistive heating of Al-clad columns allows for extremely rapid cycling of the column temperature due to their extremely low thermal mass. Figure 3.9 shows the temperature response of a 2.3 m x 0.53 mm i.d. Al-clad FSOT column installed in the GC probe, after the voltage output of the transistor of the power supply had been stepped from 0.5 V to 8.2 V and then returned to 0.5 V after a period of 25 s. Note that the voltage across the column (Figure 3.9 (a)) did not remain constant during the heating period, but increased from 6.8 V to 7.5 V. Similarly, the column voltage did not instantaneously return to its initial value of 0.45 V at the end of the heating cycle. The slow response of the column voltage can be attributed to an increase in the column resistance as the temperature is increased. The output voltage of the transistor and the resistance of the 0.261 Ω resistor remain constant during the heating period; thus, as the column resistance increases, a greater fraction of the transistor output voltage is dropped across the column. This causes the column voltage to slowly increase during heating and slowly decrease during cooling.

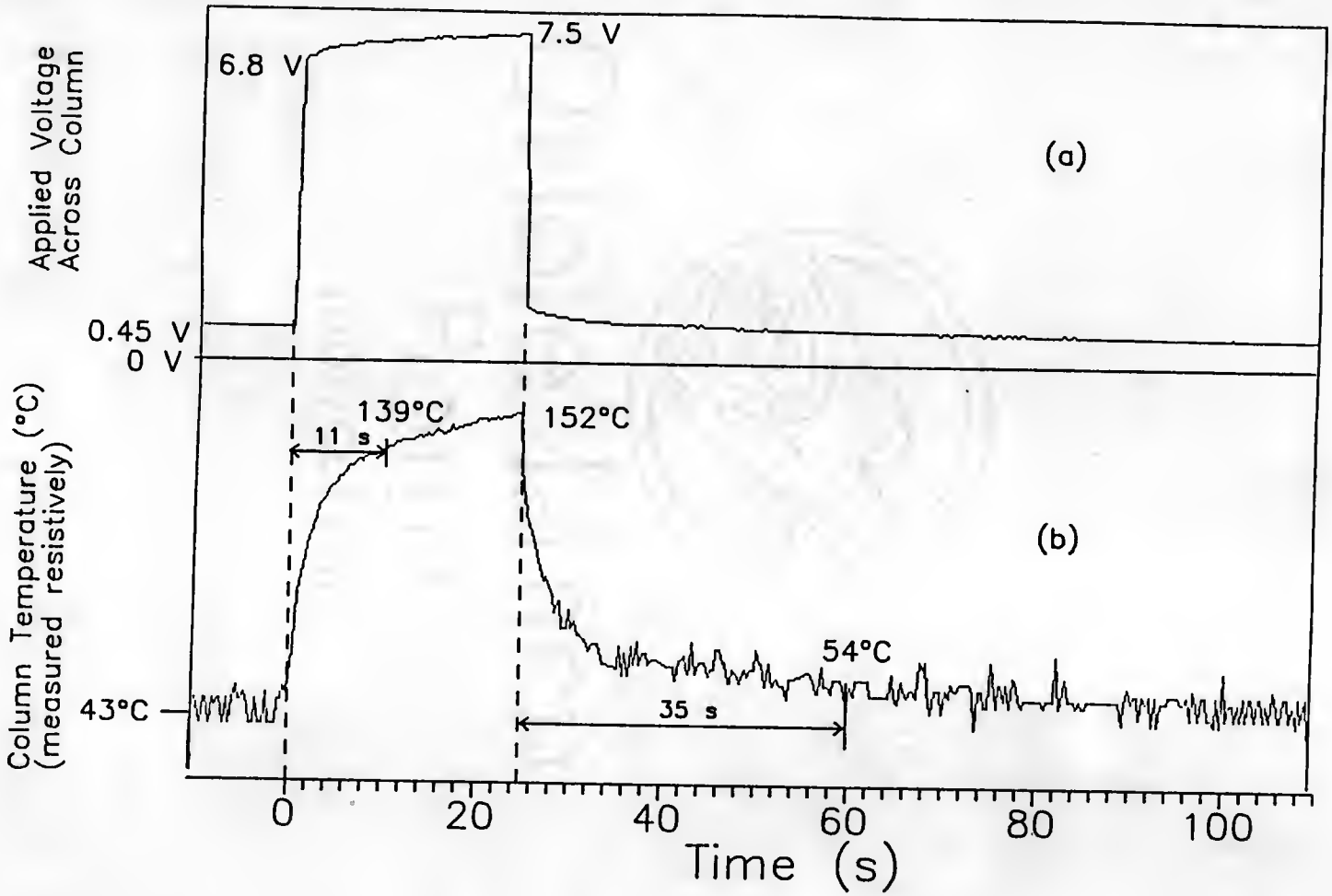

Figure 3.9. Response characteristics for a resistively-heated 2.3 m x 0.53 mm i.d. Al-clad FSOT column during a 25 s heating period: (a) applied voltage across the column, and (b) indicated temperature obtained from column resistance measurement.

During the 25 s heating cycle, the column temperature increased from 43°C to 150°C. During the first second of the 25 s heating period, the column temperature increased from 43°C to 83°C, which represents an initial heating rate of 40°C/s or 2400°C/min. The heating and cooling response of the column exhibits an exponential behavior, much like that caused by impedance in an electrical circuit. However, the response times for heating and cooling are not the same. In this example, the heating response time of the column is defined as the time required to raise the column temperature 90% of the way from 43°C to 150°C (i.e., to 139°C). As shown in Figure 3.9, this response time was found to be approximately 11 s. The temperature increase from 43°C to 139°C in 11 s represents an average rate of increase of 8.7°C/s or 524°C/min. For comparison, the ballistic heating rate of a typical gas chromatograph oven from 50°C to 150°C is only about 50°C/min [44]. In addition, the maximum heating rate for a typical on-column injector is only 150°C/min [44]. Obviously, the method of direct resistive heating offers considerable improvement in terms of rapidity of response when compared to oven heating.

In applications where extremely rapid temperature ramps are used (as in the example shown above), the speed of repetitive analyses will most likely be limited by the time required to re-equilibrate (cool) the column temperature between injections. During the first second of cooling, the column temperature dropped from 152°C to 112°C, which is an initial cooling rate of 40°C/s or 2400°C/min. Note that the initial heating and cooling rates are the same. The response time for cooling the column, defined as the time required to cool the column 90% of the way back down to 43°C from 150°C (i.e., to 54°C), was determined to be approximately 35 s. This represents an average rate of cooling of 2.7°C/s or 165°C/min.

For comparison, the temperature cool-down time for a typical gas chromatograph oven over the same temperature range would be approximately 4 minutes (about 7 times longer) [44].

As shown in Figure 3.9, there is some thermal lag associated with the heating and cooling these of columns. A small amount of thermal lag can be attributed to the voltage regulation of the power supply. The power supply regulates the voltage output of the transistor; thus, the voltage across the column changes as the temperature (and hence the resistance) of the column changes. Much of this thermal lag can be attributed to the slow thermal response of the insulation that was used to electrically isolate the column; thus, it is expected that these columns would exhibit even faster thermal response if the glass braid insulation were eliminated. This would be possible if the column could be wrapped around a grooved spool, which would separate each strand of the column and prevent electrical shorting. Nevertheless, even without any further improvements, the temperature response characteristics are impressive when compared to conventional GC ovens.

Another advantage of direct column heating is that very little electrical power (or energy) is needed. For example, approximately 35 W of electrical power applied for 25 s (0.875 kJ of energy) was required to resistively heat the 2.3 m column to 150°C. For comparison, a typical GC oven utilizes a 2400 W heater (240 V AC, 10 A) [44]. Assuming an average ballistic heating rate of 50°C/min, 3 minutes would be required to heat the oven from 50°C to 150°C. Approximately 432 kJ of energy would be consumed, which is nearly 500 times more energy than that required by direct resistive heating. In addition, a typical injector is heated separately from the oven and requires an additional 100-300 W of power

[44]. When the entire column is heated resistively and on-column injection is used, as is the case with the GC probe, no additional injector heaters are required. The power required to resistively heat a column to a particular temperature is dependent on the thermal mass of the column (eq 3.3). For columns of the same diameter and Al coating thickness, the power needed to reach a particular temperature is directly proportional to the column length. For example, a 23 m column would require ten times more power than the 2.3 m column, or 350 W, to reach 150°C.

One limitation of the present system is that the voltages sensed at the lower column temperatures are too small to yield a high degree of precision for the column resistance (and hence temperature) measurement. This is the reason for the quantization noise (at low voltages and temperatures) in the temperature profile of Figure 3.9. This limitation could be remedied if an autoranging circuit was used to automatically adjust the sensitivity of the resistance-sensing electronics.

GC Probe Performance

Figures 3.10 (a) and 3.10 (b) illustrate two different reconstructed ion chromatograms that were obtained with the GC probe and two different temperature ramps using a 3.19 m x 0.53 mm i.d. Al-clad FSOT column. A 0.5 μL on-column injection was made in both cases. The concentration of each component (identified in the figure) was 250 ng/μL in hexane. In Figure 3.10 (a), the voltage across the column was programmed, after a delay of 15 s, from 0 V (25°C) to 8.6 V in 2 minutes. The voltage was held constant for another 1.5 minutes, resulting in a final temperature of 143°C. In Figure 3.10 (b), the same initial voltage (temperature) was

Figure 3.10. Reconstructed ion chromatograms obtained with the GC probe using a 3.19 m x 0.53 mm i.d. column and two different linear column voltage programs: (a) final voltage of 8.6 V after 2 minutes, (b) final voltage of 10.8 V after 1 minute. The components of the mixture are: 1, 2-chlorophenol; 2, 2,4-dimethylaniline; 3, n-undecane; 4, 1-undecanol; 5, acenaphthylene; 6, tetradecane; 7, pentadecane.

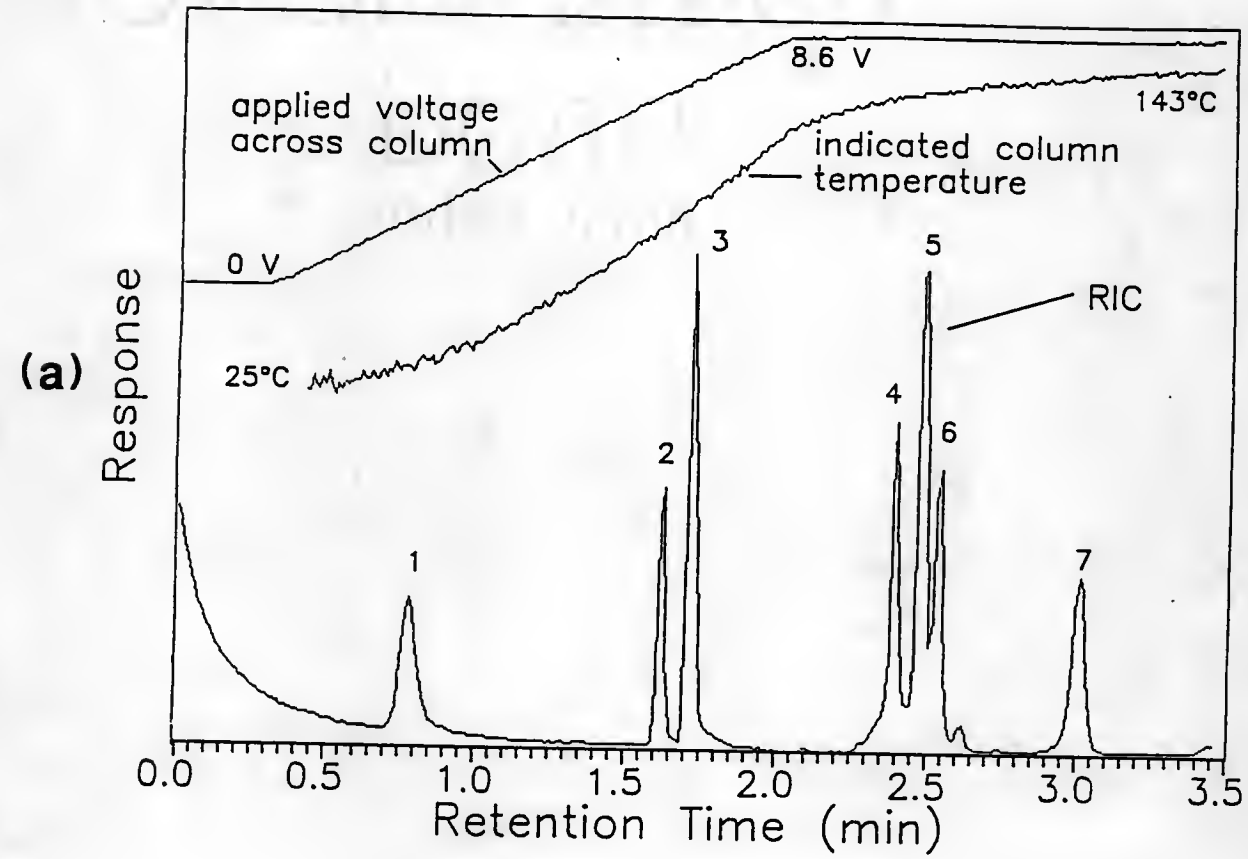
(a)
Response
applied voltage
across column
8.6 V
0 V
indicated column
temperature
143°C
25°C
RIC
1
2
3
4
5
6
7
0.0
0.5
1.0
1.5
2.0
2.5
3.0
3.5
Retention Time (min)

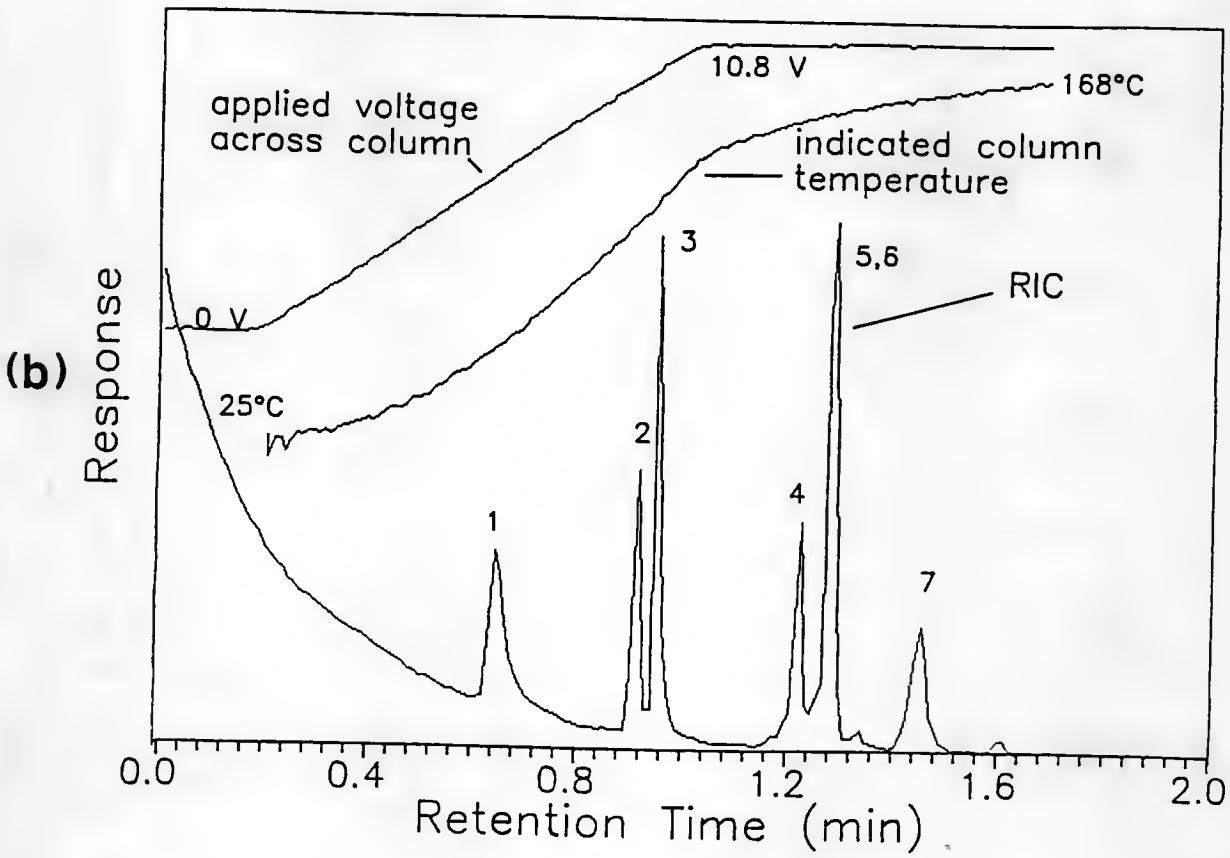
(b)
Response
applied voltage
across column
10.8 V
0 V
indicated column
temperature
168°C
25°C
RIC
1
2
3
4
5,6
7
0.0
0.4
0.8
1.2
1.6
2.0
Retention Time (min)

used as in Figure 3.10 (a). The delay was 10 s and the final voltage was 10.8 V after 1 minute. The voltage was held constant at 10.8 V for an additional 30 s, resulting in a final temperature of 168°C.

On average, the peak widths at 50% height are approximately 3 s in Figure 3.10 (a) and 2 s in Figure 3.10 (b). The earliest eluting peak (2-chlorophenol) has a larger peak width in both cases. This can be attributed to the deleterious effects of the solvent. During cold on-column injection, components that are much less volatile than the solvent are focused at the head of the column and exhibit very narrow band widths. In contrast, the volatile, early eluting components (if not well separated from the solvent front) can partition in the liquid solvent as well, resulting in increased solute peak widths [45]. This problem can often be avoided if smaller volumes of solvent are injected, or more reliably, if cryofocusing is used to trap the solutes in a narrow band at the head of the column [46]. The peak widths obtained here are extremely narrow considering that the column that was used had a stationary phase film that is normally considered thick (1.0 μm). In addition to increasing the chromatographic resolution, the capability of obtaining narrow band widths increases the sensitivity and lowers the limit of detection [3,14].

In another study, the reproducibility of retention times and peak areas obtainable with the GC probe were measured. The retention times and resulting integrated peak areas were measured for four on-column, temperature-programmed injections of 150 ng tetradecane on a 3.3 m x 0.53 mm i.d. column. Tetradecane, which has a boiling point of 232°C, eluted at 125°C with a retention time of 90.00 ± 0.81 s (relative standard deviation (RSD) of 0.9%). The integrated peak area of the m/z 198 molecular ion of tetradecane was determined with a precision of 3.5% RSD,

which is certainly within the limits of error for injections performed with a standard syringe.

Conclusions

Several important concepts for low-power and/or high-throughput analysis in GC/MS have been addressed. It has been shown that exponential flow rate programming can be used to approximate linear temperature programming. When chemical ionization is used, flow rates up to 30 mL/min can be used without detrimental effects on instrument sensitivity. Although the range of boiling points separated with flow programming is less than that which can be obtained with temperature programming, flow programming does represent a significant improvement over isothermal operation. The inherent lower elution temperatures of flow rate programming might also be attractive for the analysis of thermally labile solutes.

The direct resistive heating of Al-clad FSOT columns has also been demonstrated. This direct method of column heating obviates the need for a large chromatograph oven, and should be widely applicable in portable, low-power gas chromatographic instrumentation. This was demonstrated with the design of a compact GC probe for high-throughput analyses in GC/MS and GC/MS/MS. Measurement of the column resistance was shown to be a simple yet accurate method of directly sensing the temperature of low thermal mass Al-clad columns. It was demonstrated that linear voltage programming of the Al-clad columns can be used to approximate linear temperature programming. Future application of proportional-integral-differential (PID) feedback control of the column temperature and elimination of the column insulation is expected to further improve the thermal response characteristics of direct resistive heating of these columns.

CHAPTER 4
GAS CHROMATOGRAPHIC SAMPLE INTRODUCTION INTO THE COLLISION CELL OF A TRIPLE QUADRUPOLE MASS SPECTROMETER FOR MASS-SELECTION OF REACTANT IONS FOR CHARGE EXCHANGE AND CHEMICAL IONIZATION

Introduction and Theory

The maximum selectivity of any analytical technique can be realized if all of the variable parameters of the method are considered. These variable parameters can be considered as resolution elements that affect the informing power (i.e., the amount of information available) in the analytical method [47]. In mass spectrometry, two resolution elements which may be varied are mass analysis and ionization. The informing power of the mass analysis can be augmented by increasing the mass range, increasing the mass resolution, or increasing the number of stages of mass analysis (i.e., tandem mass spectrometry). Since the ionization method is a resolution element, it too will affect the informing power. A certain degree of "resolution" (or selectivity) can be obtained with ionization by employing techniques that allow ionization of only the desired components of a mixture, thereby excluding the ionization (and hence detection) of undesirable interferents. This selectivity of ionization is not frequently exploited, but can be controlled if careful consideration is made for the selection of reactant ions for charge exchange (CE) ionization or chemical ionization (CI) [48]. Traditionally, ion-molecule reactions for CE or CI are performed in a high-pressure (e.g., 1 torr) ion source [48-50]. However, there are limitations to

performing these reactions in the ion source. When a reactant gas is introduced into the ion source, it is rare that only a single m/z reactant ion is formed; due to the presence of other undesirable reactant ions, the ionization process may not be well-controlled. In fact, many ionization processes including CE, CI, (each with various reactant ions) and even EI may compete with the ionization technique of interest. This mixed-mode ionization certainly limits the selectivity of the ionization process. In addition, instrumental parameters such as ion source pressure affect the relative abundances of the various reactant ions; hence, reproducible CE or CI spectra are often not easily obtained.

A novel approach that eliminates the mixed-mode ionization discussed above is to mass-select the desired reactant ion before allowing it to react with the sample. Mass-selection of reactant ions has previously been used for studying ion-molecule reactions and reactive collisions. A variety of tandem mass spectrometers have been used, including sector instruments [51], a double quadrupole instrument [52], quadrupole ion traps [53-55] and triple quadrupole mass spectrometers [56-62]. Crawford and co-workers have used Kr as a charge exchange collision gas in a triple quadrupole mass spectrometer (TQMS) for monitoring carbon monoxide in the presence of hydrocarbons [63]. However, to date there has been no demonstration of the analytical utility of mass-selecting the reactant ion for mixture analysis, or of the combination of mass-selected reactions (MSRs) with GC. For this reason, a gas chromatograph has been interfaced to the collision cell of a TQMS. In gas chromatography/mass-selected reaction/mass spectrometry (GC/MSR/MS), reactant ions are selected with the first quadrupole mass filter (Q1) and are allowed to react with neutral sample molecules which elute from a GC column into the second

quadrupole collision cell (Q2). The third quadrupole is scanned for the products of the ion-molecule reactions. In this chapter, the selectivity and sensitivity of a TQMS system combining short-column GC with mass-selected reactions are discussed. Also, the capability of obtaining both molecular weight and structural information in the same chromatogram is demonstrated. A highly useful method of rapidly determining ionization energies with the TQMS is also demonstrated.

The selectivity of charge exchange (CE) and chemical ionization (CI) techniques arises from control of the energetics of the ion-molecule reactions between reactant ions and sample molecules. A CE reaction may occur if the ionization energy of the compound of interest, IE[M], is less than the recombination energy of the reactant ion, RE[$R^{+\bullet}$].

$$R^{+\bullet} + M \rightarrow M^{+\bullet} + R \qquad (4.1)$$

$$\Delta H = IE[M] - RE[R^{+\bullet}] \qquad (4.2)$$

For monoatomic species, the recombination energy of an ion is the same as the ionization energy of the neutral. However, polyatomic ions may possess excess vibrational/rotational energy; therefore, this equality cannot always be assumed. The amount of internal energy deposited into $M^{+\bullet}$ is determined by the exothermicity of the CE reaction.

Similarly, proton transfer CI reactions may occur if the proton affinity of the sample molecule, PA[M], is greater than the proton affinity of the conjugate base, R, of the reactant ion [R+H^+], PA[R].

$$[R+H]^+ + M \rightarrow [M+H]^+ + R \qquad (4.3)$$

$$\Delta H = PA[R] - PA[M] \qquad (4.4)$$

The amount of internal energy deposited into $[M+H]^+$ is equal to the difference in the proton affinities of R and M [28]. Hence, for both CE and proton transfer CI, the exothermicity of the ion-molecule reaction and the resulting extent of fragmentation can be controlled by the selection of the reactant ion. These ionization processes can be used to enhance selectivity by choosing reactant ions that will only ionize targeted compounds or by excluding the ionization of undesirable interferents. For example, if the molecular ion of benzene ($C_6H_6^{+\bullet}$, IE = 9.2 eV) is chosen as a CE reactant, only compounds with ionization energies less than 9.2 eV are ionized (typically only aromatic compounds). The energetics of ion-molecule reactions can also be used to obtain the desired amount of fragmentation. For example, if CE is used and molecular weight information is desired, then reactant ions may be chosen that have REs just above the IEs of the analytes. Alternatively, if structural information is desired, a reactant ion may be chosen that has a RE much larger than the IE of the sample molecules. The same logic can be applied to proton transfer CI, except that the difference in proton affinities determines the selectivity and the degree of fragmentation.

Experimental Section

Mass Spectrometry

A Finnigan MAT TSQ70 triple quadrupole mass spectrometer was used in these studies. All reactant gases, except for benzene and acetone, were introduced into the ion source through the gas line normally used for introduction of CI gas. Benzene and acetone were introduced into the ion source via a variable leak valve (Granville-Phillips), which was mounted

on a 1/2 in. o.d. stainless steel probe that could be inserted into the ion source through the probe inlet assembly. Reactant gases were ionized in the source with electron energies of 70-100 eV and emission currents of 200 μA. The continuous dynode electron multiplier was operated at 1000-1200 V, and the preamplifer gain was set at 10^8 V/A. The mass spectrometer vacuum cradle was maintained at 100°C to minimize sample memory effects in the collision cell. Reactant gas pressures of less than 0.3 torr were used in all cases. For experiments utilizing argon and benzene as a reactant gas mixture, the pressures of the two reactant gases were adjusted to yield approximately the same signal intensity for the $Ar^{+\bullet}$ (m/z 40) and $C_6H_6^{+\bullet}$ (m/z 78) reactant ions.

The TQMS was tuned in the normal fashion with perfluorotributylamine (FC43) to optimize ion transmission and calibrate the mass assignment. An additional tuning procedure was used to optimize the ion optics for maximum transmission of the ion-molecule reaction products. This was performed by introducing Ar into the source and n-butylbenzene into Q2. The first quadrupole (Q1) was set to pass $Ar^{+\bullet}$ and the resulting charge exchange products of $Ar^{+\bullet}$ with n-butylbenzene were monitored. The ion optics were optimized for the appearance of the product ions. It was discovered that only two parameters needed further optimization following normal tuning. The first is the Q2 offset voltage, which controls the energy of the reactant ions in Q2. The optimum Q2 ion energy was typically in the range of 1-10 eV. Since the ion energy effectively controls the residence time of the ions in Q2, it could be expected that low ion energies would be favored. The second parameter requiring additional optimization was the Q2 RF voltage. Since Q2 is an RF-only quadrupole, it is not capable of simultaneously transmitting all ions of

different m/z. In fact, at a given RF voltage, an RF-only quadrupole has a low mass cut-off, below which ions are not transmitted [64]. In addition, low m/z ions entering Q2 (e.g., $[He]^{+\bullet}$) have a very narrow range of RF voltages that allow these ions to be transmitted. The adjustment of the Q2 RF voltage was critical, since both the reactant ions and product ions had to remain stable in Q2 for product ions to be observed.

Gas Chromatography

A Varian 3400 gas chromatograph with a split/splitless injector was used. A 2.1 m x 0.25 mm i.d. DB-5 (0.25 μm film) or a 3 m x 0.18 mm i.d. (0.4 μm film) fused silica open tubular (FSOT) column (J&W Scientific) was used, depending on the analysis. Carrier gas flow rates were controlled with a mass flow controller (MKS Model 1159A) and a flow control system described previously in Chapter 2. This flow control system allows the injection port to operated at sub-ambient pressures such that low carrier gas flow rates (1-2 mL/min) can be used with short columns with vacuum outlet. It was necessary to limit the flow rates to less than 2 mL/min in the collision cell to avoid exceeding the normal operating pressure of the mass analysis region of the TSQ70. The pressure in the analyzer region, with <2 mL/min of He carrier gas flowing into the collision cell, was typically 2 x 10^{-5} torr, as indicated by a Bayard-Alpert ionization gauge. It should be noted that longer columns could be used (instead of short columns with reduced inlet pressures) to restrict the column flow rates, at the expense of longer analysis times. Split injections were performed by injecting the sample directly into the low-pressure injection port, which was connected to a mechanical pump via the splitter line. During the splitless mode of operation, the samples were injected with the

split valve closed and the injection port slightly above atmospheric pressure. The inlet pressure was then sharply reduced after allowing approximately 10 seconds for the sample to enter the column. At the flow rates used, the injection port was completely flushed with carrier gas in approximately 3 seconds. Final inlet pressures of 420 torr and 710 torr were used for the 0.25 mm i.d. and the 0.18 mm i.d. column, respectively. Temperature programming was used for all analyses.

It was important to select a carrier gas that would not be ionized by mass-selected reactant ions, since the ionized carrier gas could interfere with the ion-molecule reactions of interest. Helium was chosen for this work, since it has an ionization energy well above the recombination energies of the reactant ions used. In addition, it was expected that the small collision cross section of helium would reduce the probability of collisionally-activated dissociation (CAD) of reactant or product ions in the collision cell.

GC/MS Interface

Two different transfer lines were used for GC/MS interfaces. In both cases the effluent from the GC column was introduced directly into the collision cell of the TQMS. For one transfer line, a 1 m section of the polyimide-clad FSOT column was passed through a 1 m length of 1/16 in. o.d. stainless steel tubing. The second transfer line consisted of a 0.9 m x 0.32 mm i.d. BP-5 aluminum-clad FSOT column with a 0.5 μm film thickness (SGE). The 2.1 m FSOT column was coupled to the Al-clad column with a glass-lined zero-dead-volume fitting. Both transfer lines were resistively heated by applying an AC voltage across the tubing. This was accomplished by connecting the line voltage (120 V AC) across an

adjustable autotransformer (Variac), and connecting the output of the autotransformer to a step-down transformer (rated at 34 V, 10 A, with 120 V input). The voltage developed across the secondary of the transformer was placed across the transfer line. The temperature of the transfer line was adjusted by varying the voltage output of the autotransformer. Approximately 5-6 V AC were required to heat either transfer line to 175°C. The transfer lines were covered with glass braid insulation to minimize temperature fluctuations. The transfer line temperatures were monitored with a digital temperature sensor utilizing a low thermal mass type K thermocouple (Omega Engineering). Small alligator clips were used to make electrical connections to the transfer lines. The transfer line being used was inserted through a feedthrough into the mass spectrometer vacuum chamber. A viton ferrule and a 5 cm piece of teflon tubing was used to electrically isolate the transfer line from the vacuum manifold of the mass spectrometer. Ground for the transfer line was asserted inside the vacuum chamber, which allowed all but the last 5 cm of the column to be heated. The end of the column was inserted into the collision chamber through the same opening used for introduction of collision gas. The TSQ70 vacuum manifold has a removable glass top that allows easy access to the collision chamber. The procedure of installing the column outlet into Q2 requires about the same amount of time as normal installation of a column into the ion source. The transfer lines are mechanically simple and can be rapidly heated (or cooled) to the desired temperature.

Results and Discussion

Ionization Energy Measurements

Knowledge of the ionization energies (IEs) of reactant gases and samples is important if the energetics of the charge exchange process are to be understood and taken advantage of analytically. Since IEs of certain species may not always be available in the literature, a routine method for the determination of IEs would be a boon for the application of charge exchange ionization. A number of methods have been used to determine ionization energies, including photoionization [65,66], electron ionization [65,67], resonant photoionization [68,69], and Penning ionization [70]. However, these methods are commonly implemented on mass spectrometers specifically designed or modified for this purpose. It was found that ionization energies could be measured rapidly with the computer-controlled TSQ70 in good agreement with literature values [71]. With the sample or reactant gas introduced into the ion source, ionization or appearance energies were determined by increasing the electron energy (the potential difference between the filament and source block) in small increments (0.1-0.2 eV) and determining the approximate value at which a measurable ion signal first appeared. With the computer-controlled TSQ70, a plot of ion intensity vs. electron energy from 1-70 eV can be acquired in less than 30 seconds.

Examples of appearance energy curves are shown in Figure 4.1 for the molecular ion (m/z 134) and two fragment ions (m/z 91 and m/z 92) from n-butylbenzene. Since there is some uncertainty associated with estimation of the appearance energy (Figure 4.1), each of the ionization energies determined experimentally is reported in Table 4.1 as the average of the

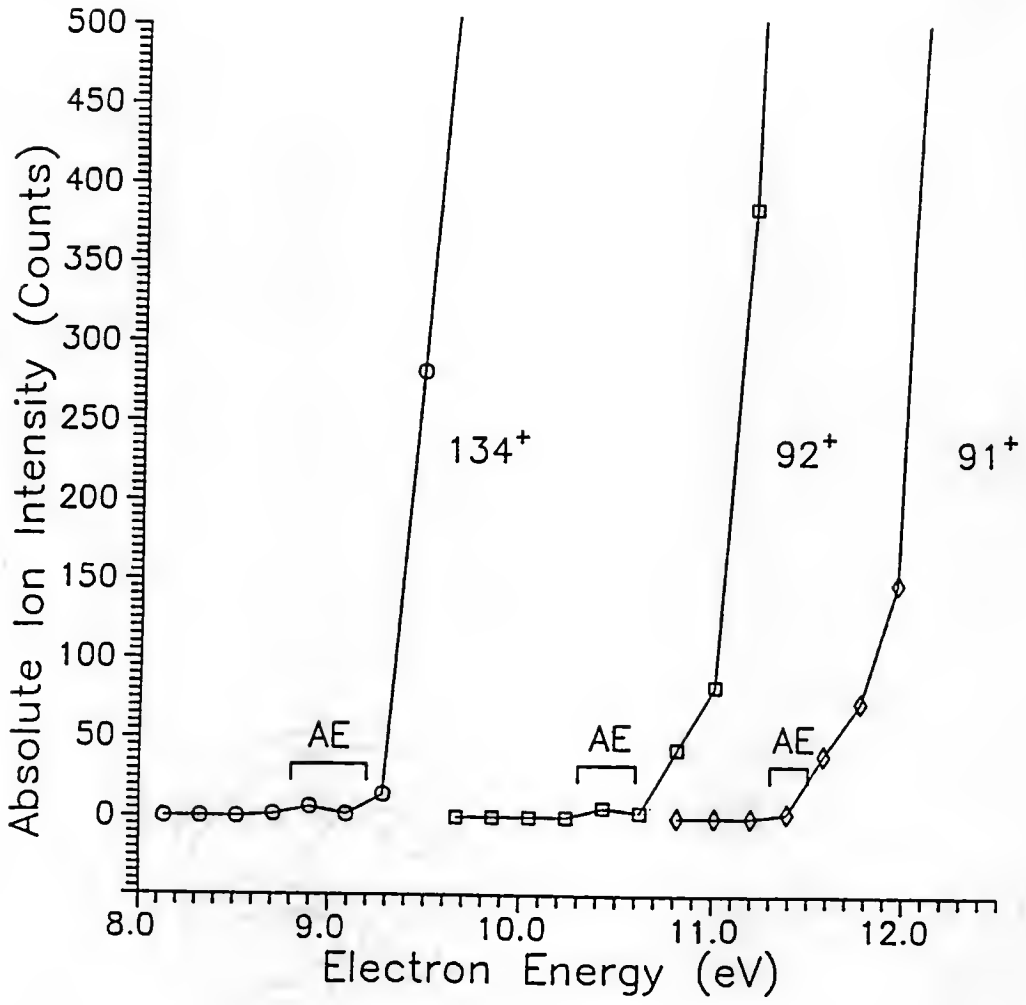

Figure 4.1. Variation of the electron energy for the determination of the appearance energy or ionization energy for three different ions (m/z 91, $[C_7H_7]^+$; m/z 92, $[C_7H_8]^{+\bullet}$; and m/z 134, $[C_6H_5C_4H_9]^{+\bullet}$) of n-butylbenzene. The brackets labeled 'AE' indicate the approximate uncertainty in the estimation of the appearance energy from a single curve.

Table 4.1. Comparison of experimentally determined ionization energies with literature values.

Species	Ion	Experimental (eV)	Literature (eV)[a]
He	$He^{+\cdot}$	24.80 ± 0.10	24.59 ± 0.01
N_2	N^+	24.50 ± 0.20	24.32 ± 0.03
He	$He_2^{+\cdot}$	20.00 ± 0.10	NF
CO_2	$(CO_2)_2^{+\cdot}$	16.40 ± 0.10	NF
Ar	$Ar^{+\cdot}$	16.10 ± 0.10	15.76 ± 0.03
N_2	$N_2^{+\cdot}$	15.70 ± 0.30	15.58 ± 0.01
N_2	$N_4^{+\cdot}$	14.70 ± 0.30	14.58 ± 0.01
Ar	$Ar_2^{+\cdot}$	14.50 ± 0.20	14.71 ± 0.01
CO_2	$CO_2^{+\cdot}$	14.40 ± 0.20	13.80 ± 0.02
CH_4	$CH_4^{+\cdot}$	13.00 ± 0.20	12.76 ± 0.24
CH_4	CH_3^+	ND	13.50 ± 0.05
C_8H_7N[b]	$C_8H_7N^{+\cdot}$	9.60 ± 0.10	9.45 ± 0.05
$C_{10}H_{14}$[c]	$C_{10}H_{14}^{+\cdot}$	9.00 ± 0.20	8.69 ± 0.01

[a] Literature values obtained from reference [71].
[b] phenylacetonitrile
[c] n-butylbenzene
NF - Data not found in the literature.
ND - Value not determined experimentally.

highest and lowest values of the observed range of possible appearance energies obtained from a single curve. The amount of uncertainty resulting from the estimation of the appearance energy from a single curve (rather than the standard deviation of several curves) is also reported with each of the determined values. This uncertainty, typically 0.2 eV, can be attributed to the low ion intensities obtained when the electron energy is near the appearance energy. The most accurate results were obtained if the first ion extraction lens after the source was set to 0.0 V with respect to the source block. This kept the field from this lens, as well as others, from perturbing the electron energy within the source and causing erroneous measurements. As shown in Table 4.1, the experimental ionization energies are in good agreement with literature values (generally within 1 or 2%). In nearly every case, the experimentally determined ionization energy was higher (typically by 0.2 eV) than that found in the literature. This error may be attributed in part to the inabilty to determine the first small increase in ion signal. Other errors may be introduced from the voltage offset in the digital-to-analog and analog-to-digital converters used by the TSQ70 to set and read back the electron energy.

Simultaneous Structural and Molecular Weight Information

Electron ionization (EI) typically provides structural information; however, in many cases low intensity molecular ions (or no molecular ions at all) are obtained. Chemical ionization (CI) is then used to obtain pseudo-molecular ions (e.g., $[M+H]^+$) for molecular weight confirmation. Since obtaining CI spectra in most mass spectrometers requires physical changes in the ion source region, EI and CI spectra cannot be obtained

simultaneously; consequently, molecular weight and structural information are not readily obtained in a single chromatographic run. With mass-selected reactions, however, the energetics of the ionization process can be tailored to the type of information desired. In addition, structural information and molecular weight information can be simultaneously acquired. This can be accomplished by sequentially selecting different reactant ions from the same reactant gas, or by introducing a mixture of reactant gases in the ion source and selecting the reactant ions during alternating scans that have different recombination energies or proton affinities. It is also possible to acquire alternating CI and CE spectra by selecting different reactant ions.

Figure 4.2 shows CE reconstructed ion chromatograms of a GC activity mixture that were obtained by selecting the $Ar^{+\bullet}$ and $C_6H_6^{+\bullet}$ reactant ions during alternating scans. The chromatogram was obtained with the 3 m x 0.18 mm i.d. column (1 m of which served as the transfer line) operated with a 25:1 split. The concentration of each component in the sample was 250 ng/μL, and a 1μL injection was made. The components of the mixture are identified in the figure. This type of mixture is commonly used for evaluating the chromatographic performance of capillary columns. It contains a wide variety of compound types (alkanes, aromatics, alcohols, and an amine), which has made it useful for investigating the ion-molecule reactions.

Ionization energies of aliphatic compounds are typically above 11 eV, while those of aromatics are typically below 10 eV. As shown in the Figure 4.2, $Ar^{+\bullet}$ (RE = 15.8 eV) ionizes all of the compounds of the mixture, while the $C_6H_6^{+\bullet}$ ion (RE = 9.2 eV) only ionizes the aromatic components. Fenselau et al. have previously evaluated benzene as a charge

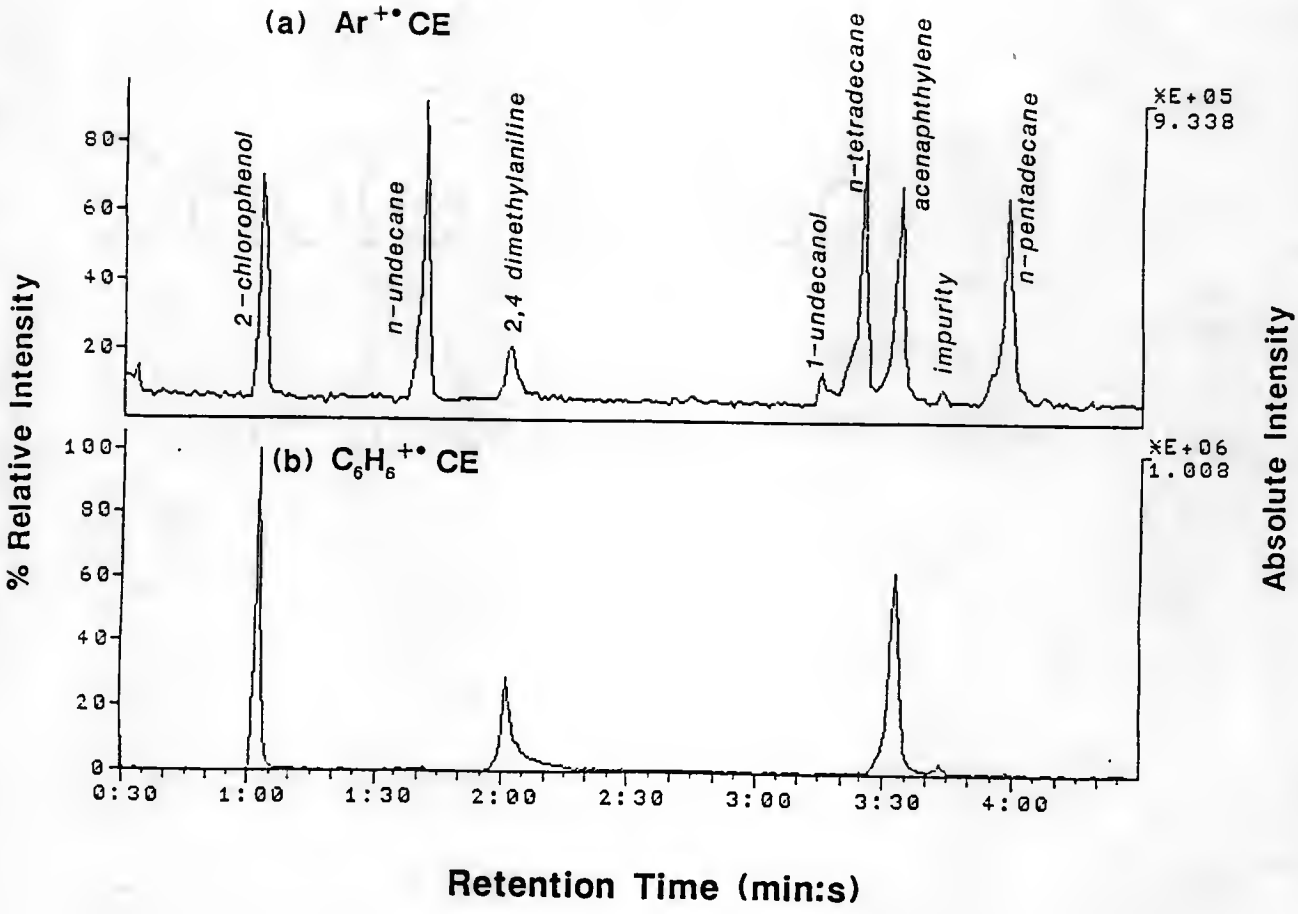

Figure 4.2. GC/MSR/MS chromatogram of GC test mixture with (a) $Ar^{+\bullet}$ charge exchange and (b) $C_6H_6^{+\bullet}$ charge exchange. The reactant ions were mass-selected with Q1 during alternate scans. The impurity in the mixture is acenaphthene.

exchange reactant [50]. However, their results showed that species not ionized by the $C_6H_6^{+\bullet}$ reactant ion were ionized by EI in the source. Clearly, the ability to mass-select the desired reactant ion and carry out these reactions in a region without the presence of ionizing electrons yields the maximum selectivity obtainable with the ionization process.

Figure 4.3 shows a comparison of the spectra of 2,4 dimethylaniline obtained from $Ar^{+\bullet}$ and $C_6H_6^{+\bullet}$ CE from the chromatogram in Figure 4.2, as well as an EI spectrum acquired separately for comparison. The CE spectra illustrate the capability of simultaneously obtaining molecular weight and structural information. Our experience has shown that the $C_6H_6^{+\bullet}$ reactant ion yields predominantly the molecular ion for aromatic compounds with little or no fragmentation. Conversely, the $Ar^{+\bullet}$ CE spectra are more energetic than 70 eV EI spectra. This can be better understood by considering the internal energy imparted upon ionization. The internal energy deposited during CE ionization is well-defined (eq 4.2), whereas the internal energy deposited during ionization by EI is not well-defined due to the wide range of energies imparted during EI with 70 eV electrons [72].

Charge exchange ionization produces odd-electron species as does EI [42,73]. It has previously been shown that CE spectra can be searched against the NBS EI library with acceptable results [73]. These concepts were investigated using the GC/MSR/MS technique. An advantage of MSRs is that two (or more) different CE reactant ions can be used, one resulting in EI-type spectra, and another yielding very little fragmentation. Thus, the CE spectra could provide an added dimmension for simultaneously providing structural and molecular weight information for the classification of unknowns. Charge exchange spectra from $Ar^{+\bullet}$, $CO_2^{+\bullet}$

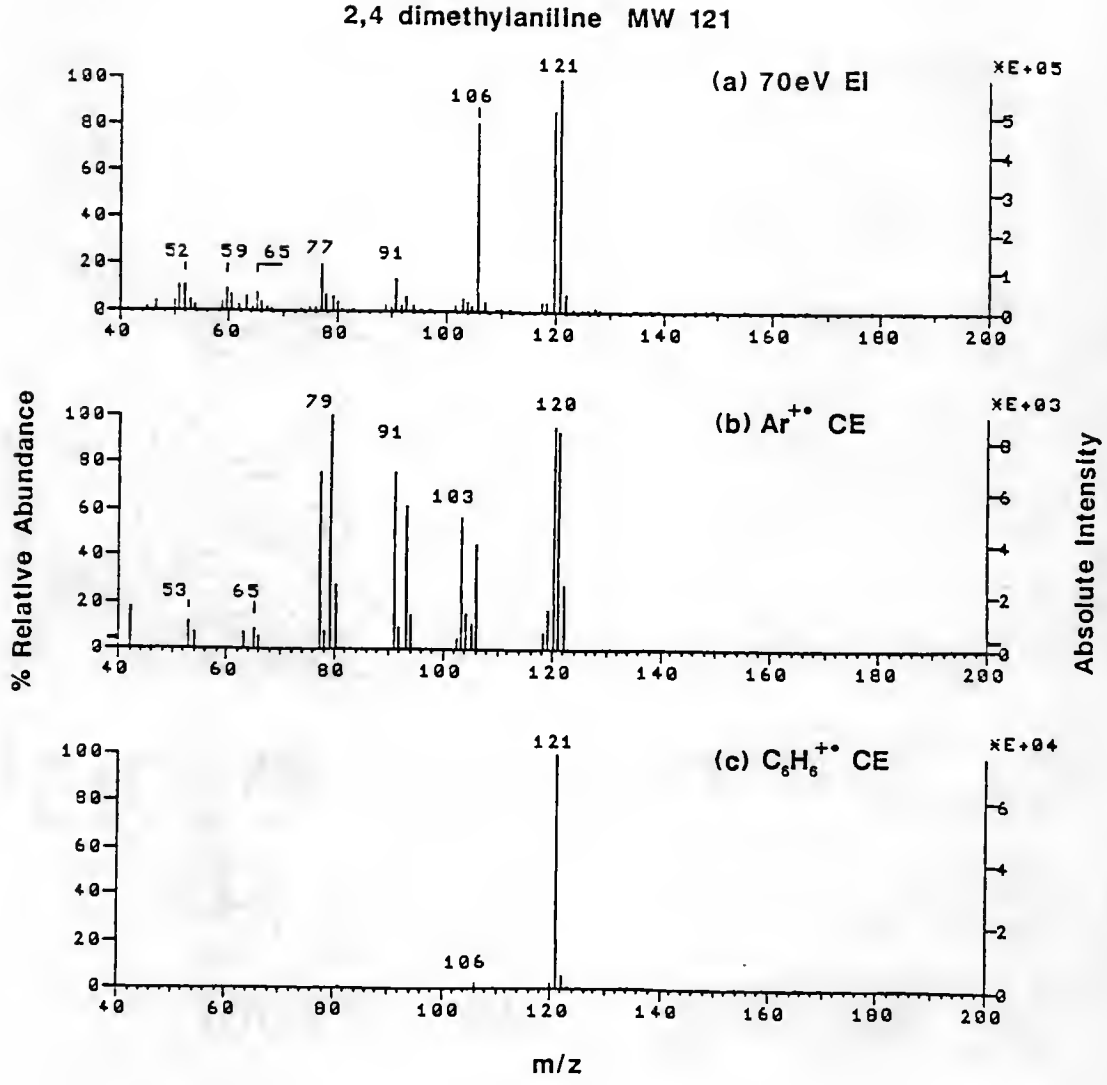

Figure 4.3. Mass spectra of 2,4 dimethylaniline: (a) 70 eV EI, (b) $Ar^{+\bullet}$ CE, and (c) $C_6H_6^{+\bullet}$ CE. The CE spectra were obtained from the chromatogram in Figure 4.2. The EI spectrum was acquired separately.

(RE = 13.8 eV), and CH_3^+ (RE = 13.5 eV) with the components in the GC test mixture were compared with EI library spectra. The results of the library searches obtained with the TSQ70 ICIS system from the three CE reactant ions as well as from EI are shown in Table 4.2. As shown in the table, the success rate of the library search for the CE spectra were comparable to those obtained with EI. In general, among the charge exchange reactants studied, the CH_3^+ CE spectra yielded the most reliable match with the EI library spectra. This might be expected, since the CH_3^+ charge exchange reactant ion deposits the least amount of energy of the three reactant ions studied and yielded the most abundant molecular ions. In cases where the compound was not found, knowledge of the molecular weight (obtainable by CE with a less energetic reactant ion) led to more accurate classification. Once the molecular weight was known, the molecular weight filter could be applied before the library search was carried out. In addition, in cases where the compound was not correctly matched, information about the compound class could be obtained from the best hits of the CE spectra, as is commonly done with EI spectra.

Selectivity of Ionization

The chromatograms in Figure 4.2 illustrate the selectivity of $C_6H_6^{+\bullet}$ CE for a relatively simple mixture. A more dramatic illustration of the selectivity of the $C_6H_6^{+\bullet}$ reactant ion is its use as a means of rapidly screening for the aromatic components of a complex mixture without high-resolution chromatographic separation. An example of these concepts is presented in Figure 4.4, which shows reconstructed ion chromatograms (RICs) of JP-4 jet fuel on a 2.1 m x 0.25 mm i.d FSOT column (1 m of this column served as the transfer line). The top two traces of the figure

Table 4.2. Comparison of EI library search results for CE with various reactant ions and EI of compounds in GC test mixture.

	Ionization Mode and Reactant Ion				
	EI	CE	CE	CE	
	--	$Ar^{+\cdot}$	$CO_2^{+\cdot}$	CH_3^+	
Compound	Library Search Match #				MW filter
2-chlorophenol	1	3	3	2	off
	1	3	3	2	on
undecane	N[a]	N	N	N	off
	5	5	2	1	on
2,4 dimethylaniline	5	3	N	4	off
	5	3	3	3	on
1-undecanol	N	N	N	N	off
	1	3	2	1	on
tetradecane	4	9	1	1	off
	2	1	1	1	on
acenaphthylene	1	7	N	N	off
	1	4	10	2	on
pentadecane	N	N	N	1	off
	1	3	1	1	on

[a]N, Not found among the top ten best fits of the library search.

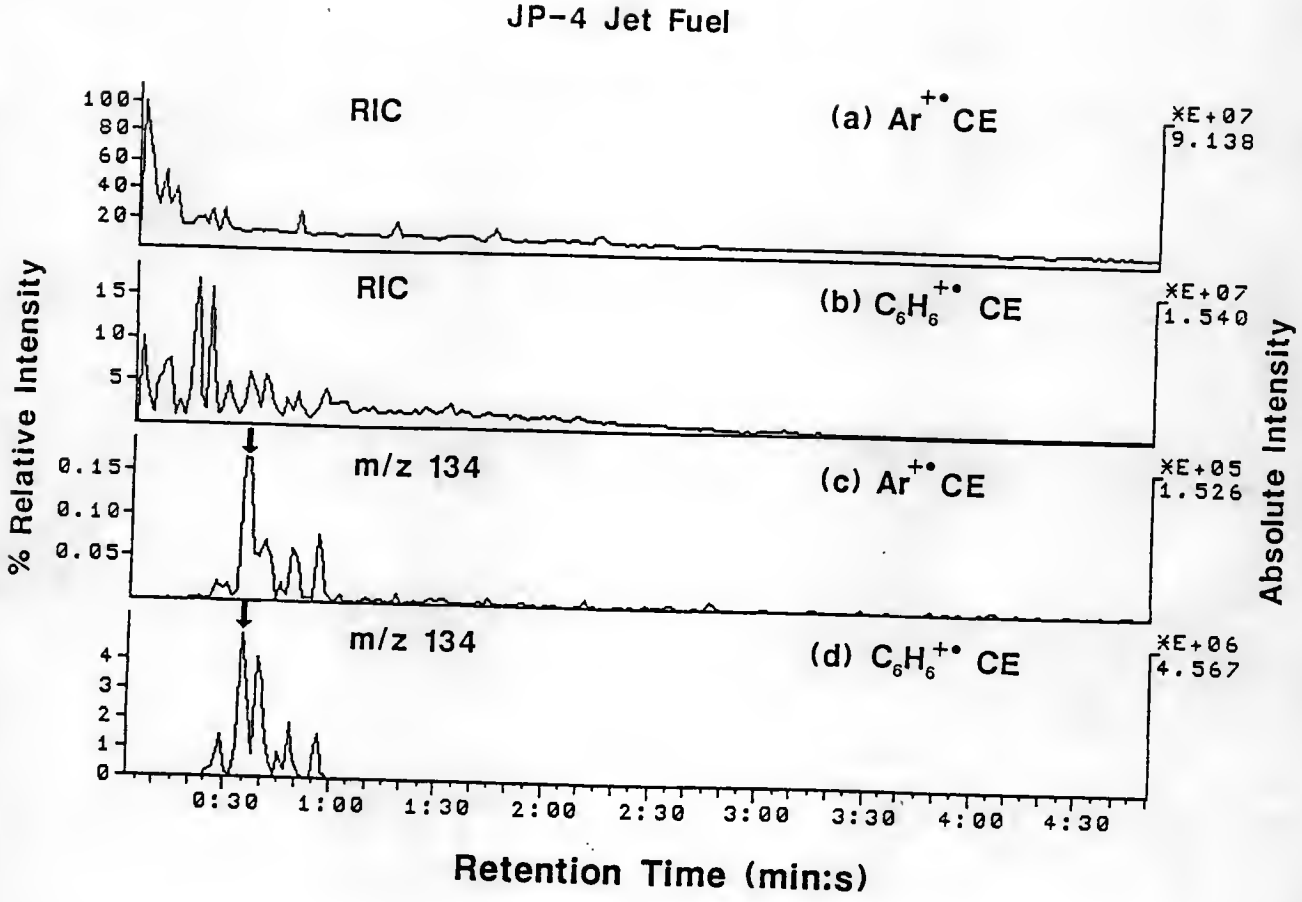

Figure 4.4. GC/MSR/MS chromatogram of JP-4 jet fuel on a 2.1 m column. Reconstructed ion chromatograms: (a) $Ar^{+\bullet}$ CE and (b) $C_6H_6^{+\bullet}$ CE. Mass chromatograms of the m/z 134 $M^{+\bullet}$ of ten-carbon alkylbenzenes: (c) $Ar^{+\bullet}$ CE and (d) $C_6H_6^{+\bullet}$ CE. The arrows indicate where spectra were obtained for Figure 4.5.

show the RICs resulting from $Ar^{+\bullet}$ and $C_6H_6^{+\bullet}$ CE, respectively. The bottom two traces show mass chromatograms for the m/z 134 ion obtained via CE from the two different reactant ions. The m/z 134 ion is the molecular ion produced from a number of different isomers of alkylbenzenes containing a total of ten carbons. Figure 4.5 shows $Ar^{+\bullet}$ and $C_6H_6^{+\bullet}$ CE spectra that were obtained from the chromatogram of Figure 4.4. The points at which these spectra were taken is indicated by the arrows in Figure 4.4. The $Ar^{+\bullet}$ CE spectrum of Figure 4.5 (a) is not easily interpreted, since molecular ions and fragment ions from both aliphatic and aromatic constituents of the jet fuel are produced. However, in the $C_6H_6^{+\bullet}$ CE spectrum of Figure 4.5 (b), only the molecular ion (m/z 134 and the ^{13}C peak at m/z 135) from the alkylbenzene(s) is produced.

Mass-selected ion-molecule reactions can be performed using unique, highly specific reactant ions. Often, selection of reactant gases for chemical ionization in the ion source is limited to low molecular weight gases (e.g., methane, ammonia, etc.), as reactant gases of higher molecular weight (e.g., 100 amu), present in a large excess compared to the sample, can produce ions due to adducts, dimers, and/or fragment ions that obscure the presence of sample ions. With mass-selected reactions, virtually any reactant ion can be used, provided that the reactant ion can be produced in the ion source and does not have the same m/z as the sample under study. An example of a unique reactant ion for chemical ionization is the protonated acetone dimer (m/z 117). A chromatogram of the GC test mixture obtained by MSR with the protonated acetone dimer is shown in Figure 4.6. The 2.1 m FSOT column was used with the 0.9 m FSOT Al-clad transfer line. It was discovered that selection of the m/z 117 ion with Q1 resulted in the production of the protonated acetone (m/z 59) in Q2.

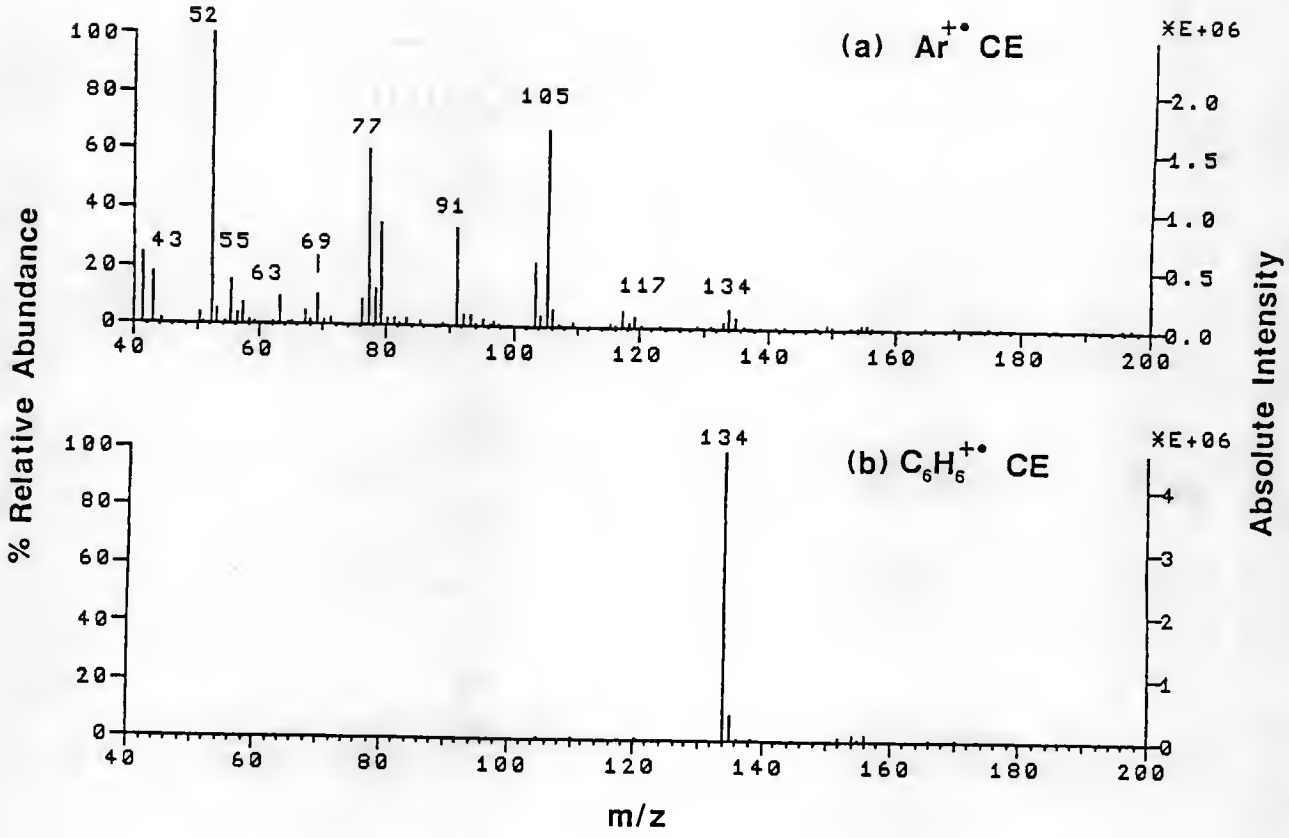

Figure 4.5. Spectra obtained from the chromatogram marked by arrows in Figure 4.4: (a) $Ar^{+\bullet}$ CE and (b) $C_6H_6^{+\bullet}$ CE. Only aromatic species of the jet fuel are ionized with benzene charge exchange, with no fragmentation.

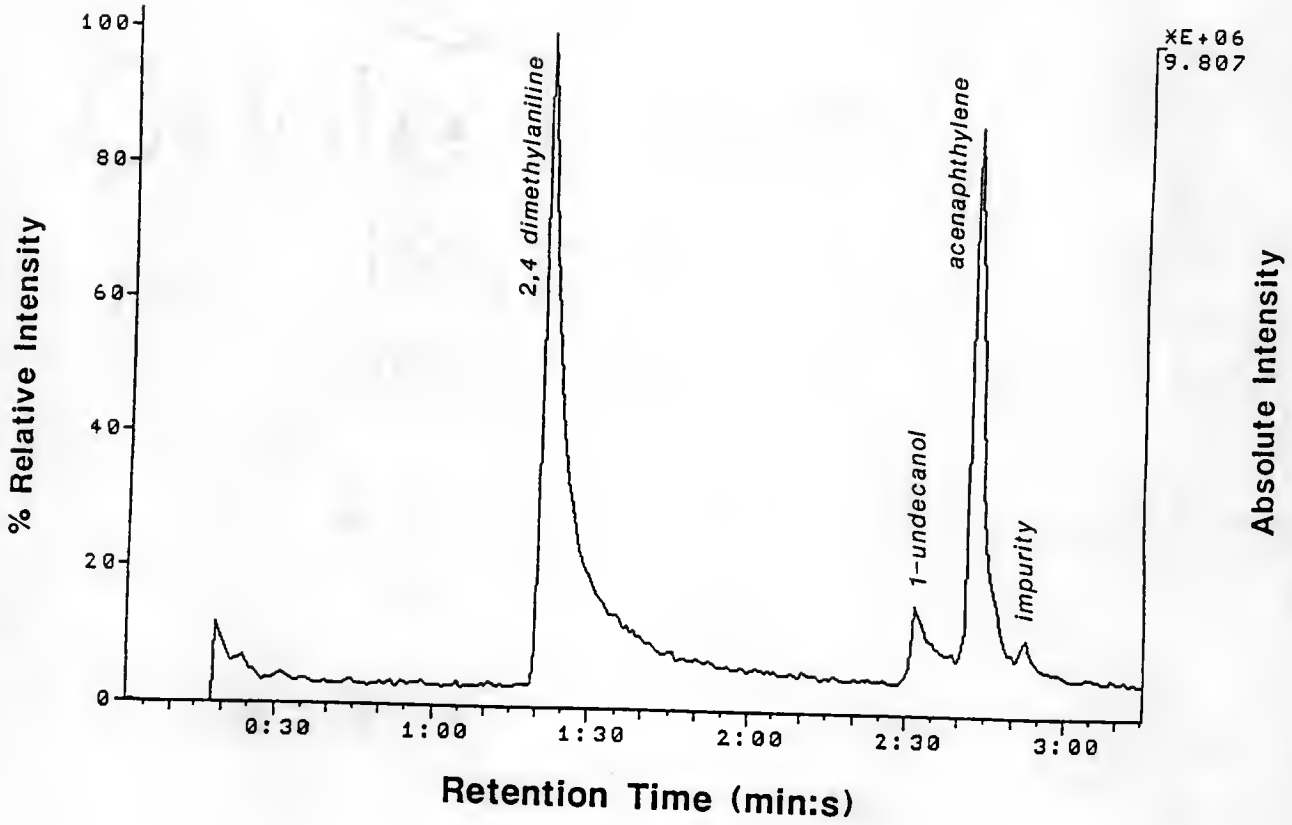

Figure 4.6. GC/MSR/MS chromatogram of GC test mixture obtained with mass-selection of the protonated acetone dimer (m/z 117) reactant ion. The impurity in the mixture is acenaphthene.

The m/z 59 ion, which was the result of metastable decomposition of m/z 117 or CAD of m/z 117 with the helium carrier gas, had an intensity of 30% relative to the m/z 117 ion. Only three of the seven components were ionized by the acetone reactant ions. Spectra for each of the components ionized are shown in Figure 4.7. The acetone reactant ions can react via proton transfer to form $[M+H]^+$ ions if the reaction is energetically favorable. Acenaphthylene and 2,4 dimethylaniline were the only mixture components protonated by the acetone reactant ions. Compounds may also form adducts with protonated acetone to yield $[M+59]^+$ ions or with the protonated acetone dimer to produce $[M+117]^+$ ions. For the components of the GC test mixture, only compounds with hydrogen bonding sites reacted to form the acetone adduct ions (e.g., 2,4 dimethylaniline, and 1-undecanol). Note that 2-chlorophenol, which does have a hydrogen bonding site, was not ionized by the acetone reagent ions. All of the spectra obtained from acetone CI exhibited no fragmentation, as shown in Figure 4.7.

Detection Capabilities of GC/MSR/MS

The ability of GC/MSR/MS to detect low levels of analyte was also examined. Initially, it was not expected that products of ion-molecule reactions in Q2 could be efficiently extracted and mass-analyzed. The products of the ion-molecule reactions have little or no axial kinetic energy when they are formed; thus, the collection efficiency of the product ions is dependent on the extraction capabilities of the Q2 ion exit lens. In fact, Enke et al. have found it necessary to fill and trap ions in Q2 for a period of time and then pulse them out with the Q2 ion exit lens in order to obtain adequate sensitivity [60]. Nevertheless, we

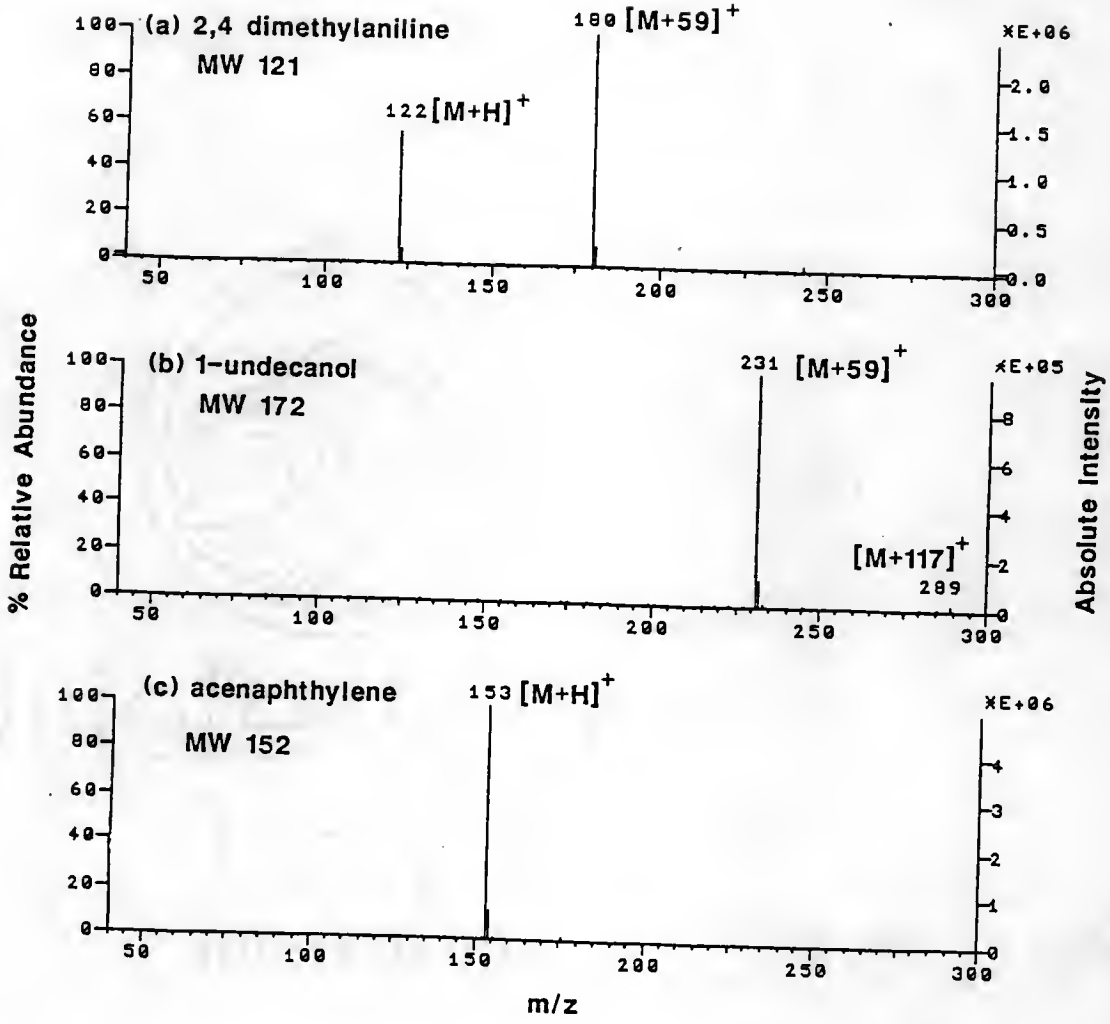

Figure 4.7. Acetone CI spectra obtained from chromatogram in Figure 4.6: (a) 2,4 dimethylaniline, (b) 1-undecanol, (c) acenaphthylene. Only components with hydrogen-bonding sites reacted to form acetone adducts.

have found that detection limits without ion trapping techniques with GC/MSR/MS are comparable or better than those obtained with GC/MS. For these experiments, benzophenone was the analyte and $C_6H_6^{+\bullet}$ was the CE reactant ion. The same column and transfer line, described previously with the acetone CI studies, was used for these experiments. Similar to the spectra of other aromatic compounds studied, benzophenone was ionized by CE with the $C_6H_6^{+\bullet}$ reactant ion to produce only the molecular ion (m/z 182). Figure 4.8 (a) shows the mass chromatogram for the m/z 182 ion of 100 pg of benzophenone for a full scan of Q3 (80-240 amu in 0.5 seconds). Figure 4.8 (b) shows the chromatogram obtained from 15 pg of benzophenone when Q3 was scanned from 181-183 amu in 0.5 seconds. The signal-to-noise ratios (S/Ns) for Figures 4.8 (a) and 4.8 (b) are approximately 9:1 and 30:1, respectively. For comparison, the specifications for the full scan sensitivity of the TSQ70 with GC/MS are quoted as 200 pg for EI with a S/N of 10:1 and 100 pg with methane CI with a S/N of 25:1. Benzene CE experiments were attempted in the ion source for comparison with the GC/MSR/MS results. With benzene CE in the ion source and a full scan of Q1, 600 pg of benzophenone could be detected with GC/MS. However, the spectra obtained from carrying out the reactions in the ion source resembled EI spectra instead of benzene CE spectra (due to mixed-mode ionization), and thus do not represent a valid comparison. The ability to obtain the molecular ion (or pseudo-molecular ion) with little or no fragmentation for an analyte provides the maximum sensitivity for trace analyis. Since such 'soft ionization' is easily performed with mass-selected reactions, the GC/MSR/MS approach provides the opportunity to 'tune' the ionization to obtain the best limits of detection.

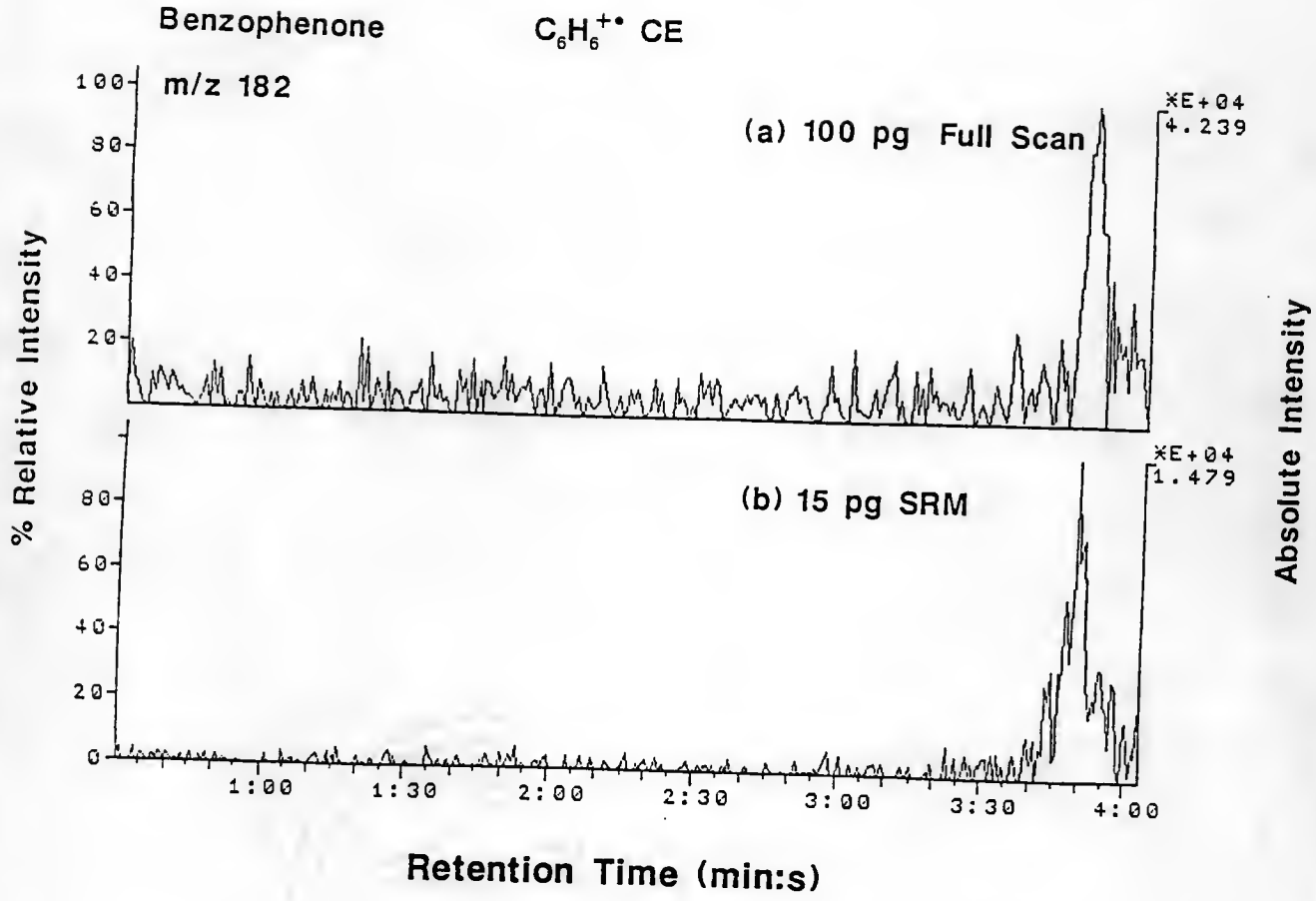

Figure 4.8. Benzene ($C_6H_6^{+\bullet}$) CE mass chromatograms for (a) 100 pg of benzophenone obtained with a full scan of Q3, and (b) 15 pg of benzophenone obtained with selected reaction monitoring (SRM) of the m/z 182 ion.

Chromatographic Integrity

The chromatographic peak shape obtained from introducing the effluent from the GC column into the collision cell is not quite as good as normally obtained when the GC effluent is introduced into the ion source. The tailing of the 2,4 dimethylaniline peak (Figure 4.2 and Figure 4.6) is most likely due to active sites and insufficient heating of the collision cell. Since the temperature of the collision cell was controlled by radiant heating from the vacuum manifold heater, the maximum temperature was limited to 100°C to avoid damage to the electron multiplier. It is expected that better chromatographic peak shape could be obtained if the collision cell were heated separately and to higher temperatures than 100°C. The best peak shape was obtained when a polyimide-clad FSOT column was used as a transfer line (Figure 4.2) instead of the Al-clad column (Figure 4.6). Although the Al-clad column is more easily heated resistively, the polyimide-clad column can be inserted closer to the quadrupole rods of the collision cell without danger of electrical arcing, minimizing sample adsorption on the stainless steel walls of the collision cell. The introduction of the GC column into the collision cell did not appear to reduce ion transmission or decrease the performance of the instrument, and has not required cleaning of any of the ion optics.

Conclusions

A new technique in which samples are introduced via GC into the collision cell of a TQMS system has been described. The GC/MSR/MS approach offers significant advantages over GC/MS for control of the selectivity and energetics of the ionization process. Ionization energies

are readily obtained with the computer-controlled TQMS. Knowledge of the ionization energies is extremely useful when selecting the proper reactant ions for charge exchange experiments. With mass-selected reactions molecular ions, pseudo-molecular ions, or characteristic fragment ions can be obtained depending on the reactant ion and the amount of internal energy deposited during ionization of the sample. The utility of searching charge exchange spectra against EI library spectra has also been demonstrated. When combined with short-column open tubular GC, mass-selected reactions can be used to rapidly screen for particular classes of compounds. For example, the aromatic content of a jet fuel can be investigated with $C_6H_6^{+\cdot}$ charge exchange, without interference from aliphatic constituents. The detection limits of GC/MSR/MS are in the picogram range, which is comparable to those which can be obtained with GC/MS. The simple, resistively-heated GC/MS transfer lines described here should make these types of experiments readily accessible on any TQMS system. With this technique, it should be possible to devise highly specific ion-molecule reactions for mixture analysis.

CHAPTER 5
CHARACTERIZATION AND OPTIMIZATION OF ION TRANSMISSION IN TRIPLE QUADRUPOLE MASS SPECTROMETRY

Introduction

Although the triple quadrupole mass spectrometer (TQMS) is currently in widespread use, the effects of many of the instrumental parameters that govern the performance of these complex ion optical devices have not been well understood. Since the pioneering work of Yost et al. [74], published studies of the nature of the ion optical parameters in triple quadrupole mass spectrometry have been limited to the work of Dawson and coworkers [75-78]. In addition, the TQMS used by Dawson is of unique ion optical design (commercially available as the Sciex TAGA 6000) and does not represent the majority of the TQMS systems in current use. For example, in the Dawson TQMS, there are no interquadrupole focusing lenses and a straight, non-enclosed quadrupole collision cell is utilized. In the commercially-available TQMS used for this work, there are six interquadrupole focusing lenses and a non-linear, enclosed collision quadrupole is used. Perhaps the real impetus for studying these ion optical effects is that the only available data concerning the ion transmission behavior of instruments of this design has been limited to a few presentations given by the instrument manufacturers at conferences [79,80].

The performance of TQMS instruments in terms of sensitivity for quantitative analysis hinges on the ability to obtain efficient ion transmission. For qualitative analysis, relative ion abundances are often

used to determine molecular structure or in studies concerning the energetics of fragmentation processes. Therefore, it is important to be able to obtain optimum and uniform transmission of ions (i.e., no mass discrimination) over the entire mass range of interest. Ion optical parameters that result in mass discrimination are said to exhibit mass-dependent behavior. It is important to understand the origins of these mass dependencies and to correct for them whenever possible. Martinez has discussed the importance of eliminating mass discrimination if dynamically-correct MS/MS spectra are to be obtained [81]. Recently, there has been a suggestion for the implementation of a standard MS/MS spectral library [82]. This idea has been somewhat controversial, since MS/MS spectra are highly dependent on the numerous operating parameters and the ion optical design of the instrument used. This has led to a recent round-robin investigation of a variety of instruments in different laboratories to determine the feasibility of such a spectral library.

In this chapter, the ion transmission characteristics of a computer-controlled TQMS are reported. In particular, the parameters which result in mass-dependent behavior, as well as the origins and strategies for minimizing these effects, have been studied. Characterization of ion transmission in the MS/MS scan modes, including the effect of using high (>50 eV) parent ion axial kinetic energies, is also presented.

Experimental Section

Instrumentation

The instrument that has been used for these characterization and optimization studies is a Finnigan MAT TSQ70. This instrument has proven to be ideal for studies of this type, since all instrumental parameters

are under microprocessor control. In fact, with older TQMS instruments, many of the experiments that have been performed would either not be possible or would have been too time-consuming to carry out. The TSQ70 is controlled by six different single board controllers, each of which has its own microprocessor. User interaction with the instrument is through a unique procedural language known as the Instrument Control Language, or ICL. ICL procedures (or programs) can be written that allow any instrument task to be performed under computer control. Another advantage of the ICL is that it is simple to use but highly structured (much like the commonly used BASIC computer language). As a result, the capability of real-time decision making exists with the ICL, which allows the instrument to react to incoming data.

Shown in Figure 5.1 is a diagram of the mass analyzer assembly of the TSQ70. As shown in the figure, the ion optics consist of three quadrupoles (Q1, Q2, and Q3) and eleven focusing lenses (L11-L42) mounted on an optical rail. Nine of the eleven lenses (L11-L33) make up 3 different three-element lens sets, known as einzel lenses [83]. In an einzel lens, the first and third elements are usually held at similar potentials with the center lens at some more negative potential (for positive ions). This results in a focused ion beam with similar kinetic energy on either side of the einzel lens. Typical voltages for a three-element einzel lens set of the TSQ70 (e.g., L11, L12, L13) for positive ions are -10 V, -100 V, and -10 V, respectively. There are two other lenses (L41 and L42) which do not make up an einzel lens, but are pre-detector lenses that serve to focus the ions exiting Q3 onto the ± 5 kV conversion dynodes; the secondary ions (or electrons) produced at the conversion dynodes are detected by the electron multiplier (EM). All of

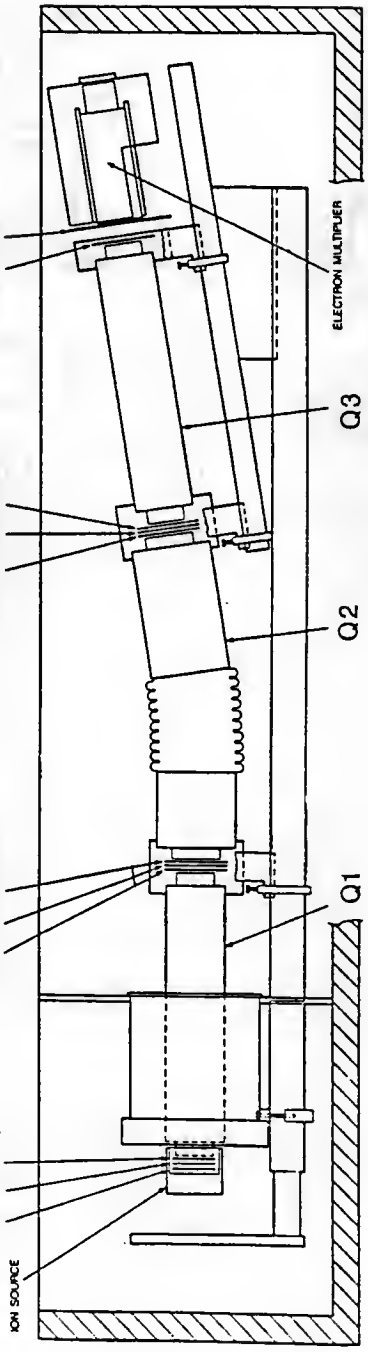

Figure 5.1. Schematic diagram of mass analyzer assembly of TSQ70 triple quadrupole mass spectrometer.

the lenses except lens L42 optimize at negative voltages for positive ions and at positive voltages for negative ions. Lens L42 has two square ion entrance holes that are in line with the conversion dynodes, instead of one round hole in the center of the lens. This lens behaves atypically in that it optimizes at positive voltages for positive ions and negative voltages for negative ions, due to its shape as well as its placement in front of the ± 5 kV conversion dynodes.

The first and third quadrupoles (Q1 and Q3, respectively) are mass filters and can be operated in the mass-selective (RF/DC) mode or can be set to pass a wide range of masses (RF-only), depending on the scan mode selected. The mass filters are used to obtain a mass spectrum or for the mass-selection of ions for MS/MS experiments. Regardless of the scan mode used, Q2 is not a mass filter, but simply serves as an ion transmission and focusing device (RF-only) during single MS experiments or as the collision (or reaction) region for MS/MS experiments. One of the unique features of the ion optical design of the TSQ70 is that it utilizes a non-linear second quadrupole (Q2) with an axis that is bent at an angle of approximately 15°. This design has been reported to offer improved signal-to-noise ratios over the conventional linear second quadrupole, particularly when used with fast atom bombardment (FAB) ionization [79]. In the conventional straight axis Q2 design, excited neutrals, photons, or X-rays produced in the ion source can traverse the length of the instrument axis and can strike surfaces in the vicinity of the detector. This can result in the production of secondary ions or electrons, producing a significant amount of noise. The bent design of Q2 reduces the amount of neutrals (and thus secondary ions) reaching the detector and improves signal-to-noise ratios. However, the bent geometry also results

in some interesting ion optical effects, which are addressed in this chapter.

One of the unique capabilities of the TSQ70 is that the ion optical parameters may be varied with mass within a single mass spectral scan such that the transmission of ions of different m/z can be optimized without compromise for a particular mass or range of masses. This turns out to be particularly advantageous in avoiding any mass discrimination that may be present in the ion optics. In order to optimize the lenses with mass, the lens voltages at specific points along the mass range are optimized. Lens potentials for the other masses are automatically interpolated between the set values. The result is called a tune table, which is a plot of lens voltage (or other ion optical parameter) vs. m/z. The concepts of mass-dependent tuning and tune tables are demonstrated in Figure 5.2. In Figure 5.2 (a), the voltage for lens L13 is held constant over the entire mass range; this is a "flat" tune table. In contrast, Figure 5.2 (b) depicts a typical tune table that would be obtained after mass-dependent optimization of lens L13, in which optima at different masses have been determined. As the mass spectrometer scans, the voltage of lens L13 follows the curve such that optimum ion transmission is obtained over the entire mass range of interest. These tune tables can be created for any of the ion optical parameters of the instrument. However, mass-dependent optimization is normally performed for only the parameters found to be mass-dependent. All of the other tune tables are left flat.

An additional advantage of the computer control is the speed with which the ion optical parameters can be optimized. Optimization which

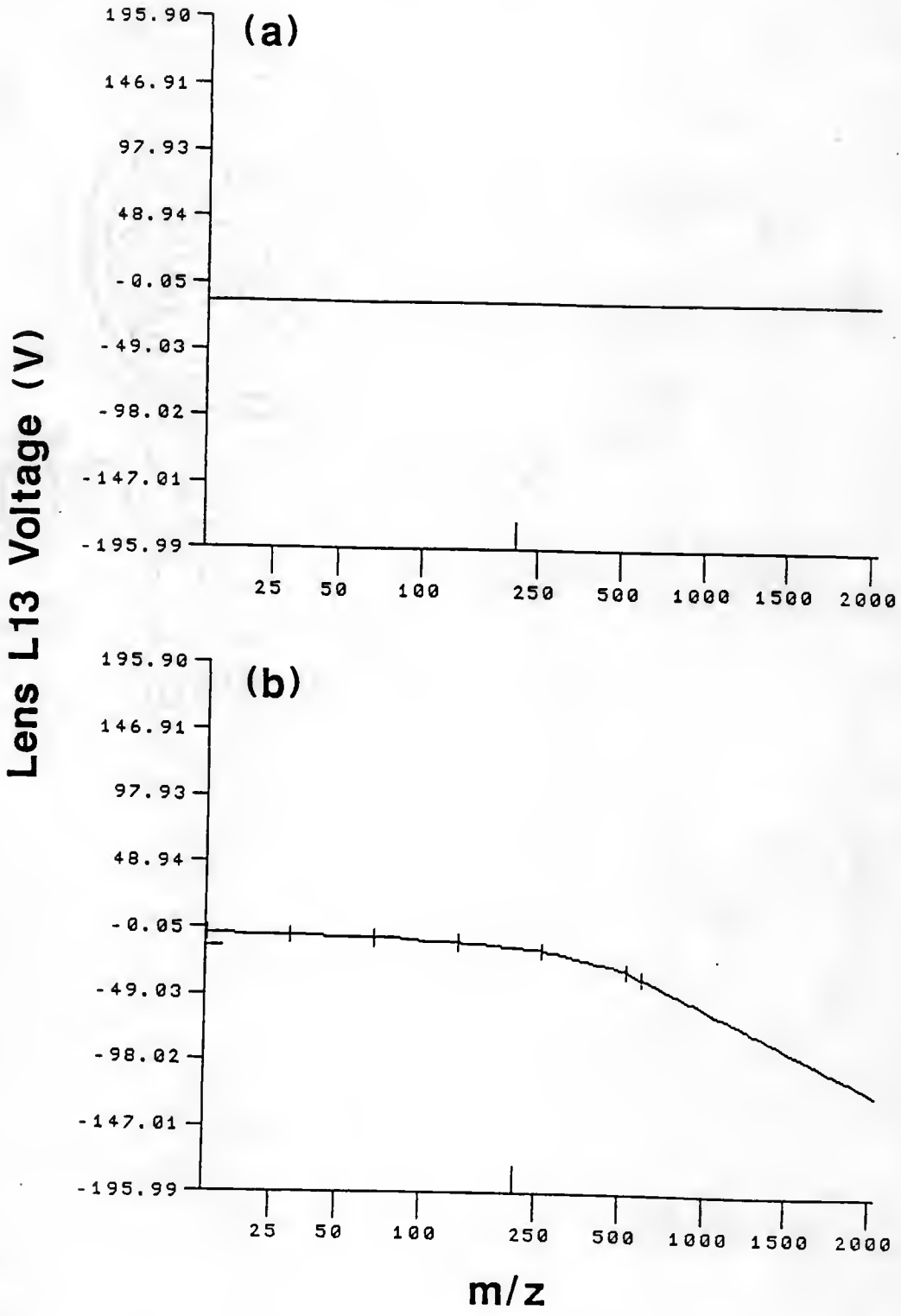

Figure 5.2. Examples of tune tables for lens L13 illustrating: (a) flat tune table in which lens voltage is constant over entire mass range, and (b) tune table in which lens voltage is varied with the mass scan to obtain optimum transmission over the entire mass range of interest.

took hours to perform on manually-controlled instruments can be performed under computer control in a matter of minutes. One innovation of this instrument that allows for such rapid optimization is that a lens voltage digital-to-analog converter (DAC) may be varied over its full range in the same amount of time that is normally required to execute one mass spectral scan. In this mode of operation, known as "DAC scan", one analyzer is set to pass a chosen m/z and the voltage on a particular lens is varied (or scanned) over the entire range. As a result, a plot of ion intensity vs. lens voltage is obtained and the optimum voltage can be determined in less than one second.

Procedures

For all of the lens characterization studies performed, a common mass calibration compound (perfluorotributylamine or PFTBA) was used. PFTBA yields a wide mass range of positive ions (m/z 31 - m/z 614) with electron ionization and is conveniently leaked into the ion source. In cases where the mass dependency of a particular lens was being investigated, all of the other lenses were held at constant, near optimum voltages, and not varied with mass. All lens voltages reported are referenced to the ion source potential, which is at ground.

Argon was used instead of PFTBA for the experiments designed to study the transmission of ions as a function of collision energy or RF voltage during MS/MS scan modes. Argon was chosen since it could not undergo collisionally-activated dissociation (CAD). The transmission of ions in the mass-selected reaction mode (described in Chapter 4) was also studied. In these experiments PFTBA was introduced into the center quadrupole collision cell, while reactant ions were mass-selected by the first

quadrupole. Ion transmission curves were obtained by plotting the intensity for selected m/z's over a wide range of lens potentials (typically 200 V) or RF voltages. With the computer-controlled TSQ70 and the ICL, a transmission curve for a number of different masses (typically 4) can be acquired in a matter of minutes.

Results and Discussion

Mass-Dependent Optimization

The presence of mass dependencies in the ion optics of single quadrupole mass spectrometers has long been known [84]. However, the effects of these mass dependencies on the transmission of ions and the resulting mass spectra have never been easily elucidated. The use of computer-controlled instrumentation like the TSQ70 has allowed for more rapid characterization and better understanding of these phenomena.

Ion optics theory predicts that all ions accelerated from a specific point in space through an electrostatic lens will follow the same trajectory regardless of the masses of the ions [83]. Thus, mass dependency does not come from the electrostatic lens per se, but rather is the result of non-idealities introduced from other forces. It was the object of this work to determine which lenses exhibited mass dependencies, and by observing trends in the data, to elucidate the origins of these mass dependencies. After determining which lenses were mass-dependent it was then possible to adopt the proper strategies for minimizing these effects. With the TQMS used here, the lenses which were found to be mass-dependent could be optimized over the entire mass range. The capability of mass-dependent tuning significantly improves the performance, as will be discussed below.

A well-behaved (ideal) lens has very similar transmission curves for ions of different m/z; the lens voltage that yields the maximum transmission (i.e., the optimum lens voltage) is therefore the same for ions of different m/z. In other words, no mass dependency is observed with an ideal lens. Figure 5.3 shows examples of typical transmission curves for two different lenses in the normal Q1 mass spectral (Q1MS) mode. Figure 5.3 (a) shows the transmission curve for a well-behaved lens (L31) (refer to Figure 5.1 for the placement of this lens and other lenses in the system). These curves demonstrate typical transmission curves obtained (for positive ions) for the first lens of an einzel lens set: maximum transmission at some low (negative) voltage, with decreased transmission at higher negative voltages due to defocusing of the ion beam, and transmission rapidly dropping to zero at positive voltages. In contrast, Figure 5.3 (b) shows the ion transmission curves for a mass-dependent lens (L13). Note that in (b) of this figure there are discrete optimum lens voltages for ions of different m/z; thus, setting the lens voltage at any one of these voltages will reduce the transmission of the other ions. One interesting discovery was that some of the lenses were found to be mass-dependent only in certain scan modes. For example, Figure 5.4 (a) shows the mass-dependent behavior for lens L42 in the normal Q3 mass spectral (Q3MS) scan mode. However, the same lens was found to be non-mass-dependent in the Q1MS scan mode, as shown in Figure 5.4 (b).

After a thorough study of the ion optics, some generalizations could be made. In the single MS scan modes (i.e., Q1MS or Q3MS), the lenses in proximity to the mass-analyzing quadrupole (i.e., the quadrupole carrying both RF and DC voltages) were found to be mass-dependent. In particular,

Figure 5.3. Ion transmission as a function of lens potential (in volts) for two different lenses in the Q1MS scan mode: (a) non-mass-dependent lens L31, (b) mass-dependent lens L13.

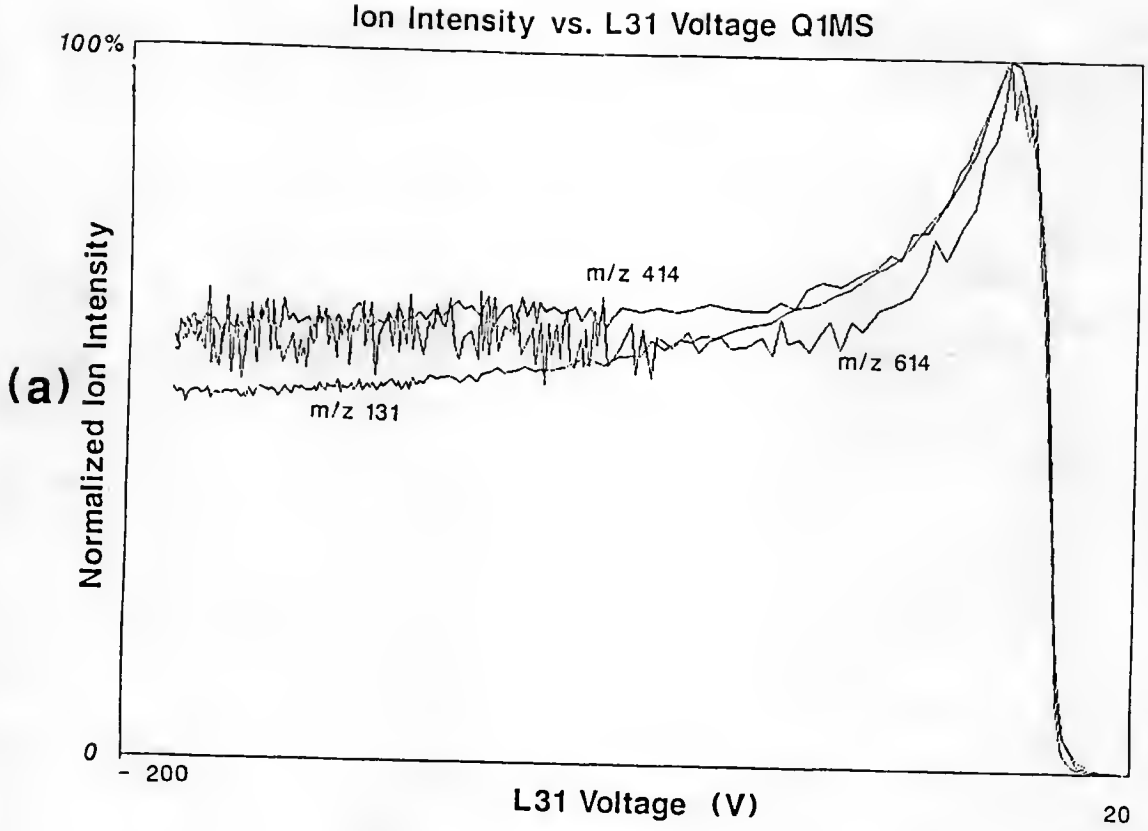
Ion Intensity vs. L31 Voltage Q1MS
100%
0
Normalized Ion Intensity
(a)
m/z 414
m/z 614
m/z 131
- 200
L31 Voltage (V)
20

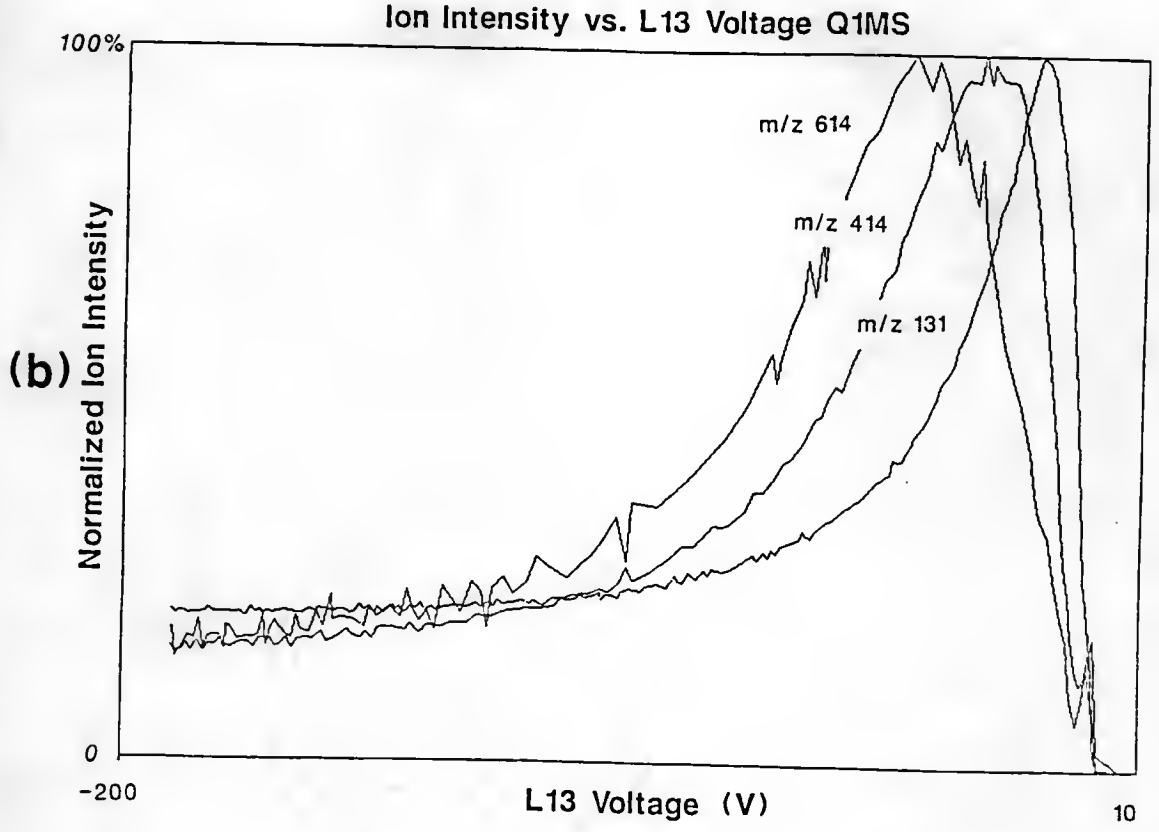
Ion Intensity vs. L13 Voltage Q1MS
100%
0
Normalized Ion Intensity
(b)
m/z 614
m/z 414
m/z 131
-200
L13 Voltage (V)
10

Figure 5.4. Ion transmission as a function of lens L42 potential (in volts) illustrating: (a) mass-dependent behavior in the Q3MS scan mode, and (b) ideal behavior in the Q1MS scan mode.

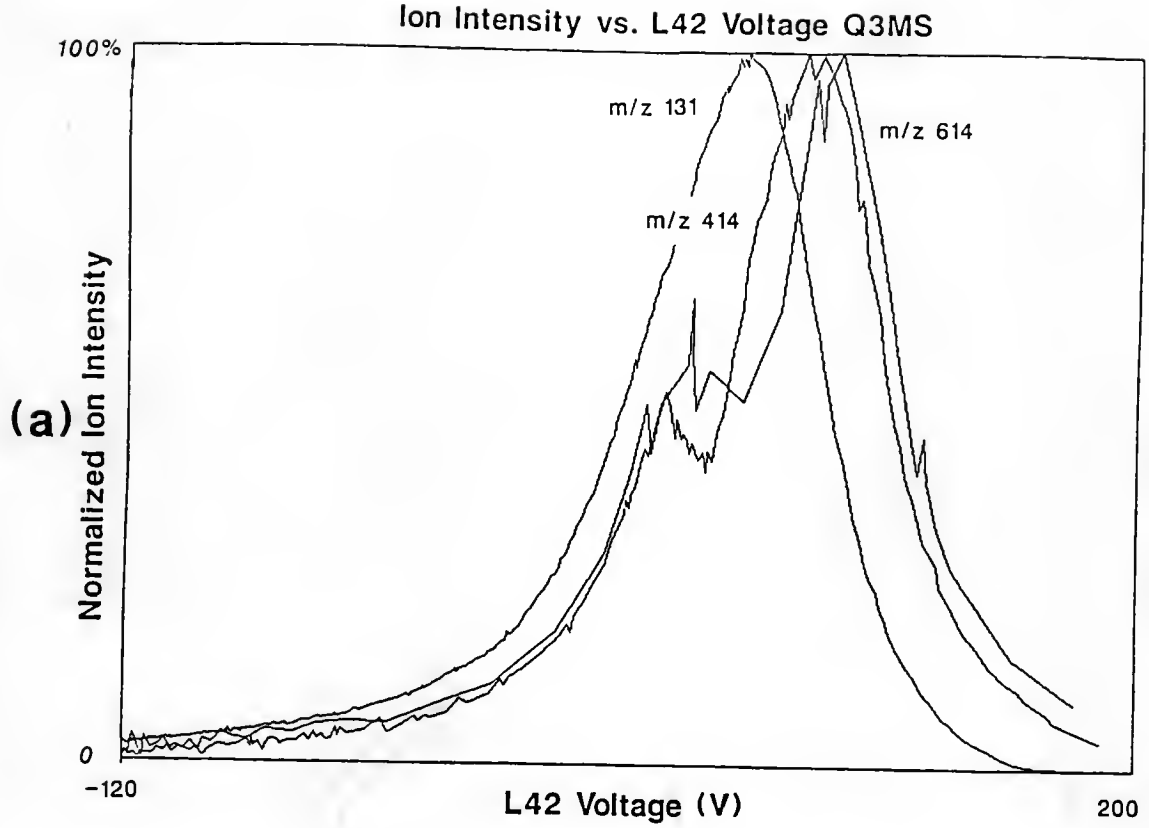
Ion Intensity vs. L42 Voltage Q3MS
100%
m/z 131
m/z 614
m/z 414
(a)
Normalized Ion Intensity
0
-120
L42 Voltage (V)
200

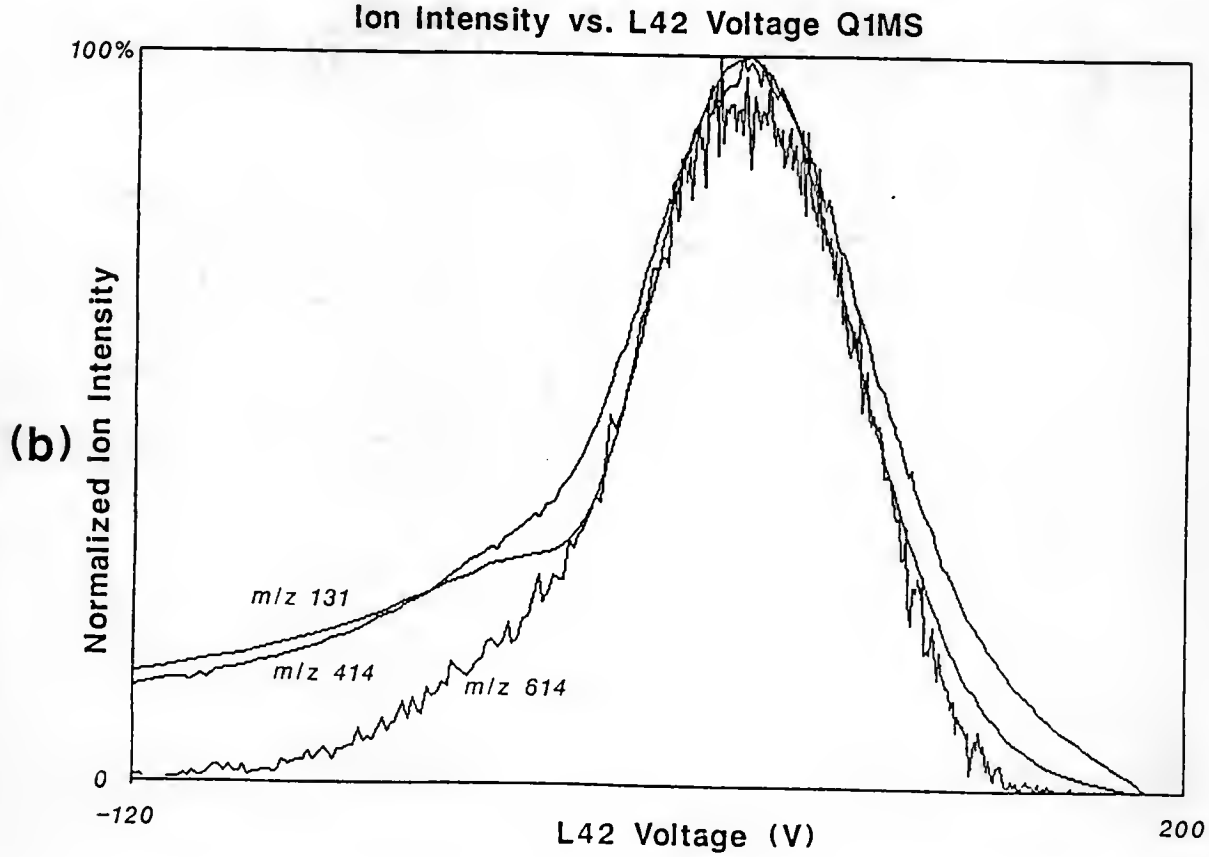
Ion Intensity vs. L42 Voltage Q1MS
100%
m/z 131
m/z 414
m/z 614
(b)
Normalized Ion Intensity
0
-120
L42 Voltage (V)
200

for Q1MS, lenses L12, L13, L21, and L22 are mass-dependent; while for Q3MS, the mass-dependent lenses are L32, L33, L41, and L42. This appears to be the case regardless of the ionization method used. For instance, positive chemical ionization (PCI) and electron capture negative CI (ECNCI) were studied and the same lenses were found to be mass-dependent. Since EI and CI require different ion volumes (the CI ion volume has a smaller ion exit aperture), the optimum lens voltages were found to be different for EI, PCI and ECNCI; therefore, the best results are obtained (i.e., maximum sensitivity) if the lens voltages are optimized for each ionization method that is to be used.

Experiments were performed in order to compare the results obtained with non-mass-dependent and mass-dependent tuning for the Q1MS scan mode. For both mass-dependent and non-mass-dependent optimization, initial voltages of -10 V, -100 V, and -10 V were used for all of the three-element einzel lens sets; initial voltages of -10 V and +50 V were used for the pre-detector lenses, L41 and L42, respectively. For non-mass-dependent tuning, all of the lenses were then optimized only at m/z 219. The DAC scan method was used to determine the lens voltage that yielded the maximum ion signal for m/z 219 for each lens, starting with lens L11 and ending with lens L42. For mass-dependent optimization, the lenses which were found to be non-mass-dependent in the Q1MS scan mode (L11, L23, L31, L32, L41, and L42) were optimized with DAC scan only at m/z 219. Then, the lenses which were previously determined to be mass-dependent in the Q1MS scan mode (L12, L13, L21, and L22) were each optimized (one m/z at a time) at m/z 69, m/z 219, m/z 414, and m/z 502. An example of a typical tune table that was obtained with mass-dependent optimization is shown in Figure 5.2 (b). A significant improvement in sensitivity was

observed when mass-dependent optimization was performed, as shown by the QlMS electron ionization (EI) spectra of PFTBA in Figure 5.5. Spectrum (a) of Figure 5.5 was obtained after the non-mass-dependent tuning method was used, while the spectrum in Figure 5.5 (b) was acquired after mass-dependent optimization had been performed. Both spectra are normalized to the full scale intensity of spectrum (b), and both are enlarged by a factor of 10 beyond m/z 325. Note that the ion intensity is increased by 30% at m/z 69 and by 42% at m/z 502 when mass-dependent optimization was performed. Optimization at only m/z 219 caused this ion to be the base peak in (a), while m/z 69 was the base peak in (b). The ion intensities for m/z 219 are essentially the same in both cases. Clearly, mass-dependent optimization is preferred, since optimization at a single mass will cause the sensitivity to be compromised at other masses.

There has been some concern that mass-dependent optimization would not yield the correct ion intensity ratios for qualitative EI spectra. This is of particular concern, since EI spectra are used for comparison with standard library spectra. Indeed, the correct (and natural) ion abundances are obtained only when there is no mass discrimination in the ion optics. Since mass-dependent tuning provides maximum transmission for each m/z, and therefore effectively removes any discriminating character in the ion optics, the natural abundances of the ions are obtained. Moreover, ion intensity ratios are affected by other parameters such as ion source temperature and mass analyzer transmission characteristics; therefore, any attempt to defocus a lens to obtain the 'correct' ratios is not recommended. Although these studies have been performed on a specific TQMS instrument, it is expected that the same mass-dependencies would be observed with other instruments of similar ion optical design.

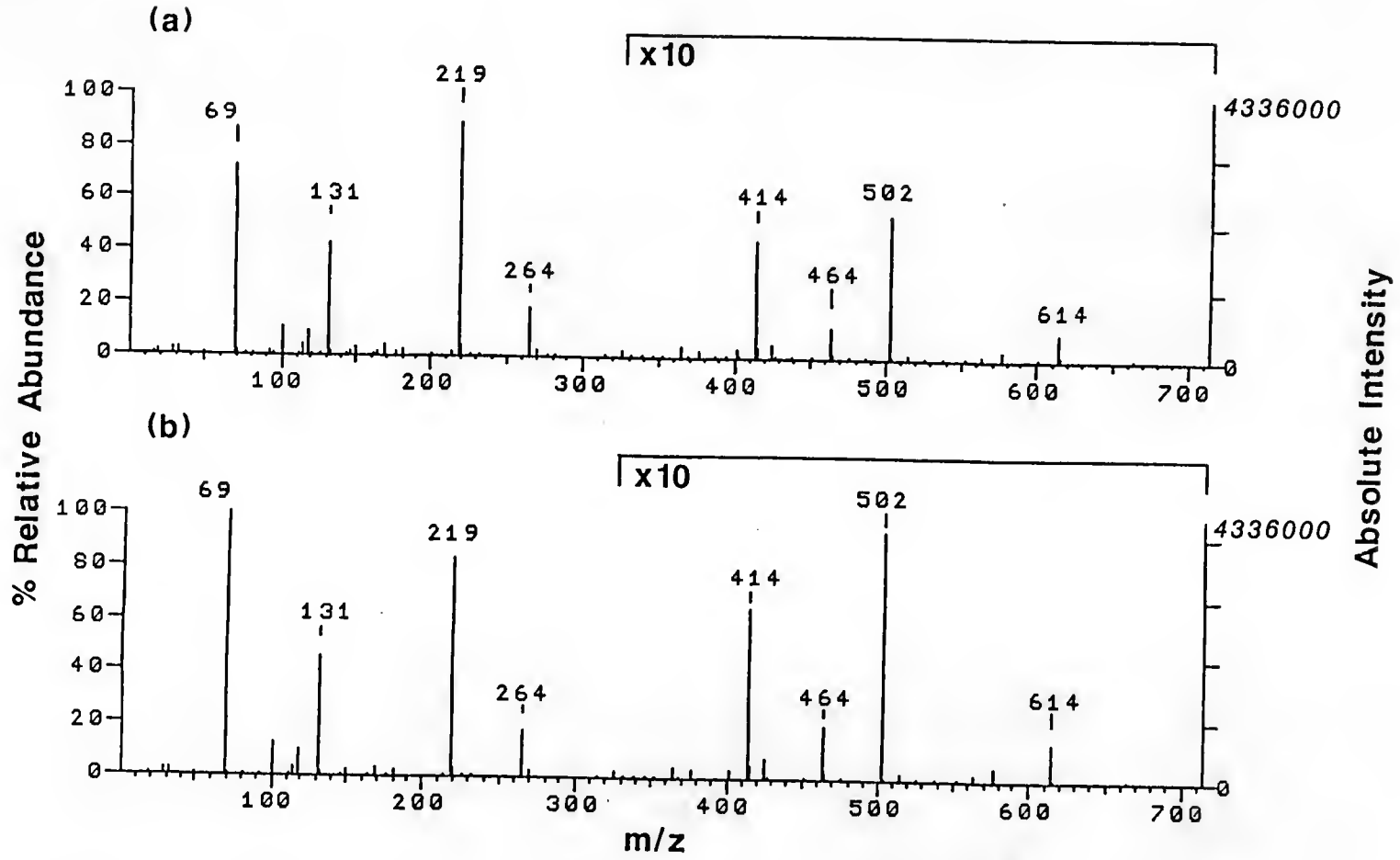

Figure 5.5. EI mass spectra of PFTBA: (a) lenses were optimized for transmission of only m/z 219 (i.e., non-mass-dependent tuning), (b) mass-dependent lens optimization was used.

Preliminary results obtained by a coworker on a Finnigan MAT TSQ45 system in this laboratory have suggested that this is the case.

Quadrupole Mass Filters

Operation. The basic operating principles of quadrupole mass analyzers have been presented in a number of excellent review articles [76,85-87]. The detailed characteristics of performance of these devices are discussed in a book edited by Dawson [84]. In order to explain some of the characteristic behavior of the ion optics, some basic theory of operation of quadrupole mass filters is reviewed here.

In a quadrupole mass filter, RF and DC voltages are applied to a set of four hyperbolic rods (one pair of rods being of opposite polarity to the other pair). These potentials are all referenced to a DC voltage corresponding to the quadrupole offset voltage which defines the axial ion kinetic energy in the quadrupole. The motion of ions within quadrupoles is described mathematically by a second-order differential equation known as the Mathieu equation [84].

$$\frac{d^2u}{d\xi^2} + (a_u - 2q_u \cos 2\xi)u = 0 \qquad (5.1)$$

The solutions of this equation define the position of an ion at any time within the device, where u is a position-dependent parameter (representing the x or y displacement of an ion) and ξ is a time-dependent variable. Ion trajectories within a quadrupole are either stable or unstable depending on the values of the Mathieu parameters 'a' and 'q'. The Mathieu parameters are given by

$$q_u = \frac{4V_{RF}e}{mr_o^2\omega^2} \tag{5.2}$$

$$a_u = \frac{8V_{DC}e}{mr_o^2\omega^2} \tag{5.3}$$

where V_{RF} is the zero-to-peak RF voltage of angular frequency ω, V_{DC} is the DC voltage, e is the charge and m is the mass of the ion, and r_o is the inscribed radius of the quadrupole. An ion is said to have stable trajectories if its excursions in the x or y directions do not exceed the defined boundaries of the applied field. Conversely, unstable trajectories represent conditions in which the displacement of the ion increases without bound until it is eventually ejected and is not transmitted through the device. Consequently, a stability diagram can be drawn (shown in Figure 5.6) where 'a' and 'q' are plotted on the y and x axes, respectively. Ions that have Mathieu parameters within the triangular envelope of the stability diagram have stable trajectories; those outside of the area are unstable. When operating as a mass filter, RF and DC voltages are applied such that only a narrow range of masses (usually one) have stable trajectories at any one instant in time, and are transmitted to the detector. This is achieved by using a scan line that slices through the very tip of the stability diagram. The range of masses which will be stable is determined by the DC/RF ratio (i.e., the slope of the scan line). In order to obtain a scan over a range of m/z's, the RF and DC voltages are increased linearly with time (at constant DC/RF) so that ions of increasing m/z are brought within the narrow window of stability. Mass resolution is increased (with a reduction of the

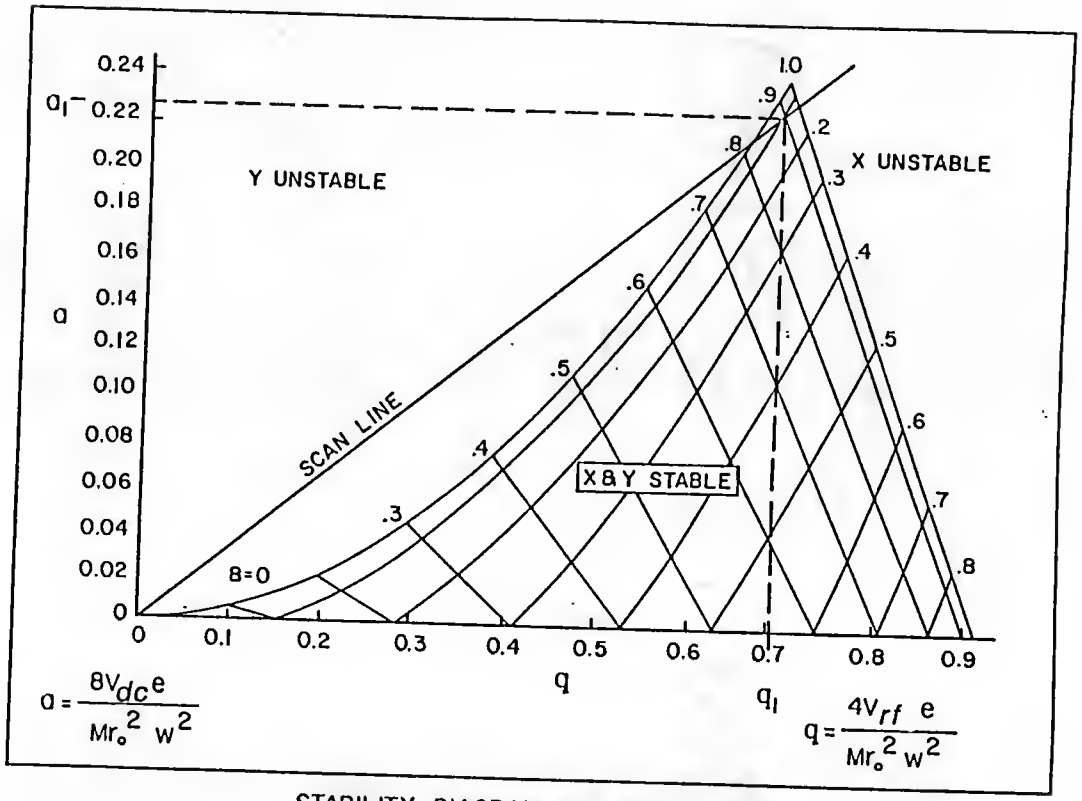

STABILITY DIAGRAM FOR BOTH X & Y

Figure 5.6. Stability diagram for a quadrupole mass filter (from reference [90]).

number of ions transmitted) by moving the scan line closer to the tip of the stability region.

Origins of mass dependencies. As stated previously, only the lenses near mass filters exhibited mass-dependent behavior. Lenses next to RF-only quadrupoles were not found to be mass-dependent. The mass dependencies in the lenses that are observed with this TQMS can most likely be attributed to the fringing fields present at both ends of the mass filters. In the TSQ70, the fringing fields at both ends of the quadrupole mass filter may penetrate the immediate lens regions, thereby affecting the efficiency with which ions may be transmitted. It has previously been shown that fringing fields can cause ions to have unstable trajectories as they attempt to enter or exit the quadrupole, which can significantly reduce the number of ions transmitted [76]. A number of alternative ion optic designs have been employed in attempt to circumvent the fringing field problem. One TQMS has been designed without focusing lenses between adjacent quadrupoles [77,78]. Instead, the rod sets are closely coupled such that the ions never leave one quadrupole field before entering the next. The effects of fringe fields in single quadrupole instruments have been shown to be reduced if the ions are allowed to experience the RF field before experiencing the DC field. This has been accomplished with either a short RF-only quadrupole [88] or dielectric tube [83,89] placed at the entrance of the mass filter.

Alternatively, with the computer-controlled TQMS used in this work, the effects of the fringing fields can be minimized with mass-dependent optimization of the lenses. Since the lens voltages may be changed as a function of mass, all ions may be transmitted with equal efficiency. Ion transmission in quadrupole mass spectrometers has been shown to be a

function of the initial position and velocity of the ions as they are injected into the mass filter [76,84]. The initial conditions that result in transmission define the ion acceptance of the mass filter. Theoretical calculations have demonstrated that the optimum acceptance for an RF/DC mass filter is obtained if the ions spend approximately two RF cycles in the fringe field, assuming that the ion source/lens system emittance is well-matched to the mass filter acceptance [76,84]. If ions of different mass are injected into the quadrupole at constant energy, all ions would not spend the optimum time in the fringe field, which would result in mass discrimination. For this reason, an optimum ion velocity for different masses, instead of an optimum kinetic energy, is expected in cases where fringing fields are present. The velocity (v) of an ion is given by

$$v = (2E/m)^{1/2} \tag{5.4}$$

where E is the kinetic energy and m is the ion mass. Thus, as the mass is increased, the kinetic energy must increase accordingly if the optimum ion velocity is to be maintained. Indeed, most quadrupole mass spectrometers include a programmed ion energy which permits the quadrupole offset voltage (and hence the ion kinetic energy through the mass filter) to be increased (most often linearly) with mass, in order to increase transmission of high-mass ions [76,90]. Unfortunately, increasing the ion velocity through the quadrupole has the undesired effect of decreasing the number of RF cycles the ion experiences and hence the resolution [76]. Programming the lens potentials with mass, in contrast, can increase the ion velocity of higher mass ions through the fringing fields without affecting their velocity within the quadrupole. The calculation of an

optimum ion velocity is in agreement with the experimental results obtained for mass-dependent lenses. In all cases, mass-dependent lenses required higher absolute lens potentials and hence higher kinetic energies for optimum transmission of higher mass ions. Table 5.1 shows the optimum lens potentials and the calculated optimum ion velocities for ions of different masses obtained with mass-dependent lens L13 in the QlMS mode. As shown in the table, the optimum lens voltage increases, but the optimum ion velocity remains essentially constant. With a relatively low Q1 offset (ca. -2 V), one can roughly estimate the ions' average velocity between L13 and Q1 as half the velocity calculated at the L13 potential; hence, the optimum average velocity is ~1.7 x 10^3 m/s. Given an approximate distance of ~0.5 mm between L13 and Q1, this corresponds to a transit time of ~0.85 μs, or approximately 1 cycle of the 1.2 MHz RF. This is in good agreement with Dawson's theoretical optimum of 2 RF cycles [76], considering the rough estimates that were made for the average ion velocity and the distance between L13 and Q1. The low-mass ions (m/z 69 and m/z 131) have slightly higher optimum velocities, which is not fully understood. However, this may be attributed to an additional energy spread induced by the fringing fields. It is expected that computer simulation of the ion trajectories with a program such as SIMION [91] may eventually help to elucidate this behavior.

Ion Transmission Characteristics of the Center Quadrupole

Low mass cut-off. In triple quadrupole mass spectrometry the center quadrupole operates in the RF-only mode. It is a popular misconception that an RF-only quadrupole is capable of passing all masses simultaneously. However, transmission of ions through an RF-only

Table 5.1. Optimum lens potentials and ion velocities for various masses obtained with mass-dependent lens L13 in the QlMS mode.

m/z	Optimum Lens Potential (V)	Optimum Ion Velocity (m/s)
69	-7.5	4.6×10^3
131	-10.4	3.9×10^3
219	-14.0	3.5×10^3
414	-23.0	3.3×10^3
502	-29.5	3.4×10^3
614	-36.5	3.4×10^3

quadrupole is subject to the same constraints as an RF/DC quadrupole. The difference is that since the applied DC voltage is zero, a = 0, and the scan line follows the x-axis (q-axis) of the stability diagram in Figure 5.6 [80,92]. Thus, for an ion to be stable it must have a value of 'q' between 0 and 0.908. Since there are a range of q's over which a particular mass is stable, it follows from eq 5.2 that there is also a range of RF voltages over which a particular mass is stable. This means that proper choice of the RF level is critical to avoid low mass cut-off. Low mass cut-off occurs when the RF voltage has been set high enough such that ions below a certain m/z have q's greater than 0.908, and are not transmitted. In addition, since q is constrained to values between 0 and 0.908 for stable trajectories, it can be seen from eq 5.2 that the range of RF voltages allowing stable ion trajectories decreases linearly with the mass of the ion.

Figure 5.7 is a demonstration of the principles discussed above. In this experiment, ion intensities for the daughters from the collisionally-activated dissociation (CAD) of m/z 219 from PFTBA are plotted against Q2 RF voltage. As shown in the figure, there is an optimum RF voltage for the transmission of each ion of different m/z; thus, the Q2 RF voltage is a mass-dependent parameter as well. Also note that the transmission curves become more narrow with decreasing m/z as discussed above. This brings forth a fundamental limitation of the second quadrupole. In single MS experiments (i.e., Q1MS or Q3MS), only one m/z is passed through Q2 at any one instant in time. Thus, the Q2 RF voltage can be optimized and programmed with mass to obtain the maximum transmission of ions of each different m/z. However, during MS/MS scans, Q2 is required to simultaneously transmit parent ions, as well as daughter ions of different

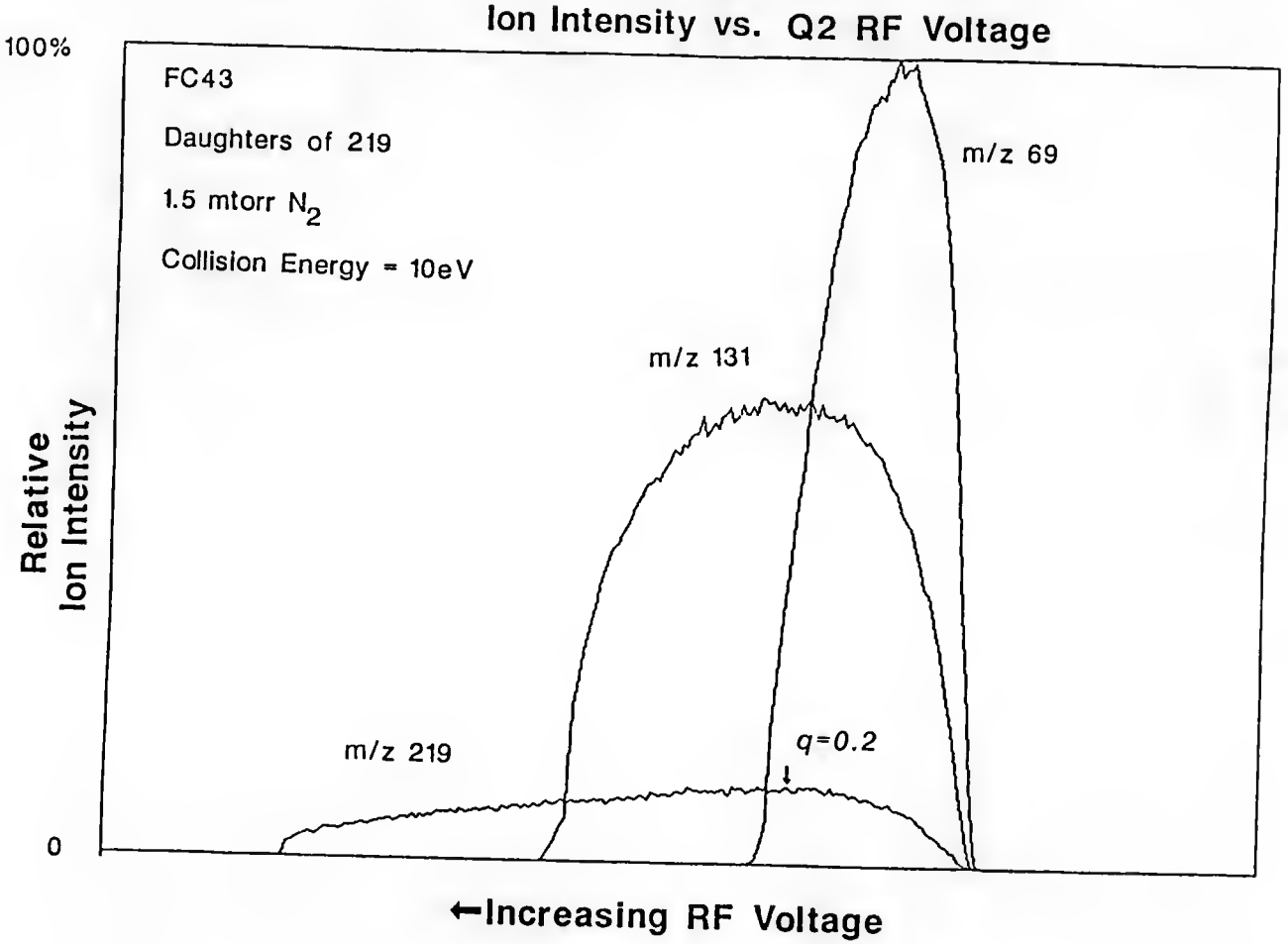

Figure 5.7. Transmission of parent ion (m/z 219) and resulting daughter ions (m/z 69, 131) of PFTBA with Q2 RF voltage illustrating mass-dependent optimum RF voltages. The RF voltage corresponding to a q-value of 0.2 for the parent ion is indicated by the arrow.

m/z. Since different m/z ions have different optimum RF voltages, maximum transmission of all ions during MS/MS may not always be possible. For this reason, the RF voltage must be optimized in a manner to accomplish the goals of the particular experiment of interest. For example, if good qualitative daughter spectra are desired, then the RF voltage is optimized for a low m/z daughter ion such that all of the resulting daughter ions could be observed. For quantitative work, where only one or a few daughter ions are monitored, the RF voltage is optimized such that maximum sensitivity is obtained for the particular parent ion-to-daughter ion transition under study.

In the TSQ70, the Q2 RF level is automatically set by the level chosen for the parent ion in an MS/MS experiment. The default setting of the Q2 RF level corresponds to a q-value of 0.2 for the parent ion. Rarely does this default setting correspond to the optimum for the observation of daughter ions. In fact, as shown in Figure 5.7, setting the RF level for the optimum for the parent ion m/z 219 (q = 0.21) severely limits the transmission of daughter ions of lower mass. The lowest m/z ion that will have a stable trajectory in the center quadrupole, $(m/z)_{cut\text{-}off}$, is determined by the m/z of the parent ion, $(m/z)_p$, and the q-value of the parent ion, q_p, as shown by eq 5.5.

$$(m/z)_{cut\text{-}off} = \frac{q_p(m/z)_p}{0.908} \qquad (5.5)$$

If the q-value of the parent is chosen to be 0.2, then eq 5.5 reduces to

$$(m/z)_{cut\text{-}off} = 0.220(m/z)_p \qquad (5.6)$$

As can be seen in Table 5.2, with increasing m/z of the parent ion, the lower mass limit may prevent useful daughter ions from being observed. This is demonstrated in Figure 5.8 which shows the intensities of the ions obtained with CAD of the m/z 502 ion of PFTBA as a function of Q2 RF voltage. The RF voltage corresponding to a q-value of 0.2 for the parent ion (m/z 502) is indicated in the figure. If a daughter spectrum was acquired with the default q-value of 0.2, then the lowest m/z ion that could be observed would be m/z 110 (Table 5.2); thus, the m/z 69 ion would not be present in the daughter spectrum. As shown in Figure 5.8, operation at a q-value of 0.13 for the parent ion would include all of the daughter ions and would yield more complete structural information. This is not to say that all daughter experiments should be operated at a q-value of 0.13, rather, intelligent choice of q should be made based on the experimental conditions being used. By plotting the ion transmission curves as a function of RF voltage, the choice of an appropriate RF level certainly becomes more apparent.

The appearance of abundant fine structure (or beat patterns) in plots of parent ion transmission versus Q2 ion kinetic energy or Q2 RF voltage have also been reported [74,80,92]. An example of this behavior (although perhaps not as dramatic as that observed by others [80,92]), can be seen by observing the transmission of the parent ion (m/z 502) in Figure 5.8. These beat patterns are due to the transverse periodic (sinusoidal) trajectories of the parent ion beam and to the small size of the exit aperture of the collision cell (usually required to attain suitable pressures for CAD). If the trajectories of the parent ions correspond to an integral number of half-cycles, the parent ions will exit Q2 close to

Table 5.2. Lower m/z limit of the daughter (DG) ion possible with the RF-voltage applied to Q2 to yield a q-value of 0.2 for the parent ion.

m/z Parent Ion	Lowest m/z DG Ion
69	15
31	29
219	48
264	58
414	91
502	110
614	135
652	143
2000	440
4000	880

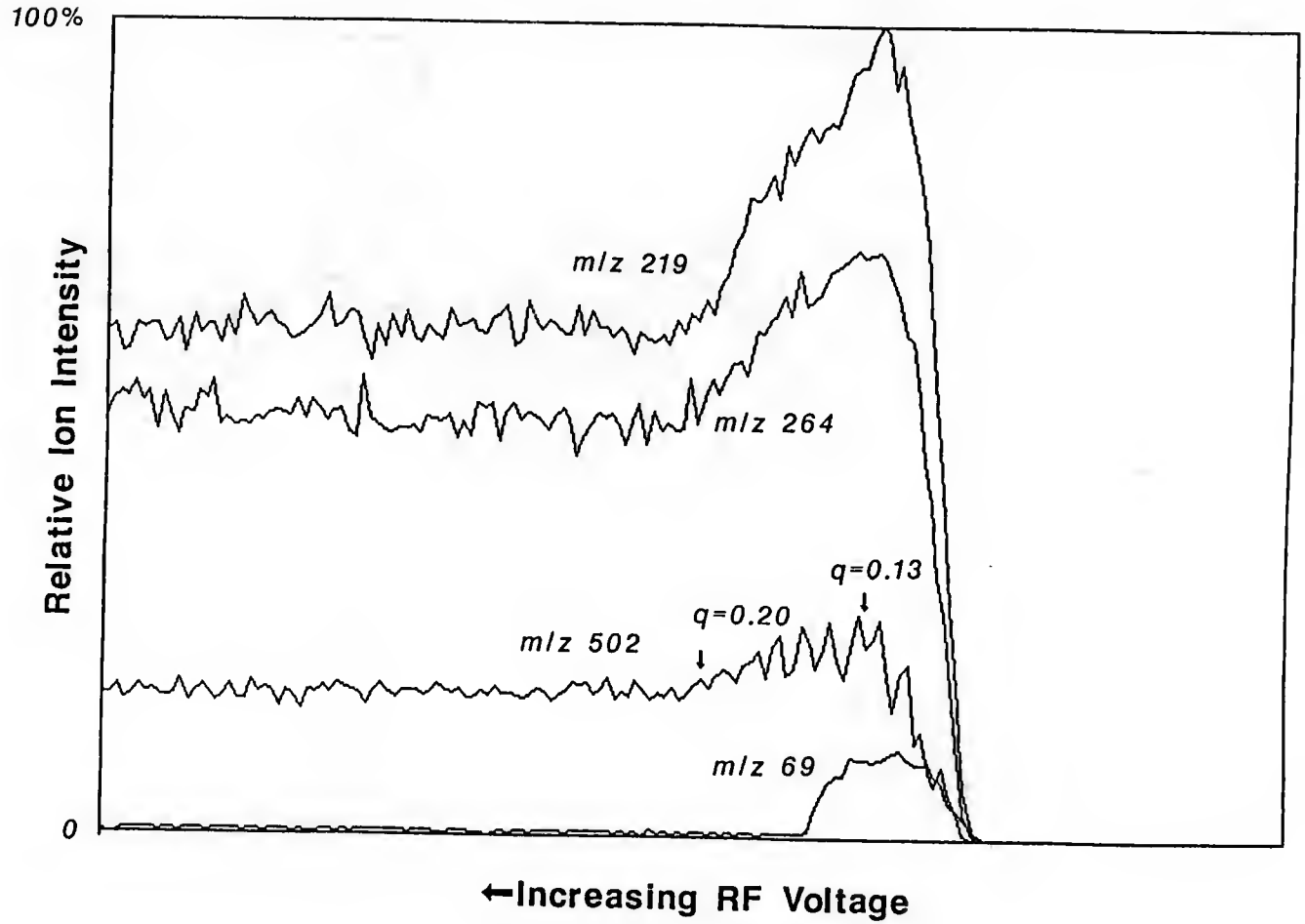

Figure 5.8. Ion transmission as a function of the Q2 RF voltage for the daughter ions from the CAD of m/z 502 of PFTBA. Note that with the default parent ion q of 0.2, the m/z 69 ion would not be observed in the daughter spectrum. Instead, operation at a parent ion q of 0.13 would yield the complete daughter spectrum.

the axis, and thus a maximum in parent ion transmission is observed. However, if the parent ion beam exits Q2 during the midpoint of a half-cycle, some of the ion excursions exceed the size of the exit aperture of the collision cell, and thus a minimum in transmission is observed. The beat patterns are not normally observed for daughter ions, since they are formed along the entire length of the collision cell [80]. However, this behavior does make the comparison of parent-to-daughter ion ratios rather unpredictable and in many cases useless, due to the non-uniform transmission of the parent ion. For this reason, other types of collision cells (e.g., hexapoles and octapoles) have recently been investigated, both for the purposes of obtaining uniform ion transmission as well as increasing the range of masses which can be simultaneously transmitted through the collision cell [93-95].

Effects of ion energy. In MS/MS experiments one of the most important parameters for controlling the degree of fragmentation during CAD is the collision energy. The collision energy is varied directly by adjusting the quadrupole offset voltage on Q2 (i.e., a quadrupole offset voltage of 10 V results in 10 eV ion kinetic energy in Q2). Because of the importance of the collision energy for MS/MS, the effects of this parameter on ion transmission through the second quadrupole were studied. It has been shown that the optimum RF voltage is mass-dependent (Figure 5.7); thus, it was anticipated that the optimum RF voltage might be kinetic energy-dependent as well. This is demonstrated in Figure 5.9, which illustrates ion transmission as a function of the Q2 RF potential for three different Q2 offset voltages. In this experiment, Q1 was set to pass argon ions (Ar^+, m/z 40), Q2 contained no collision gas (base pressure ~1 x 10^{-6} torr), and Q3 was scanned from m/z 37.5 to m/z 42.5. As seen in the figure, the optimum RF level increases with increasing Q2

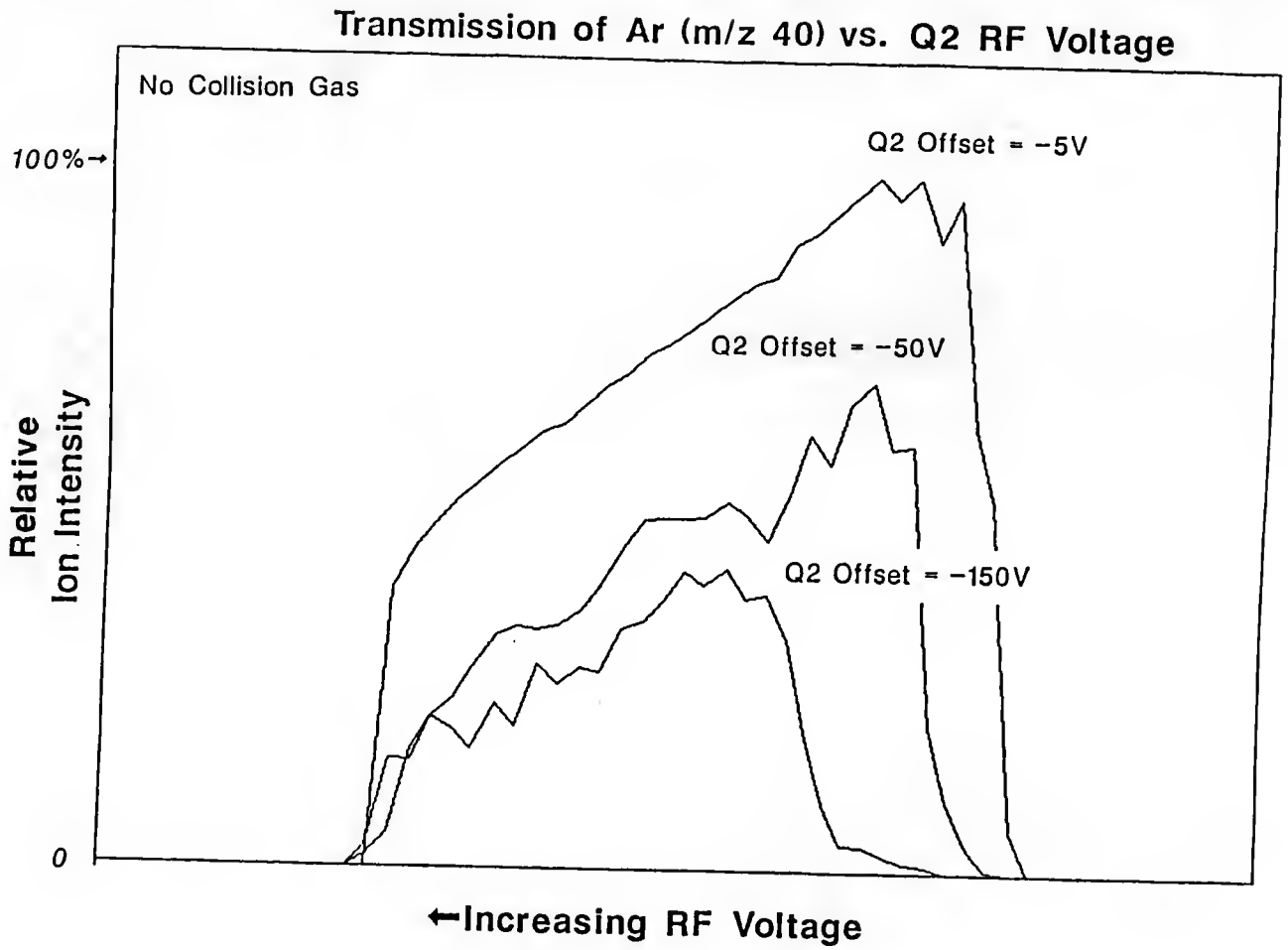

Figure 5.9. Ion transmission of Ar^+ (m/z 40) with Q2 RF voltage, illustrating that the optimum RF voltage is dependent on the Q2 offset voltage (collision energy) that is used.

offset voltage. This behavior can most likely be attributed to the bent geometry of Q2. For a non-linear quadrupole, it has been shown that ions experience an outward force causing them to be displaced from the quadrupole axis. The magnitude of the displacement, ΔX, is periodic and is dependent on the radius of curvature of the quadrupole axis, R [79].

$$\Delta X = \frac{16E}{mq^2\omega^2R} (1-\cos(q\xi/2^{1/2}) \qquad (5.7)$$

The ions are eventually lost and transmission decreases if ΔX becomes too large. At higher ion kinetic energies, higher RF voltages (higher q-values) are required to contain the ions through the bend of the quadrupole. This relationship and the data that are presented above demonstrate the necessity to optimize the Q2 RF voltage for the particular Q2 offset voltage that is to be used.

Figure 5.9 indicates that the ion containment efficiency in Q2 at a particular RF voltage is dependent on the ion axial energy. This energy dependence may also explain in part why different mass daughter ions have different optimum RF voltages (Figure 5.7). Upon CAD of the parent ion, the kinetic energy of a newly formed daughter ion, E_{DG}, is given by [78,80]

$$E_{DG} = E_P(m_{DG}/m_P) \qquad (5.8)$$

where E_P is the kinetic energy of the parent ion (which is equal to the collision energy), m_{DG} is the mass of the daughter ion, and m_P is the mass of the parent ion. Since different mass daughter ions have different

kinetic energies, it is not surprising that the optimum RF amplitude is mass-dependent.

In CAD experiments, the masses of the daughter (product) ions are of lower mass than the parent ion. This is in contrast to the mass-selected reaction mode discussed previously in Chapter 4. In mass-selected reactions (MSRs), the product ions are typically of higher mass than the parent (reactant) ions. The range of RF voltages that result in stable trajectories for low-mass ions is very narrow (eq 5.2). Since the reactant ions (typically low mass) must be efficiently contained in Q2 for the product ions to be observed, proper choice of RF level is critical. This is illustrated in Figure 5.10, which shows ion transmission as a function of Q2 RF voltage for the $C_2H_5^+$ reactant ion and the resulting product ions formed by reaction of this ion with PFTBA (m/z 502 and m/z 652) in Q2. Note that benzene from a previous experiment was also present in Q2, which resulted in the formation of m/z 277 ($[C_4F_9+C_6H_6-HF]^+$) and m/z 105 ($[C_6H_6+C_2H_3]^+$). As shown in the figure, product ions are observed only when the reactant ion is transmitted. In addition, the optima for maximum transmission for different m/z product ions occur at the same Q2 RF voltage. This might be attributed to the fact that the product ions are formed with little or no axial kinetic energy, since they were produced by proton transfer from neutral molecules in Q2. The product ions do eventually gain kinetic energy and are drawn out of Q2 by the ion exit lens. If a constant ion extraction potential is used, the product ions have essentially the same range of kinetic energies; thus, different mass product ions would be expected to have the same optimum RF voltage. This is in contrast to the results obtained for the daughter scan mode in which ions of different mass have different kinetic energies and exhibited different optimum Q2 RF voltages.

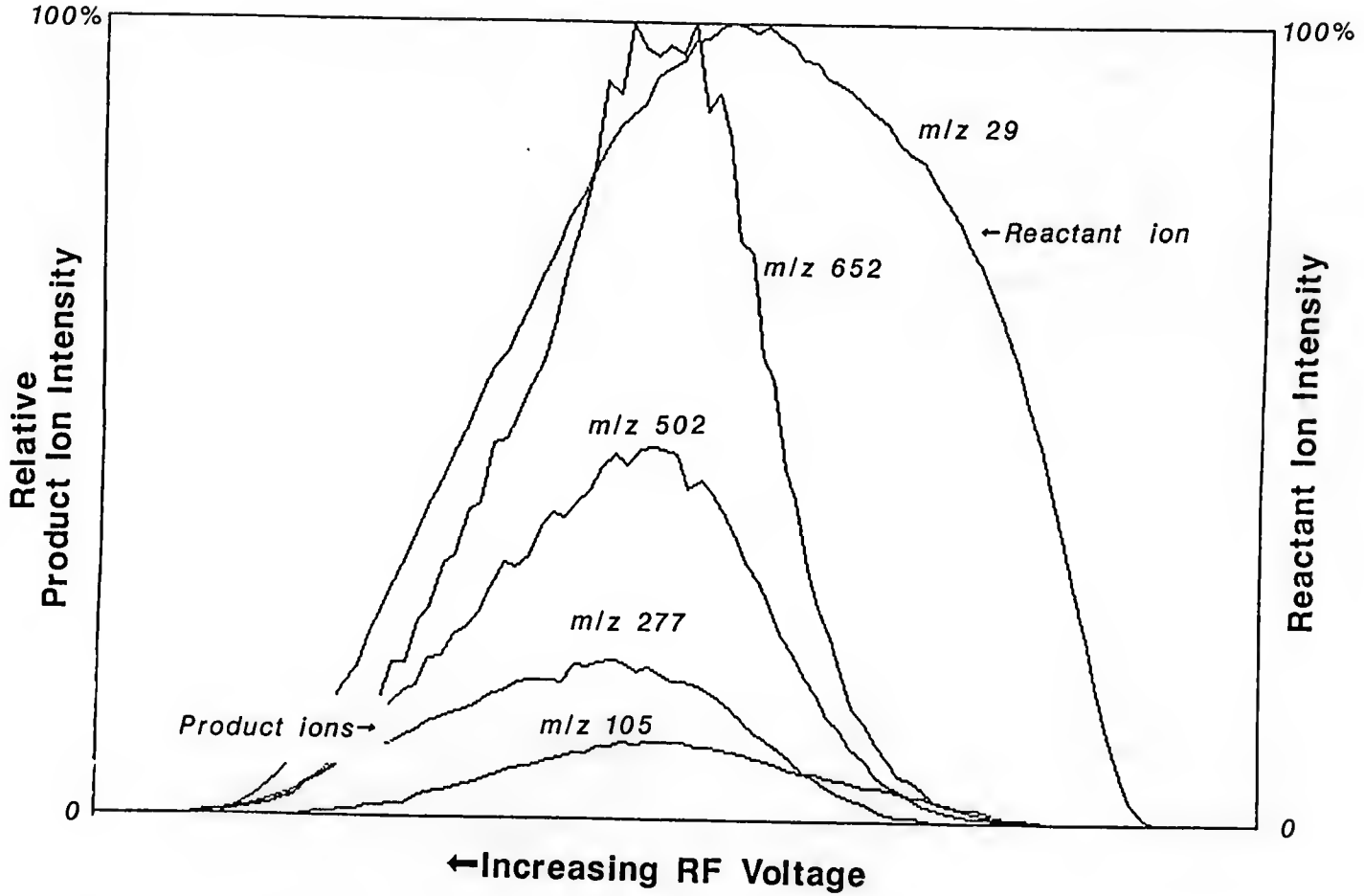

Figure 5.10. Ion transmission as a function of Q2 RF voltage for the $C_2H_5^+$ (m/z 29) reactant ion and the resulting product ions formed by reaction of this ion with PFTBA and benzene in Q2.

Ion Transmission at High Collision Energies

Many compounds of analytical concern (e.g., polycyclic aromatic hydrocarbons) form very stable ions that are particularly difficult to fragment during MS/MS. For example, daughter ions for the CAD of the molecular ion of pyrene are not observed at all with collision energies less than 100 eV [80]. Even at high collision energies and collision gas pressures, the yield of daughter ions from these stable parent ions can be very low. Therefore, proper optimization is crucial for efficient detection of the low-abundance daughter ions. In addition, it has been found that operation at collision energies above approximately 50 eV requires some special considerations for adjustment of the ion optical parameters. After tuning for the Q1MS and Q3MS scan modes, the lens voltages obtained are used in the MS/MS scan modes. For MS/MS scans, all ion optical parameters prior to Q2 (i.e., L11-L23) are obtained from those optimized during Q1MS tuning. The ion optics following Q2 (i.e., L31-L42) are taken from those optimized during Q3MS tuning. Most of the lenses behave in the MS/MS modes as they do in the single MS scan modes; thus, no special optimization for these lenses is required. However, it has been found that lenses on either side of Q2 (L23 and L31) play a key role in the transmission of ions during MS/MS, especially when collision energies above 50 eV are used. This is shown in Figure 5.11 for the case of L23 for the 100 eV CAD of m/z 219 from PFTBA. Ion transmission is improved dramatically if the L23 voltage is made at least as negative as the Q2 offset voltage. In fact, as shown by the inset of Figure 5.11 there is a linear relationship between the optimum L23 voltage and the Q2 offset voltage. It should be noted that the step increase in ion transmission is nearly insignificant at smaller Q2 offset voltages (i.e.,

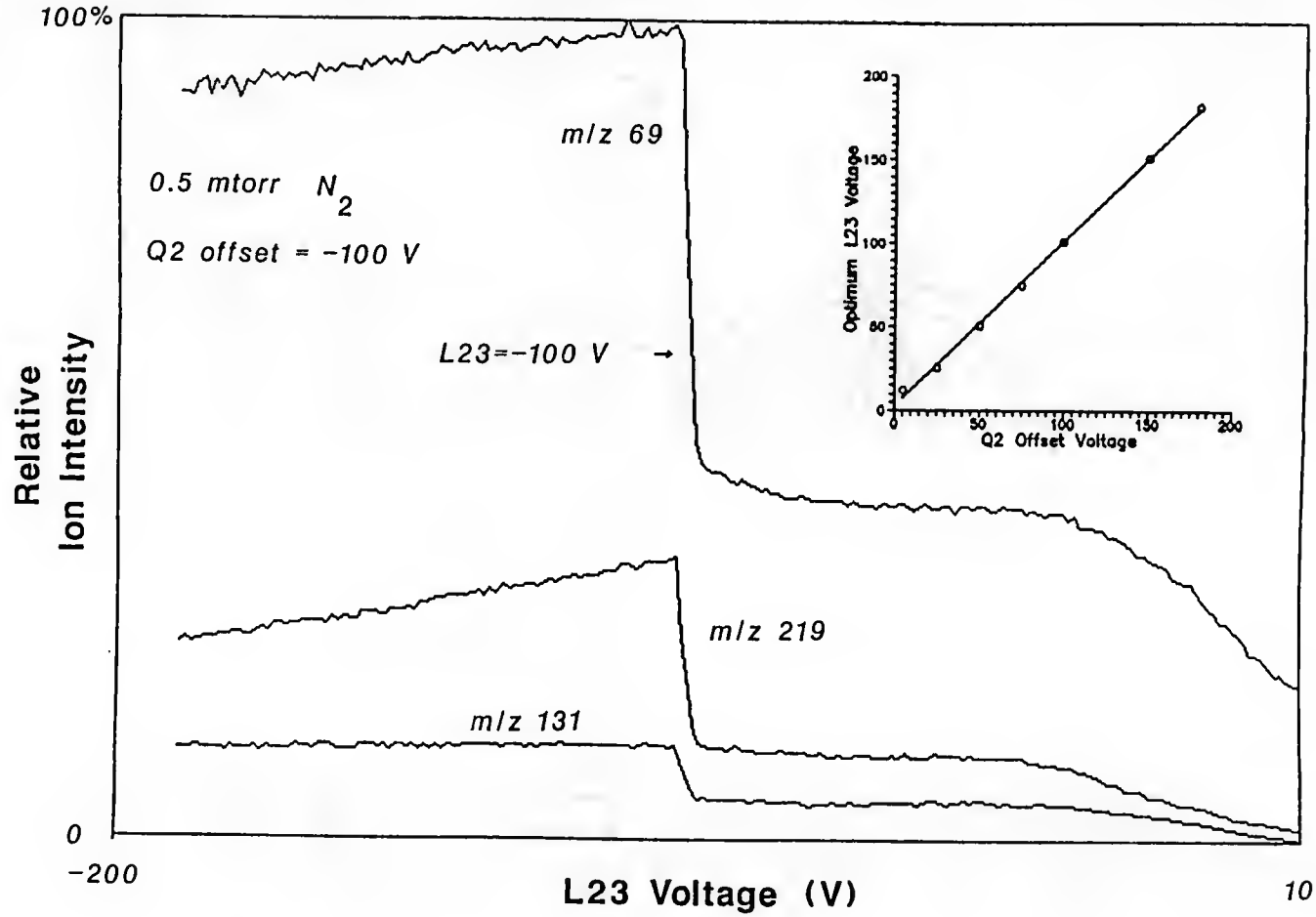

Figure 5.11. Ion transmission as a function of the lens L23 voltage for the 100 eV CAD of the m/z 219 fragment ion of PFTBA. The inset of this figure illustrates the linear relationship between the optimum L23 voltage and the Q2 offset voltage.

more positive than ca. -50 V). The causes for this apparent behavior are discussed in more detail below.

Figure 5.12 shows the transmission of m/z 40 from Ar^+ in the daughter scan mode as a function of collision energy. Curve A in Figure 5.12 was obtained using ion optical parameters that were found to be optimum with a collision energy of 10 eV. As shown in the figure, ion transmission rapidly diminishes if the Q2 offset is made more negative than approximately -50 V. It was found that this loss in transmission that occurs is due to two major factors. The first is the aforementioned dependence of optimum Q2 RF voltage on collision energy. The second is ion entrance and exit conditions that exist when the Q2 offset is made more negative than ca. -50 V. Typically, the lenses are optimized at relatively low Q2 offset voltages (e.g., -10 V). Thus, when MS/MS is performed, the ion beam becomes defocused if the Q2 offset is made more negative than -50 V. However, ion transmission through Q2 can be significantly improved by optimizing the Q2 entrance and exit lenses (L23 and L31) for the collision energy being used. Trace B of Figure 5.12 illustrates the transmission curve for Ar^+ that is improved significantly after proper optimization of these lenses and the Q2 RF voltage had been performed at each collision energy. The capability to obtain uniform ion transmission over a range of kinetic energies is especially important when studying the energetics of the CAD process. These data demonstrate that the effects of the various instrumental parameters should be taken into consideration if the collision energy is varied over a wide range, particularly if energies above ca. 50 eV are used.

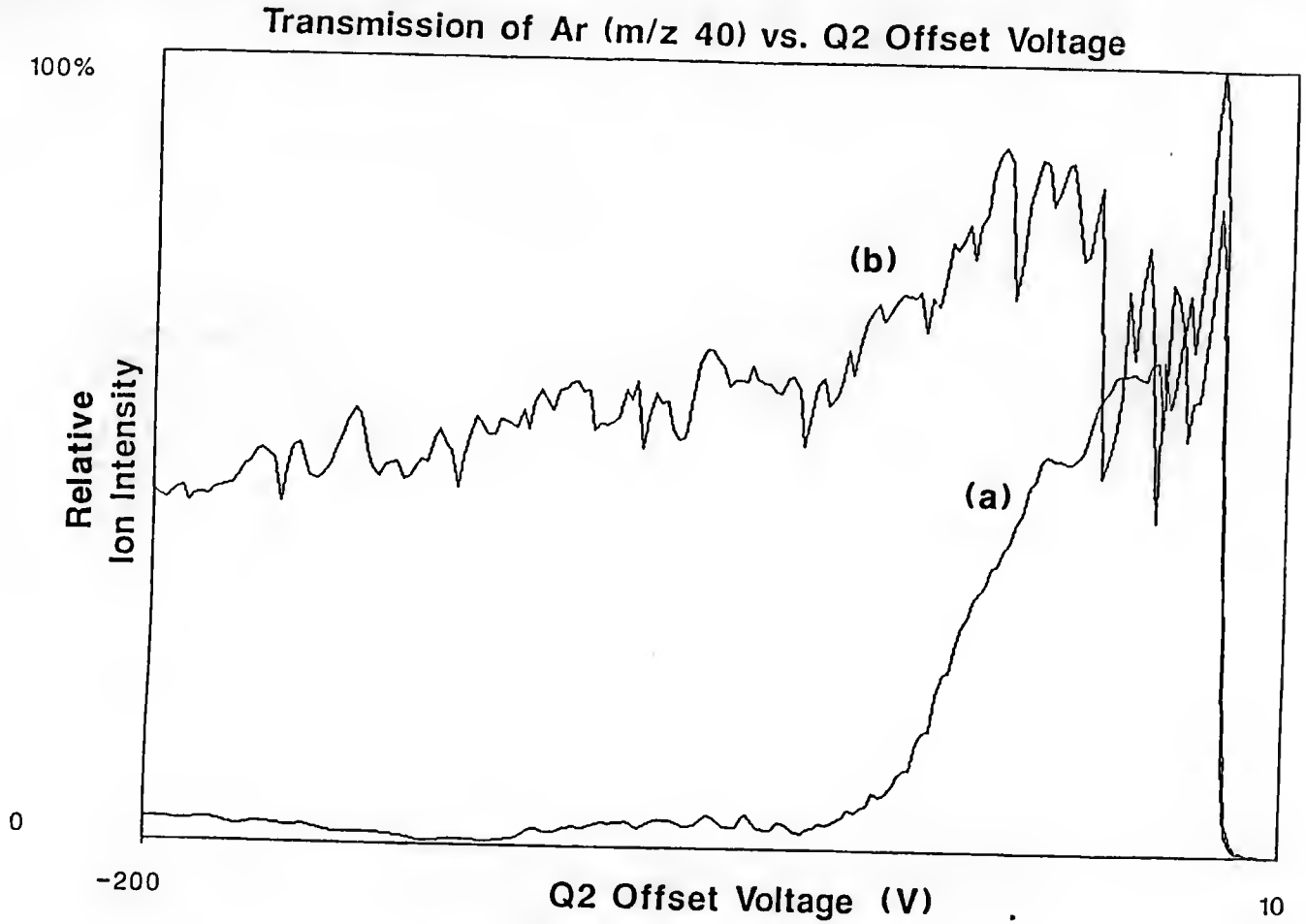

Figure 5.12. Ion transmission of Ar^+ with Q2 offset voltage. For (a), the ion optical parameters used were those found to be optimum for 10 eV collisions. For (b), lenses and the Q2 RF voltage were optimized at each collision energy.

Conclusions

The ion transmission characteristics of a computer-controlled TQMS have been studied for MS and MS/MS operational modes. Studies that have traditionally been laborious and time-consuming with manually-controlled instruments can be rapidly performed with the computer-controlled TSQ70. The results of these studies have provided a better understanding of the effects of the instrumental parameters.

It was found that ion optical lenses positioned close to quadrupole mass filters exhibited mass-dependent transmission behavior if fixed lens potentials were used. These mass dependencies were attributed to the presence of fringing fields that exist near the quadrupole rods carrying both RF and DC voltages. The mass dependencies can be eliminated if the lens voltage is programmed with the mass scan, as can be done with the TSQ70. As a result, optimum transmission can be obtained (at least for single MS scans) over the entire mass range.

Ion transmission in MS/MS experiments was shown to be particularly dependent on the characteristics of the second quadrupole. Ion confinement in the second quadrupole at a particular RF voltage was shown to be dependent on the ion kinetic energy. When CAD was performed in Q2, transmission of daughter ions at a given RF voltage was found to be mass-dependent. In contrast, product ions of mass-selected reactions in Q2 were found to have the same optimum RF voltage, regardless of the ion mass. The effects of the ion energy on transmission was found to be more pronounced at high collision energies (i.e., above 50 eV). Part of this energy-dependent behavior can be attributed to the bent design of the second quadrupole. Ions traversing Q2 at high axial energies require higher RF amplitudes to be efficiently transmitted around the bend. The

lenses on either side of Q2 also have a dramatic effect on ion transmission at high collision energies. All of these parameters must be considered if results obtained over a wide range of collision energies are to be compared.

CHAPTER 6
CONCLUSIONS AND FUTURE WORK

Conclusions

The research reported in this dissertation has demonstrated extensions to the analytical capabilities of GC/MS, and GC/MS/MS, particularly in GC sample introduction and ion transmission. These research efforts have led to a better understanding of the fundamental concepts in both of these areas. These types of studies are particularly significant considering the growing popularity of MS/MS and the widespread availability of commercial instrumentation for its use.

It was demonstrated that vacuum outlet operation in open tubular gas chromatography results in a significant increase in the optimum carrier gas velocity when compared to atmospheric outlet operation. The increase was shown to be more prevalent with short and/or wide-bore open tubular columns, both of which are attractive for use in GC/MS and GC/MS/MS due to the inherent selectivity available with mass spectrometry. Theoretical calculations have been an invaluable aid in understanding the effects of low operating pressures on open tubular columns. The advantages of operating the column inlet as well as the column outlet at vacuum have been stressed. The use of sub-ambient inlet pressures with short columns allows optimum chromatographic performance to be obtained. In addition, lower inlet pressures result in lower carrier gas flow rates, allowing the maximum sensitivity to be obtained when electron ionization is used. Reduced inlet pressures and flow rates have allowed short wide-bore

columns to be used with the GC probe and have permitted short columns to be interfaced to the collision cell of a TQMS without exceeding the normal operating pressure of the instrument.

Alternatives to conventional oven heating and temperature programming in gas chromatography were demonstrated with exponential flow rate programming and direct resistive column heating. Direct resistive heating of metal-clad open tubular columns appears to exhibit tremendous potential for applications requiring portable instrumentation due to the low-power requirements and the simplicity of the electronics required for temperature control. Direct resistive temperature sensing was shown to be an accurate method of determining the temperatures of the metal-clad columns. It appears that this method would be applicable to the direct measurement of column temperatures in chromatograph ovens as well. Moreover, the rapid heat-up and cool-down rates of directly-heated columns makes them attractive for performing high-throughput analysis in the laboratory. These concepts were demonstrated with the compact GC probe and associated electronics that were designed for use in GC/MS.

A new technique, GC/MSR/MS, was described, which involves mass-selection of a single m/z reactant ion and reaction of this ion with the effluent from a GC column which is introduced into the center quadrupole collision cell of a triple quadrupole mass spectrometer (TQMS). One of the advantages of mass-selected reactions (MSRs) is the enhanced selectivity that is obtained by the selection of a single m/z reactant ion for reaction with sample molecules via charge exchange, proton transfer, or adduct formation chemical ionization. In addition, it was shown that both molecular weight and structural information are readily obtained in the same chromatogram by alternating between two (or more) reactant ions.

The combination of short open tubular GC columns with MSRs allows for highly selective and rapid mixture analyses to be performed. The GC/MSR/MS technique exhibits considerable promise, since the selectivity of the technique is limited only by the choice of specific ion-molecule reactions. The potential application of this technique to selective negative ion reactions should also add to the attractiveness of the method.

A thorough study of the ion transmission characteristics of a computer-controlled TQMS has been performed. It was shown that electrostatic lenses positioned on either side of quadrupole mass filters exhibited mass-dependent behavior. The origins of the mass dependencies were attributed to the fringing fields imposed by the mass filters. The ion transmission behavior of the second quadrupole (Q2) was also studied. The importance of selecting the proper Q2 RF voltage for obtaining both qualitative and quantitative results was stressed. The inter-relation of the MS/MS ion optical parameters was found to be very complex. The best transmission efficiencies in MS/MS experiments were obtained when the appropriate parameters were optimized at the collision energy that was used. Finally, the importance of computer control for investigating the ion optical behavior and correcting for undesirable effects (e.g., mass-dependencies) is evident from these studies.

Suggestions for Future Work

Reduced Column Pressures with Conventional GC Detectors

The advantages of low column pressures are readily obtained with the GC/MS combination; however, low-pressure operation of conventional GC detectors has not been previously investigated. The commonly used flame

ionization detector (FID) and electron capture detector (ECD) could be evaluated for low-pressure operation. As was shown in Chapter 2, high-vacuum operation (e.g., <1 torr) may not be necessary. In fact, for a 3 m x 0.25 mm i.d. open tubular column, operation at an outlet pressure of 100 torr was predicted to yield nearly the same chromatographic results as operation with an outlet pressure of 1 torr.

The effects of the low-pressures on the hydrogen flame of the FID have not been previously studied, thus it is not known if the hydrogen flame of the FID would remain lit at the low pressures. Perhaps the ECD would be more easily evaluated due to its simplicity. The ECD employs a ß-emitting ^{63}Ni foil which acts as a source of thermal electrons at atmospheric pressure. However, operation of the ECD at the low pressures might inhibit the thermalization of the ß particles. These problems would have to be addressed and the effects of the operating pressure on the sensitivity of these detectors would have to be evaluated if vacuum operation is to be a attractive alternative to conventional operation.

Directly-heated Open Tubular Columns

There are several improvements that could be made to the existing technology in addition to other possibilities that have yet to be explored with directly-heated capillary columns. It is expected that heating rates would be significantly increased if the glass-braid insulation were removed from the column. If this were to be done, a new column spool would have to be designed that would prevent electrical shorting of successive coils of the column. Improvements in the design of the power supply and associated electronics might also be advantageous. For example, application of proportional-integral-differential feedback

control of the column temperature and an autoranging circuit for measurement of the column resistance is expected to significantly improve the characteristics of direct resistive heating.

Smaller diameter columns could also be applied in the GC probe to yield better chromatographic resolution for a given column length than the wide-bore columns. This would not require a new design for the injection port. Rather, a wide-bore column could be used as a pre-column and would serve as the injection port for the narrow-bore column. In order for this to be feasible, a low thermal mass column coupling would have to be designed to electrically connect the two columns without creating a cold spot. Another advantage of the smaller bore columns is that they can be coiled to a smaller diameter, which would allow further reduction in the size of the GC probe or other portable GC instrumentation.

It might also be possible to take advantage of the Peltier effect for the rapid heating and cooling of metal-clad open tubular columns [38]. The feasibility of utilizing Peltier heating and/or cooling in open tubular GC was speculated (but never demonstrated) at the University of Florida in a discussion between S. O. Colgate, R. A. Yost, and this author. With the Peltier effect, thermoelectric heating or cooling occurs if a voltage drop is placed across the junction of two dissimilar metals (i.e., a thermocouple). Depending on the direction and magnitude of the current, the junction can be made to heat or cool. Therefore, it should be possible to coat fused silica columns with two different metals for the purposes of thermoelectric temperature control. If the appropriate metals were chosen for coating, the column itself could be used as a thermocouple, allowing conventional commercially-available temperature sensing electronics to be used for measuring the column temperature.

Perhaps the real challenge for this project would be devising a suitable method of coating the desired metals on the columns. Recently, stainless steel tubing with an inner surface of fused silica has become commercially available (Restek Inc.). The manufacturers claim that the fabrication process for this tubing involves depositing the fused silica inside the stainless steel tubing with a chemical reaction, instead of depositing the stainless steel on the outside of the fused silica. If this same process were employed, it should be possible to fabricate virtually any type of column with metallic coatings for thermoelectric temperature control.

Resonance Excitation and Ion Storage in Q2

There are a number of different processes that could be investigated that might enhance the characteristics of MS/MS in triple quadrupole mass spectrometry. One process that warrants evaluation is resonance-enhanced collisionally-activated dissociation (RECAD) in the center quadrupole collision cell. Typically, the degree of fragmentation of the CAD process in a TQMS is controlled by varying the parent ion axial kinetic energy in Q2. It was shown in Chapter 5 that operation at high collision energies usually requires special considerations for tuning. Nevertheless, in most cases, operation at high axial collision energies results in reduced transmission efficiencies. An alternative, and perhaps more efficient method of collisional activation would be to increase the parent ion oscillatory (instead of axial) kinetic energy via resonance excitation. To perform RECAD, a supplementary RF voltage could be applied to the quadrupole rods of Q2 at the fundamental resonant frequency of a particular m/z ion. Application of the RF voltage at the correct frequency and amplitude would increase the orbital velocity (and thus the

kinetic energy) of the ion of interest. Fragmentation would be induced via collisions of the resonance-excited ion with neutral gas molecules. The RECAD process is already being used in the ion trap mass spectrometer (ITMS) and has proven to be a very efficient method of performing CAD [96]. Resonance excitation has also been used with an RF-only quadrupole operated as a "notch filter" [97]. In this mode, the supplementary RF amplitude is set high enough such that the oscillations of a selected ion become large and the ion is ejected from the quadrupole field. The notch filter mode might prove to be useful for ejecting undesirable reactant ions that are formed in Q2 during mass-selected ion-molecule reaction experiments. For example, in Chapter 4 it was stated that even with mass-selection of the protonated acetone dimer (m/z 117) with Q1, protonated acetone (m/z 59) was formed (either by metastable decomposition or CAD) in Q2. Application of resonance excitation might be used to eject the m/z 59 ion, and thereby further increasing the selectivity of mass-selected reactions.

There are a number of considerations that would have to be addressed if RECAD were to be successfully employed. One reason for the inherent efficiency of RECAD in the ion trap is the long ion storage times (hundreds of milliseconds) that are possible [96]. In contrast, the residence time of ions in the center quadrupole is on the order of microseconds. The residence time, t, of an ion in Q2 is given by

$$t = L(m/2E)^{1/2} \qquad (6.1)$$

where L is the collision cell path length, m is the ion mass, and E is the ion axial kinetic energy. Using this equation, an ion with a mass of

100 amu and 10 eV of axial energy has a residence time of 32 μs in the collision cell of the TSQ70 (L = 14 cm). A residence time this short may not be long enough to allow efficient RECAD to occur. It may be possible to store ions in Q2 to increase their residence times. It has previously been shown that the ion lenses on either side of the second quadrupole collision cell can be used as "electrostatic mirrors" to store and pulse the ions out of the collision cell [60-62,98]. Ion storage in Q2 might also be attractive for increasing reaction times for ion-molecule reactions. The TSQ70 is well-suited for these types of studies, since all ion optical parameters are under computer control.

LITERATURE CITED

1. Yost, R. A.; Fetterolf, D. D.; Hass, J. R.; Harvan, D. J.; Weston, A. F.; Skotnicki, P. A.; Simon, N. M. Anal. Chem. 1984, 56, 2223-2228.

2. Trehy, M. L.; Yost, R. A.; McCreary, J. J. Anal. Chem. 1984, 56, 1281-1285.

3. Trehy, M. L.; Yost, R. A.; Dorsey, J. G. Anal. Chem. 1986, 58, 14-19.

4. McClennen, W. H.; Richards, J. M.; Meuzelaar, H. L. C. Proceedings of the 36th ASMS Conference on Mass Spectrometry and Allied Topics 1988, 403-404.

5. Richards, J. M.; McClennen, W. H.; Bunger, J. A.; Meuzelaar, H. L. C. Proceedings of the 36th ASMS Conference on Mass Spectrometry and Allied Topics 1988, 547-548.

6. Giddings, J. C. Anal. Chem. 1962, 34, 314-319.

7. Tijssen, R.; van den Hoed, N.; van Kreveld, M. E. Anal. Chem. 1987, 59, 1994-1996.

8. Gaspar, G.; Annino, R.; Vidal-Madjar, C.; Guiochon, G. Anal. Chem. 1978, 50, 1512-1518.

9. van Es, A.; Janssen, J.; Bally, R.; Cramers, C.; Rijks, J. J. High Resolut. Chromatogr. Chromatogr. Commun. 1987, 10, 273-279.

10. Schutjes, C. P. M.; Vermeer, J. A.; Rijks, J.; Cramers, C. J. Chromatogr. 1982, 253, 1.

11. Hyver, K. J.; Phillips, R. J. J. Chromatogr. 1987, 399, 33-46.

12. Ewels, B. A.; Sacks, R. D. Anal. Chem. 1985, 57, 2774-2779.

13. Lanning, L. A.; Sacks, R. D.; Mouradian, R. F.; Levine, S. P.; Foulke, J. A. Anal. Chem. 1988, 60, 1994-1996.

14. Cramers, C. A.; Scherpenzeel, G. J.; Leclercq, P. A. J. Chromatogr. 1981, 203, 207-216.

15. Leclercq, P. A.; Scherpenzeel, G. J.; Vermeer, E. A. A.; Cramers, C. A. J. Chromatogr. 1982, 241, 61-71.

16. Leclercq, P. A.; Cramers, C. A. J. High Resolut. Chromatogr. Chromatogr. Commun. 1987, 10, 269-272.

17. Leclercq, P. A.; Cramers, C. A. J. High Resolut. Chromatogr. Chromatogr. Commun. 1985, 8, 764-771.

18. Hatch, F. W.; Parrish, M. E. Anal. Chem. 1978, 50, 1164-1168.

19. Johnson, J. V.; Yost, R. A. Anal. Chem. 1985, 57, 758A.

20. Golay, M. J. E. Nature 1958, 182, 1146-1147.

21. Giddings, J. C.; Seager, S. L.; Stucki, L. R.; Stewart, G. H. Anal. Chem. 1960, 32, 867-870.

22. Guiochon, G. Anal. Chem. 1978, 50, 1812-1821.

23. Ettre, L. S. Introduction to Open Tubular Columns, Perkin-Elmer Corp.: Norwalk, CT, 1979, 52-57.

24. Omega Engineering Inc., Stamford CT, 06906.

25. Kelley, J. D.; Walker, J. Q. Anal. Chem. 1969, 41, 1340-1342.

26. Scott, R. P. W.; Hazeldean, G. S. F Gas Chromatography 1960; Scott, R. P. W., Ed.; Butterworth: London, 1960, 144.

27. Jennings, W. J. Analytical Gas Chromatography, Academic Press, Inc.: Orlando, FL, 1987, 77-78.

28. Harrison, A. G. Chemical Ionization Mass Spectrometry, CRC Press, Inc.: Boca Raton, FL, 1983; Chapter 2.

29. Nygren, S. J. Chromatogr. 1977, 142, 109-116.

30. Zlatkis, A.; Fenimore, D. C.; Ettre, L. S.; Purcell, J. E. J. Gas Chromatogr. 1965, 3, 75-81.

31. Walsh, J. T.; Merritt, C. J. Gas Chromatogr. 1967, 5, 420-423.

32. Costa Neto, C.; Koffer, J. T.; De Alencar, J. W. J. Chromatogr. 1964, 15, 301-313.

33. Nygren, S.; Mattsson, P. E. J. Chromatogr. 1976, 123, 101-108.

34. Nygren, S.; Anderson, S. Anal. Chem. 1985, 57, 2748-2751.

35. Nygren, S.; Olin, A. J. Chromatogr. 1986, 366, 1-12.

36. Lee, M. L.; Yang, F. J.; Bartle, K. D. Open Tubular Gas Chromatography: Theory and Practice; John Wiley & Sons: New York, 1984; Chapter 4.

37. Sears, F. W.; Zemansky, M. W.; Young, H. D. University Physics, 5th ed.; Addison-Wesley: Reading, MA, 1978; Chapter 16.

38. Sears, F. W.; Zemansky, M. W.; Young, H. D. University Physics, 5th ed.; Addison-Wesley: Reading, MA, 1978; Chapter 28.

39. Rudat, M. A. Proceedings of the 30th ASMS Conference on Mass Spectrometry and Allied Topics, 1982, 868.

40. Davies, N. W. Anal. Chem. 1984, 56, 2618-2620.

41. Davies, N. W. J. Chromatogr. 1985, 325, 23-35.

42. Lee, E. D.; Hsu, S.; Henion, J. D. Anal. Chem. 1988, 60, 1990-1994.

43. Lee, M. L.; Yang, F. J.; Bartle, K. D. Open Tubular Gas Chromatography: Theory and Practice; John Wiley & Sons: New York, 1984; Chapter 2.

44. Varian Model 3300/3400 Operator's Manual, Varian Associates Inc., Walnut Creek, CA 94598.

45. Grob, K. On-Column Injection in Capillary Gas Chromatography; Huethig: Heidelberg, 1987; Chapter B.

46. Bretell, T. A.; Grob, R. L. Am. Lab. 1985, 17(11), 50-68.

47. Fetterolf, D. D.; Yost, R. A. Int. J. Mass Spectrom. Ion Proc. 1984, 62, 33-49.

48. Jelsus, B. L.; Burnaby, M.; Fenselau, C. Biomed. Mass Spectrom. 1974, 1, 96-102.

49. Einolf, N.; Munson, B. Int. J. Mass Spectrom. Ion Phys. 1972, 9, 141-160.

50. Subba Rao, S. C.; Fenselau, C. Anal. Chem. 1978, 50, 511-515.

51. Hsu, C. S.; Cooks, R. G. Org. Mass Spectrom. 1976, 11, 975-983.

52. Busch, K. L.; Kruger, T. L.; Cooks, R. G. Anal. Chim. Acta 1980, 119, 153-156.

53. Van Berkel, G. J.; Glish, G. L; McLuckey, S. A. Proceedings of the 36th ASMS Conference on Mass Spectrometry and Allied Topics 1988, 300-301.

54. Van Berkel, G. J.; Glish, G. L; McLuckey, S. A. Proceedings of the 36th ASMS Conference on Mass Spectrometry and Allied Topics 1988, 639-640.

55. Glish, G. L; Van Berkel, G. J.; Asano, K. G.; McLuckey, S. A. Proceedings of the 36th ASMS Conference on Mass Spectrometry and Allied Topics 1988, 1112-1113.

56. Schmit, J. P.; Dawson, P. H.; Beaulieu, N. Org. Mass Spectrom. 1985, 20,269.

57. Schmit, J. P.; Beaudet, S.; Brisson, A. Org. Mass Spectrom. 1986, 21, 493.

58. Jalonen, J. J. Chem. Soc. Chem. Commun. 1985, 872.

59. Fetterolf, D. D.; Yost, R. A.; Eyler, J. R. Org. Mass Spectrom. 1984, 19,104-105.

60. Dolnikowski, G. G.; Kristo, M. J.; Enke, C. G.; Watson, J. T. Int. J. Mass Spectrom. Ion Proc. 1988, 82, 1-15.

61. Beaugrand, C.; Devant, G.; Jaouen,D.; Mestdagh, H.; Rolando, C. Proceedings of the 35th ASMS Conference on Mass Spectrometry and Allied Topics, 1987, 345-346.

62. Beaugrand, C.; Devant, G.; Jaouen,D.; Mestdagh, H.; Rolando, C.; Supérieure, E. N. Proceedings of the 36th ASMS Conference on Mass Spectrometry and Allied Topics, 1988, 811-812.

63. Crawford, R. W.; Alcaraz, A.; Reynolds, J. G. Anal. Chem. 1988, 60, 2439-2441.

64. Dawson, P. H., Quadrupole Mass Spectrometry and its Applications; Elsevier Scientific Publishing Co.: Amsterdam, 1976; Chapter 2.

65. Duckworth, H. E.; Barber, R. C.; Venkatasubramanian, Mass Spectroscopy; Berry, M.; Davies, P. C. W.; Isham, C. J.; Main, I. G., Eds., Cambridge University Press: New York, 1986; 40-69.

66. Chupka, W. A., Ion-Molecule Reactions; Franklin, J. L., Ed., Plenum Press: New York, 1972; 33-76.

67. Maeda, K.; Semeluk, G. P.; Lossing, F. P. Int. J. Mass Spectrom. Ion Phys. 1968, 1, 395.

68. Peatman, W. B.; Borne, T. B.; Schlag, E. W. Chem. Phys. Lett. 1969, 3, 492.

69. Villarejo, D.; Herm, R. R.; Ingrham, M. G. J. Chem. Phys. 1967, 46, 4995.

70. Brion, C. E.; McDowell, C. A.; Stewart, W. B. Chem. Phys. Lett. 1972, 13, 79.

71. Rosenstock, H. M.; Draxl, K.; Steiner, B. W.; Herron, J. T. J. Phys. Chem. Ref. Data Supp., 1977, 6, 1.

72. Märk, T. D. Gaseous Ion Chemistry and Mass Spectrometry; John Wiley & Sons: New York, 1986; Chapter 3.

73. Hunt, D. F.; Gale, P. J. Anal. Chem. 1984, 56, 1111-1114.

74. Yost, R. A.; Enke, C. G.; McGilvery, D. C.; Smith, D.; Morrison, J. D. Int. J. Mass Spectrom. Ion Phys. 1979, 30, 127-136.

75. Dawson, P. H. Int. J. Mass Spectrom. Ion Phys. 1982, 42, 195-211.

76. Dawson, P. H. Mass Spectrom. Rev. 1986, 5, 1-37.

77. Dawson, P. H.; French, J. B.; Buckley, J. A.; Douglas, D. J.; Simmons, D. Org. Mass Spectrom. 1982, 17, 205-211.

78. Dawson, P. H.; French, J. B.; Buckley, J. A.; Douglas, D. J.; Simmons, D. Org. Mass Spectrom. 1982, 17, 212-219.

79. Syka, J. E. P.; Schoen, A. E.; Ceja, P. C.; Smith, R. M. Proceedings of the 34th ASMS Conference on Mass Spectrometry and Allied Topics 1986, 718-719.

80. Schoen, A. E.; Syka, J. E. P. Proceedings of the 34th ASMS Conference on Mass Spectrometry and Allied Topics 1986, 722-723.

81. Martinez, R. I.; Ganguli, B. Rapid Commun. Mass Spectrom. 1988, 2, 41-46.

82. Martinez, R. I.; Dheandhanoo, S. J. Res. Natl. Bur. Stand. 1987, 92, 229-237.

83. Fite, W. L. Proceedings of the 31st ASMS Conference on Mass Spectrometry and Allied Topics 1983, 19-43.

84. Dawson, P. H., Ed., Quadrupole Mass Mass Spectrometry and Its Applications, Elsevier Scientific Publishing Co.: Amsterdam, 1976.

85. Campana, J. E. Int. J. Mass Spectrom. Ion Proc. 1980, 33, 101-117.

86. Miller, P. E.; Denton, M. B. J. Chem. Educ. 1986, 63, 617-622.

87. Lawson, G.; Todd, J. F. J. Chem. Brit. 1972, 8, 373-380.

88. Brubaker, W. M. J. Vac. Sci. Technol., 1973, 10, 291.

89. Fite, W. L. Rev. Sci. Instrum., 1976, 47, 326.

90. Finnigan MAT Series 4500 GC/MS Operator's Manual, Finnigan MAT Corp., San Jose, CA, 95134.

91. Dahl, D. A.; Delmore, J. E. Proceedings of the 34th ASMS Conference on Mass Spectrometry and Allied Topics 1987, 257-258.

92. Miller, P. E.; Denton, M. B. Int. J. Mass Spectrom. Ion Proc. **1986**, 72, 223-238.

93. Hagg, C., Szabo, I. Int. J. Mass Spectrom. Ion Proc. **1986**, 73, 237.

94. Hagg, C., Szabo, I. Int. J. Mass Spectrom. Ion Proc. **1986**, 73, 295.

95. Syka, J. E. P.; Szabo, I. Proceedings of the 36th ASMS Conference on Mass Spectrometry and Allied Topics **1988**, 1328-1329.

96. Louris, J. N.; Cooks, R. G.; Syka, J. E. P.; Kelley, P. E.; Stafford, G. C.; Todd, J. F. J. Anal. Chem., **1987**, 59, 1677-1685.

97. Reinsfelder, R. E.; Denton, M. B. Int. J. Mass Spectrom. Ion Proc. **1981**, 37, 241-250.

98. Yost, R. A., Triple Quadrupole MS/MS for Mixture Analysis, proposal to the National Science Foundation, **1982**.

BIOGRAPHICAL SKETCH

Mark Edward Hail, son of Carl W. Hail and Catherine C. Hail, was born in Lexington, Kentucky. Mark lived in Ashland, Kentucky, until the age of 12. The Hail family moved to Shelbyville, Kentucky, in 1975. He graduated from Shelby County High School in 1980.

In the fall of 1980 Mark enrolled at the University of Kentucky (UK) in Lexington. In the spring of 1983 he joined Lambda Chi Alpha fraternity and during the next year served as president of the local chapter. He spent the following two summers performing undergraduate research under the direction of Dr. F. James Holler. Mark received two fellowships during these two summers, including the Stephen Harris Cook Memorial and an Ashland Oil fellowship. Under Dr. Holler's guidance, he developed a strong interest in analytical chemistry and chemical instrumentation. Mark graduated from UK in the spring of 1984.

In August 1984, Mark began his graduate work in analytical chemistry under the direction of Dr. Richard A. Yost. On July 30, 1988, Mark married Amy Marianne Duffy, a talented musician (flutist) whom he has known since high school. Upon completion of his graduate studies, he will begin work in the engineering division of Finnigan-MAT Corporation in San Jose, California.

I certify that I have read this study and that in my opinion it conforms to acceptable standards of scholarly presentation and is fully adequate, in scope and quality, as a dissertation for the degree of Doctor of Philosophy.

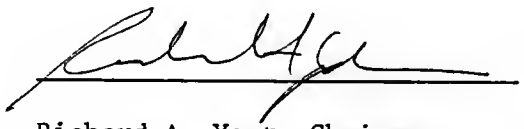

Richard A. Yost, Chairman
Associate Professor of Chemistry

I certify that I have read this study and that in my opinion it conforms to acceptable standards of scholarly presentation and is fully adequate, in scope and quality, as a dissertation for the degree of Doctor of Philosophy.

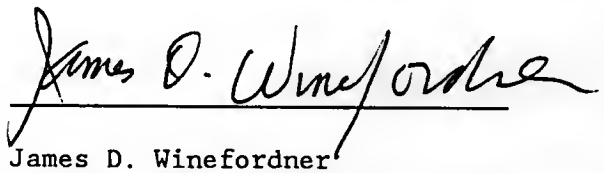

James D. Winefordner
Graduate Research Professor of Chemistry

I certify that I have read this study and that in my opinion it conforms to acceptable standards of scholarly presentation and is fully adequate, in scope and quality, as a dissertation for the degree of Doctor of Philosophy.

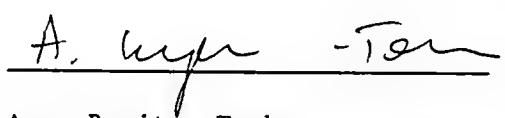

Anna Brajter-Toth
Associate Professor of Chemistry

I certify that I have read this study and that in my opinion it conforms to acceptable standards of scholarly presentation and is fully adequate, in scope and quality, as a dissertation for the degree of Doctor of Philosophy.

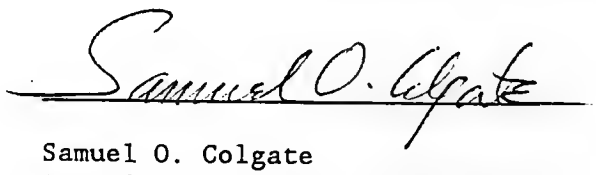

Samuel O. Colgate
Associate Professor of Chemistry

I certify that I have read this study and that in my opinion it conforms to acceptable standards of scholarly presentation and is fully adequate, in scope and quality, as a dissertation for the degree of Doctor of Philosophy.

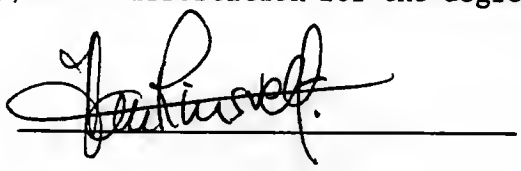

Henri A. Van Rinsvelt
Professor of Physics

This dissertation was submitted to the Graduate Faculty of the Department of Chemistry in the College of Liberal Arts and Sciences and to the Graduate School and was accepted as partial fulfillment of the requirements for the degree of Doctor of Philosophy.

May 1989

_____

Dean, Graduate School

UNIVERSITY OF FLORIDA
3 1262 08554 2743